The evolution of the Brewer-Dobson circulation and the ozone layer during the last three decades

Albert Ossó Castillón

Thesis to get the degree of a doctor of philosophy

The evolution of the Brewer-Dobson circulation and the ozone layer during the last three decades

Albert Ossó Castillón

8 July 2014

Universitat de Barcelona
Facultat de Física i Química
Departament d'Astronomia i Meteorologia

Director
Prof. Jerónimo Lorente Castelló

Tutor
Prof. Jerónimo Lorente Castelló

Als meus pares, Enric i Enriqueta

"Ningú ha viscut més temps que un nen mort, i Matusalem va morir jove. El Cel i la Terra són tant vells com jo, i deu mil coses son una sola."

Zhuang Zi, 300 a. de C.

"*I went to the woods because I wished to live deliberately, to front only the essential facts of life, and see if I could not learn what it had to teach, and not, when I came to die, discover that I had not lived.*"

Henry David Thoreau

Acknowledgments

No puc començar d'altra manera que expressant la meva sincera gratitud a les nombroses i meravelloses persones que m'han inspirat al llarg de la meva vida. Primerament a la meva mare *Enriqueta* i al meu pare *Enric*, que m'han cuidat amb tot l'amor que només uns pares poden donar. Als meus germans *Marta* i *Ernest*, intel · ligents i brillants, els quals estimo per sobre de tot. Als meus avis *Maria*, *Enric* i *Eulàlia* que em van cuidar i estimar com uns pares. Quina fantàstica família que tinc!

Als meus primers mestres formals i no formals que m'han transmès coneixement i inspiració. Recordo especialment en *Josep Valls*, en *Jordi Mercadé*, la *Neus Codina*, en *David Jou* i en *Gaspar Orriols*.

A l'*Álvaro Corral* i en *Josep Enric Llebot*, que van confiar en mi i em van introduir en el món de la recerca científica. Al meu director de tesi, en *Jerónimo Lorente*, que em va donar la confiança per portar a terme aquest projecte i m'ha donat suport en tots i cadascun dels moments. To *Dave Thompson* who hosted me at Colorado State University and whose personality and talent inspires me.

A la *Laura*, la meva millor amiga, a qui la meva estimació ha estat i sempre serà infinita.

Finalment, però no per això menys importants, als meus companys del DAM. El meu agraïment i estima és molt especial per a la *Yolanda Sola*. La seva amabilitat i comprensió, el seu talent i entusiasme fa que treballar amb ella sigui un goig continu. Al *David, al Didac*, a la *Míriam* i al *Pedro* amb qui he trobat uns amics per sempre. I a les *Mireies* amb qui el temps compartit amb elles al DAM i les aventures passades a Colorado han fet que la meva estima cap a elles sigui de les més grans.

A tots gràcies!

Contents

List of Figures

List of Tables

0.1 Nomenclature

Atmosphere-Ocean Global Circulation Models: AOGCM

Brewer-Dobson Circulation: BDC

Brewer-Dobson Circulation Index: BDCI

Brewer-Dobson Circulation Index based in temperature: BDCI_T

Brewer-Dobson Circulation Index based in residual vertical velocity: BDCI_W*

Chlorofluorocarbon: CFC

Climate-Chemistry Model: CCM

Empirical Orthogonal Function: EOF

El Niño-Southern Oscillation: ENSO

Eliassen-Palm flux: EP-flux

Global Circulation Model: GCM

Greenhouse Gases: GHGs

North Atlantic Oscillation: NAO

Northern Annular Mode: NAM

Northern Hemisphere: NH

Ozone-Depleting substances: ODSs

Polar Stratospheric Clouds: PSC

Potential Vorticity: PV

Quasi-Biennial Oscillation: QBO

Southern Annular Mode: SAM

Southern Hemisphere: SH

Sea Level Pressure: SLP

Summer North Atlantic Oscillation: SNAO

Stratosphere-Troposphere Exchange: STE

Standard Deviation: (SD)

Transformed Eulerian Mean: TEM

Tropical Lower Stratosphere: TLS

Total Ozone Column: TOC

Ultraviolet: UV

Estudi de l'evolució de la circulació de Brewer-Dobson i de la capa d'ozó al llarg de les tres últimes dècades

Resum

El 1985 Joseph Farman i els seus col · legues de la British Antarctic Survey van publicar un article [Farman et al. 1985] que mostrava que la columna total d'ozó sobre l'Antàrtida durant la primavera havia disminuït de manera alarmant entre el 1975 i el 1984. Estudis posteriors van confirmar aquesta disminució i el terme "forat de la capa d'ozó" va esdevenir popular.

L'ocurrència d'aquest fenomen va revitalitzar l'interès de la comunitat científica per l'estudi de l'estratosfera. Des d'aleshores s'ha avançat molt en la comprensió dels processos que hi tenen lloc. Aquests avenços han estat possibles gràcies al desenvolupament de les eines de teledetecció i de sofisticats models numèrics. Aquests models ens permeten contrastar els nostres coneixements teòrics amb observacions i així determinar-ne la validesa.

La visió que es tenia en el passat de l'estratosfera com una capa isolada dels fenòmens de la troposfera ha canviat totalment. Avui és àmpliament acceptat que els processos que es desenvolupen a la troposfera afecten l'estat de l'estratosfera i a l'inrevés, els fenòmens que tenen lloc a l'estratosfera poden afectar la troposfera.

Malgrat tots els avenços fets en els últims anys, el nostre coneixement sobre els processos de l'estratosfera no és complet. Hi ha importants incerteses sobre la manera com el canvi climàtic afectarà l'estratosfera i sobre la recuperació dels nivells d'ozó estratosfèric.

En aquest context, la motivació d'aquesta tesi és contribuir a l'estudi de l'evolució de la capa d'ozó, de les temperatures de l'estratosfera i de la circulació de Brewer - Dobson (BDC) al llarg de les tres últimes dècades. Conèixer i quantificar els factors que determinen l'evolució d'aquests fenòmens i comprovar si els models numèrics actuals són capaços de reproduir l'evolució observada és de vital importància si volem pronosticar la seva evolució futura en un escenari de canvi global.

S'hi aborden aquestes preguntes:

1. En quina mesura l'oscil · lació de l'Atlàntic Nord (NAO) influeix en l'evolució de la columna total d'ozó a l'hemisferi nord durant l'hivern i l'estiu?
2. Com són de consistents les tendències observades de la BDC?
3. En quina mesura l'actual generació de models generals de circulació atmosfèrica que consideren les interaccions amb l'oceà ["Atmosphere-Ocean Global

Circulation Models" (AOGCMs)] i els actuals models químics-climàtics acoblats [coupled chemistry-climate models (CCMs)] reprodueixen les tendències en les temperatures observades a l'estratosfera?

En el **capítol 1** presentem a mode d'introducció alguns dels conceptes que seran usats en els capítols posteriors. Primerament, presentem una breu descripció del clima de l'estratosfera. A continuació introduïm les equacions que regeixen la circulació a l'estratosfera i les usem per descriure els mecanismes que forcen l'intercanvi de massa entre la troposfera i l'estratosfera. Finalment fem una breu descripció de les reaccions fotoquímiques de producció i destrucció de l'ozó estratosfèric.

En el **capítol 2** per tal d'intentar contestar la primera qüestió analitzem com l'Oscil · lació de l'Atlàntic Nord (NAO) afecta la distribució de la columna total d'ozó a l'hemisferi nord. Per dur a terme aquest estudi examinem el patró espacial de correlació entre la NAO i la columna total d'ozó, l'alçada de la tropopausa tèrmica i diferents alçades geopotencials tant a l'hivern com durant l'estiu. Aquest estudi mostra que la NAO influencia d'una manera molt important la distribució d'ozó tant a l'hivern com a l'estiu. L'estudi també mostra que aquesta influència no està limitada a l'Atlàntic Nord sinó que abasta tot l'hemisferi nord.

La majoria del models prediuen una acceleració de la BDC en els pròxims cinquanta anys com a resposta a l'increment de la concentració dels gasos d'efecte hivernacle a l'atmosfera. Si aquesta acceleració es produís, alteraria de manera molt determinant la distribució de diferents compostos químics a l'estratosfera, com per exemple l'ozó. Aquesta predicció però, es fonamenta bàsicament en simulacions numèriques i l'evidència observacional és molt pobre. La pròpia definició de la BDC fa que aquesta sigui molt difícil de determinar per mitjans observacionals.

La pretensió del **capítol 3** és contestar la segona pregunta. Per això utilitzem les tendències de temperatures a l'estratosfera com un mitjà indirecte per inferir possibles tendències en la BDC al llarg de les últimes tres dècades. Primerament utilitzem el model químic-climàtic acoblat WACCM per analitzar la idoneïtat d'inferir tendències en la BDC a partir de l'anàlisi de les tendències de temperatura. Seguidament analitzem l'estructura meridional de les tendències de les diferències entre les mitjanes zonals i les mitjanes globals de temperatura. La diferència entre la mitjana zonal i la global és en primer ordre independent de l'augment de la concentració de CO_2 i vapor d'aigua i respon primàriament a canvis en la circulació (com la BDC). L'anàlisi es realitzarà per quatre rangs d'altitud representatius de la baixa, mitja i alta estratosfera. S'analitzaran les tendències per anomalies provinents de radiosondatges, satèl · lits i reanàlisis. L'estudi demostra que tot i que l'estructura meridional de les tendències és coherent amb una acceleració de la BDC, aquestes no són estadísticament significatives en cap dels nivells estudiats. A més a més hi ha importants diferències entre diferents bases de dades. L'estudi remarca la necessitat de disposar de més i millors bases de dades de temperatura a l'estratosfera si volem validar les prediccions fetes pels models.

En el **capítol 4** tractem la tercera qüestió. Per això analitzarem la capacitat del conjunt de models AOGCMs del projecte CMIP5 i dels CCMs del projecte de validació CCMVal2 per reproduir l'evolució de les temperatures de l'estratosfera en les últimes tres dècades. Aquest capítol mostra que hi ha importants discrepàncies entre models i observacions i entre els mateixos models. En acabar, es proposen possibles causes que expliquin aquestes discrepàncies.

Finalment, en el **capítol 5** es presenta un sumari de la tesi i una prospectiva que suggereix possibles futures línies de recerca.

La present tesi es basa en aquestes publicacions:

- Ossó, A., Y. Sola, J. Bech, and J. Lorente, 2011. Evidence for the influence of the NAO on total ozone column at northern low- and mid-latitudes during winter and summer seasons. *J. Geophys. Res., 116*.
- Ossó, A., Y. Sola, K. Rosenlof, B. Hassler, J. Bech, J. Lorente, 2014. How robust are trends in the Brewer-Dobson Circulation derived from observed stratospheric temperatures? (Submitted to *Journal of Climate* 04-17-2014).
- Thompson, D.W.J., D.J. Seidel, W.J. Randel, C. Zou, A.H. Butler, C. Mears, A.Ossó, C. Long, R. Lin, 2012. The mystery of recent stratospheric temperature trends. *Nature 491*, 692–697.
- Bech J., Y. Sola, A. Ossó, J. Lorente, 2014. Analysis of 14 years of broadband ground based solar UV index observations in Barcelona. *Int. J. Climatol.*
- Sola, Y., J. Lorente, A. Ossó, 2012. Analyzing UV-B narrowband solar irradiance: Comparison with erythemal and vitamin D production irradiances. *Journal of Photochem. Photobiol. B 117*, 90-96.

Preface

In 1985 Joseph Farman and his colleagues of the British Antarctic Survey published a paper [Farman et al. 1985] showing that the total ozone content of the atmosphere during the Antarctic spring had decreased dramatically between 1975 and 1984. Subsequent studies confirmed this decrease and the term *Antarctic ozone hole* became popular. The occurrence of this phenomenon revitalized the interest of the climate community in the stratosphere. Since then many remarkable advances have been made in our understanding of stratospheric processes. These advances have been possible by the advent of remote sensing measurements of the atmosphere together with the sophistication of the atmospheric simulations. Nowadays it is known that stratospheric climate is determined by a complex coupling of dynamic, radiative and chemical processes.The view of the stratosphere as an isolated layer have changed completely and today it is widely accepted that both the tropospheric processes affect the stratospheric climate, and the other way around, the stratospheric processes affect the climate in the troposphere. Despite all the progresses made, our knowledge is far to be complete. There are still large uncertainties about how climate change is affecting the stratosphere and to what extent it will influence the stratospheric ozone recovery. Moreover recent studies [e.g., Thompson et al. 2012] evidenced that there are important discrepancies among observational data sets and between observations and numerical simulations of recent stratospheric temperature trends.

Overview

The aim of this thesis is to contribute on the understanding of the past evolution of the ozone layer and the Brewer-Dobson circulation.

With this objective the following question will be addressed:

1. To what extent are the long-term trends of total ozone affected by the North Atlantic Oscillation (NAO) during winter and summer seasons?
2. How robust are the observed trends in the Brewer-Dobson Circulation (BDC)?
3. Is the current generation of coupled atmosphere-ocean global circulation models (AOGCMs) and coupled climate-chemistry models (CCMs) reproducing the observed stratospheric temperature trends over the last three decades?

Chapter 1 presents an introduction to the basic concepts that are transverse to chapter 2 and chapter 3. First, a description of the mean state of the stratosphere is provided. Then, an introducing of the basic equations used to describe the stratosphere followed by a description of the mechanisms involve in the troposphere-stratosphere exchange processes is presented. Finally a description of the basic processes involved in the production, transport and destruction of ozone are reviewed.

Chapter 2 deals with question 1 and is built on the bases of the article Ossó et al. [2012]. In this chapter the influence of the North Atlantic Oscillation on the total ozone content of the atmosphere is examined during winter and summer seasons.

Chapter 3 deals with questions 2 and is built on the bases of the article Ossó et al. [2014]. First, a brief review of our current understanding of the stratospheric temperature trends is provided. Then, residual vertical velocity trends and temperature trends from the CCM WACCM output is examined. Finally, stratospheric temperatures are used to infer trends in the BDC during the last 3 decades.

Chapter 4 presents a brief discussion on the performance of the current AOGCMs and CCMs on reproducing the stratospheric temperature trends derived from observation.

Finally a summary and outlook of the thesis is provided in **chapter 5.**

This PhD study is primary built on the following peer-reviewed publications:

- Ossó, A., Y. Sola, J. Bech, and J. Lorente, 2011: Evidence for the influence of the NAO on total ozone column at northern low- and mid-latitudes during winter and summer seasons. *J. Geophys. Res., 116, D24.*
- Ossó, A., Y. Sola, K. Rosenlof, B. Hassler, J. Bech, J. Lorente, 2014: How robust are trends in the Brewer-Dobson Circulation derived from observed

stratospheric temperatures? (Submitted to *Journal of Climate* 04-17-2014).

- Thompson, D.W.J., D.J. Seidel, W.J. Randel, C. Zou, A.H. Butler, C. Mears, A.Ossó, C. Long, R. Lin, 2012: The mystery of recent stratospheric temperature trends. *Nature 491*, 692–697.

Other contributions made during this thesis:

- Bech J., Y. Sola, A. Ossó, J. Lorente, 2014: Analysis of 14 years of broadband ground based solar UV index observations in Barcelona. *Int. J. Climatol.*
- Sola, Y., J. Lorente, A. Ossó, 2012: Analyzing UV-B narrowband solar irradiance: Comparison with erythemal and vitamin D production irradiances. *Journal of Photochem.Photobiol. B 117*, 90-96.

1 Introduction

Overview

The aim of this chapter is to describe the basic dynamical mechanisms responsible for the troposphere-stratosphere connections. This introductory chapter first reviews the observed mean state of the stratosphere in section 1.1. Second, in section 1.2, the Transformed Eulerian Mean formulism is described. Third, the dynamical mechanisms involved in the troposphere-stratosphere mass exchange, with especial emphasis in the mechanism driving the Brewer-Dobson Circulation (BDC), are explained in section 1.3. In section 1.4, the basic processes responsible for the observed stratospheric ozone distribution are reviewed. At the end, section 1.5 summarizes the primary questions addressed in this thesis.

1.1 The observed mean state of the stratosphere

The troposphere is the region that has attracted most scientific attention since it contains approximately 80% of the mass of the total atmosphere and 99% of its water vapor. Indeed, most of the weather phenomena take place in the troposphere affecting human life. Traditionally, the stratosphere has been viewed as a passive stratified layer with no influence on tropospheric processes. However, this view has changed radically during the last decades. Nowadays, it is broadly accepted that both the troposphere affects the stratosphere state, and the other way around, the stratosphere influences tropospheric climate [e.g., Baldwin and Dunkerton 1999, 2001].

Mean temperatures in the stratosphere are at first order determined by a balance between infrared radiative cooling and radiative heating due to the absorption of solar ultraviolet radiation (UV) by ozone [Andrews et al. 1987]. Indeed, it is the presence of large concentrations of ozone in the stratosphere that makes temperatures increase upward from the tropopause to a maximum in the stratopause.

Figure 1.1 shows the ERA-40 zonal-mean temperature and wind climatologies as a function of height and latitude for December-February and June-August. ERA-40 refers to the forty years reanalysis performed by the European Centre for Medium-Range Weather Forecasts (ECMWF). Available online at www.ecmwf.int/research/era/ERA-40_Atlas.

In the lower stratosphere, the temperature distribution is characterized by a minimum at tropical latitudes and over the pole cap of the winter hemisphere. Higher

up, the temperature increases continuously from the winter pole to the summer pole in qualitative agreement with radiative equilibrium conditions. Nevertheless, the observed meridional temperature gradient between poles is weaker than expected from radiative equilibrium calculations. This is a direct consequence of the adiabatic expansion heating and cooling due to vertical movements associated with the stratospheric overturning meridional circulation. This overturning circulation, called the Brewer-Dobson Circulation (BDC) [Brewer 1949; Dobson 1956], drives stratospheric temperatures away from their radiative equilibrium, some tens of degrees below in the tropical tropopause and some tens of degrees above in the BDC extratropical downwelling regions.

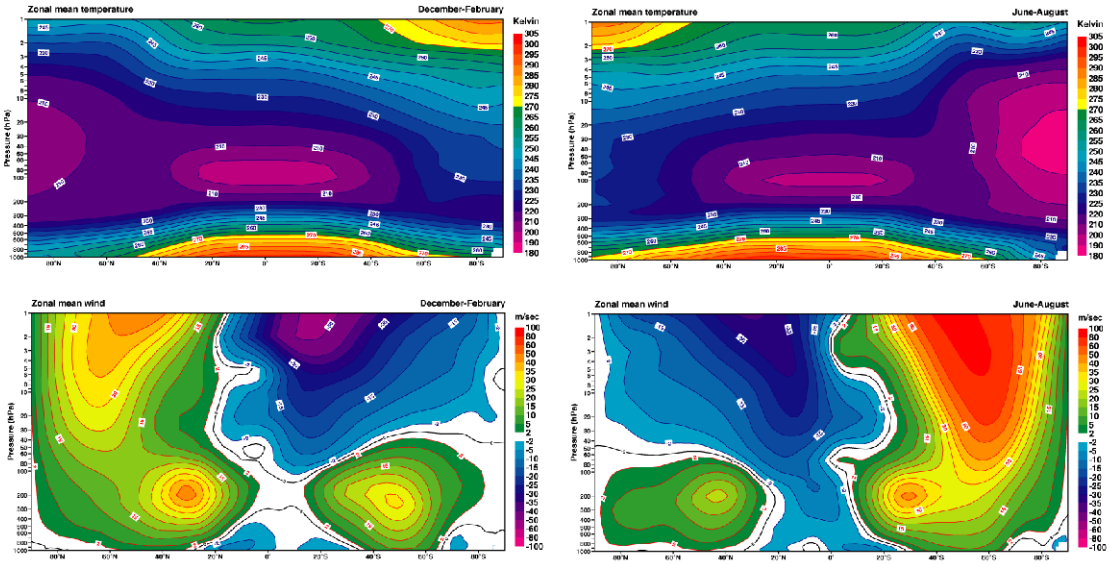

Figure 1.1: Upper panels show the climatological mean (1958-2001) zonal-mean temperatures for December-February (left panel) and June-August (right panel). Bottom panel show the climatological mean zonal-mean wind for the same months. Figure from www.ecmwf.int/research/era/ ERA-40_Atlas.

The main characteristics of the zonal-mean zonal wind in the stratosphere could be derived through the thermal wind relationship from the observed temperature distribution. This is possible because the stratosphere is in quite good approximation with geostrophic and hydrostatic balance. The main features are a westerly jet in the winter hemisphere with a maximum at stratopause levels and an easterly jet in the summer hemisphere, both in qualitatively agreement with the observed temperature structure (Fig. 1.1). The westerly jet maximum is located around 60^{o} - 65^{o} and it is called the polar night jet [Holton 1992]. It delimits a region called the stratospheric polar vortex, a highly isolated (especially in the SH) stratospheric mass of air over the Pole Cap that is characterized by a high cyclonic vorticity and extremely low temperatures.

1.2 Eulerian and Transformed Eulerian mean

Much of the atmospheric variability is captured by the zonal-mean fields. Therefore, it is useful to split the atmospheric field variables into a zonally-averaged term and an eddy term, which describes the longitudinal departures of the total field from its zonal-mean. Thus, any field variable A could be expanded as A=$\bar{\text{A}}$+A´, where

$$\overline{A} = \frac{1}{2\pi a cos\phi_0} \int_0^{2\pi a cos\phi_0} A(x, y, z, t)dx \tag{1.1}$$

is the zonally-averaged field and $A' = A - \bar{A}$ represents the eddy component of the total field A. The sort of average described by eq. 1.1 is called *Eulerian Mean*.

This thesis mainly deals with dynamic processes that take place in the extratropics. Over this region, large-scale horizontal motions as well as large-scale waves which interact with the mean flow are nearly in hydrostatic and geostrophic balance. In such conditions, the *quasi-geostrophic* approximation of the primitive equations constitutes a good framework for our purposes. The main simplifications of this approximation are considering the horizontal advection of momentum and temperature only occurring due to the geostrophic winds, neglecting the vertical advection of momentum and approximating the static stability parameter by a basic-state static stability parameter, which is a function of height only [e.g., Holton and Hakim 2012].

Applying the Eulerian-Mean average to the set of quasi-geostrophic equations on the midlatitude β plane approximation[1] we obtain:

$$\frac{\partial \overline{u}}{\partial t} = f_0 \overline{v}_a - \frac{\partial(\overline{u'v'})}{\partial y} + \overline{X} \tag{1.2}$$

$$\frac{\partial \bar{T}}{\partial t} = -N^2 H R^{-1} \bar{w} - \frac{\partial(\overline{v'T'})}{\partial y} + \frac{\bar{J}}{c_p} \tag{1.3}$$

$$\frac{\partial \bar{v_a}}{\partial y} + \rho_0^{-1} \frac{\partial(\rho_0 \bar{w_a})}{\partial z} = 0 \tag{1.4}$$

[1]This approximation consists to expand the latitudinal dependence of the Coriolis parameter in a Taylor series about a reference latitude $\emptyset_0$:$f = f_0 + \beta y$where $\beta = (\frac{df}{dy})_{\phi_0}$

$$f_0 \frac{\partial \bar{u}}{\partial z} + RH^{-1} \frac{\partial \bar{T}}{\partial y} = 0 \tag{1.5}$$

where $z \equiv -H \ln(\frac{p}{p_s})$is the vertical log-pressure coordinate with H~7km,$\rho_0 \equiv \rho_s \exp(\frac{-z}{H})$ is the basic density state, $\bar{X}$designates the zonal-drag due to small-scale eddies,$\bar{J}$ is the heating rate due to diabatic processes and the subscript "a" refers to ageostrophic terms.

Note that the zonal-mean y-component of the momentum equation vanishes because

$$\overline{v}_g \equiv \frac{1}{2\pi a cos\phi_0} \int_0^{2\pi a cos\phi_0} \frac{1}{f_0} \frac{\partial \Phi}{\partial x} dx = 0 \tag{1.6}$$

by periodicity. Here Φ represents the geopotential height.

Equations 1.2 to 1.5 form a closed set for the mean-flow variables $(\bar{u}, \bar{T}, \bar{v_a}, \overline{w}_a)$, given $\overline{X}$,$\overline{J}$and suitable boundary conditions. Equation 1.2 is the *zonal-mean zonal momentum equation* on a β plane and states that the acceleration of the quasi-geostrophic zonal-mean zonal flow (left-hand side (lhs) term) equals to the Coriolis force acting on the ageostrophic meridional component of the flow (first term on the right-hand side [rhs]) plus the meridional convergence of zonal eddy momentum flux (second term on the rhs) plus the term that accounts for the zonally average zonal drag force due to small-scale eddies. Equation 1.3 is the *zonal-mean thermodynamic equation* and can be interpreted as follows: the zonal-mean temperature tendency (lhs term) is product of the adiabatic heating/cooling due to vertical motion (first term on the rhs) plus the meridional convergence of eddy heat fluxes (second term on the rhs) plus the diabatic heating (third term on the rhs). Equation 1.4 is the *mass continuity equation* for the meridional plane and finally, equation. 1.5 is the *thermal wind equation* that states that the vertical shear of the zonal-mean quasi-geostrophic zonal wind is proportional to the latitudinal gradient of temperature. A similar set of equations can be deduced for the disturbance terms [e.g., Andrews et al. 1987].

Andrews and McIntyre [1976] formulated an alternative version of this set of equations, called *The Transformed Eulerian Mean* equations (TEM). This approach uses the fact that in equation 1.3 there is a strong cancellation between the eddy heat flux convergence and the adiabatic cooling, while the diabatic term is a small residual. Indeed, are precisely the diabatic processes associated with this residual term which induced the "*residual meridional circulation*".

The residual meridional circulation $(\overline{v}*, \overline{w}*)$ is defined by:

$$\overline{w}^* \equiv \overline{w}_a + RH^{-1}\frac{\partial(\overline{v'T'}/N^2)}{\partial y} \tag{1.7}$$

$$\overline{v}^* \equiv \overline{v}_a - \rho_0^{-1}RH^{-1}\frac{\partial(\rho_0\overline{v'T'}/N^2)}{\partial z} \tag{1.8}$$

Substituting the equations 1.7 and 1.8 into the equations 1.2 to 1.5 we obtain the TEM equations:

$$\frac{\partial\overline{u}}{\partial t} - f_0\overline{v}^* = \rho_0^{-1}\nabla\cdot\overrightarrow{F} + \overline{X} \equiv \overline{G} \tag{1.9}$$

$$\frac{\partial\overline{T}}{\partial t} + N^2HR^{-1}w^* = \frac{\overline{J}}{c_p} \tag{1.10}$$

$$\frac{\partial\overline{v}^*}{\partial y} + \rho_0^{-1}\frac{\partial(\rho_0\overline{w}^*)}{\partial z} = 0 \tag{1.11}$$

$$f_0\frac{\partial\overline{u}}{\partial z} + RH^{-1}\frac{\partial\overline{T}}{\partial y} = 0 \tag{1.12}$$

where $\overrightarrow{F} \equiv F_y\hat{j} + F_z\hat{k}$, *the Eliassen-Palm flux* (EP flux), is a vector in the meridional plane, which for large scale quasi-geostrophic eddies has the components: $F_y = -\rho_0\overline{u'v'}$ and $F_z = \frac{\rho_0 f_0 R\overline{v'T'}}{N^2H}$. $\overline{G}$denotes the total zonal force due to both small- and large-scale eddies. Note that the divergence of the EP flux represents the eddy forcing of both the eddy heat and momentum fluxes. Thus, a map of the EP flux divergence provides a clear diagnosis of the zonal force exerted by the large-scale quasi-geostrophic eddies. These equations reconciled the different pictures of the stratospheric meridional circulation obtained from the "conventional" Eulerian-mean meridional circulation and from analysis of the mean Lagrangian motion of air parcels in the meridional plane [Butchart 2014]. They provide a useful diagnosis tool of the eddy forcing to the mean flow and have been successfully applied in the study of the tracer transport in the stratosphere.

1.3 Stratosphere-Troposphere exchange

Two mechanisms are responsible for the mass transport between the troposphere and the stratosphere: (1) The residual mean meridional circulation -the BDC- that slowly transfers mass upward across the tropopause in the tropics and poleward and downward in the extratropics and (2) rapid quasi-isentropic mass transport and mixing across the tropopause that occurs by wave-breaking in the lowermost stratosphere (Fig. 1.2).

1.3.1 The BDC, what it is

The BDC [Brewer 1949; Dobson 1956] is a slow, hemispheric scale, meridional overturning circulation in the stratosphere, with air moving upwards in the tropics and polewards and downwards in the extratropics. The BDC consists of a "shallow" branch, a strong circulation driven by synoptic and planetary waves breaking in the lower stratosphere, juxtaposed on a "deep" branch, a weaker circulation driven by planetary waves breaking in the mid and upper stratosphere [Plumb 2002; Birner and Bönish 2011]. The vertical motion drives stratospheric temperatures away from their radiative equilibrium, some tens of degrees below in the tropical tropopause and some tens of degrees above in the downwelling regions. Variations in the strength of the BDC are seasonal, with stronger cells in the winter hemisphere [Rosenlof 1995]. Moreover, due to the differences in wave-activity between the two hemispheres, the annual average BDC is stronger in the Northern Hemisphere (NH) than it is in the Southern Hemisphere (SH).

The BDC is a prominent dynamical phenomenon in the stratosphere and affects physical and chemical processes. Most significantly, it meridionally and vertically transports chemical trace gases. These include ozone, which absorbs nearly all of the biologically harmful highly-energetic ultraviolet radiation and alters the radiative balance in the stratosphere. The BDC moves ozone-rich air from the tropics, where ozone is produced, to mid and high latitudes and it is responsible for the high values of ozone observed at mid latitudes during the winter-spring season. The BDC also almost completely determines the residence time in the atmosphere of the chlorofluorocarbons (CFCs) that act as catalysts in the photochemical reactions responsible for ozone loss. Consequently, the BDC influences stratospheric ozone recovery [Solomon 1999; Antarctic Ozone Bulletin 2012 and references therein].

1.3.2 The driving mechanism of the BDC

The physical mechanism driving the BDC is the extratropical pump. This mechanism is based on the recognition of the non-local effects in the atmosphere. The pioneering works of Eliassen [1951] and Dickinson [1968] showed that the extratropical stratosphere acts upon the tropical stratosphere like a global-scale suction pump,

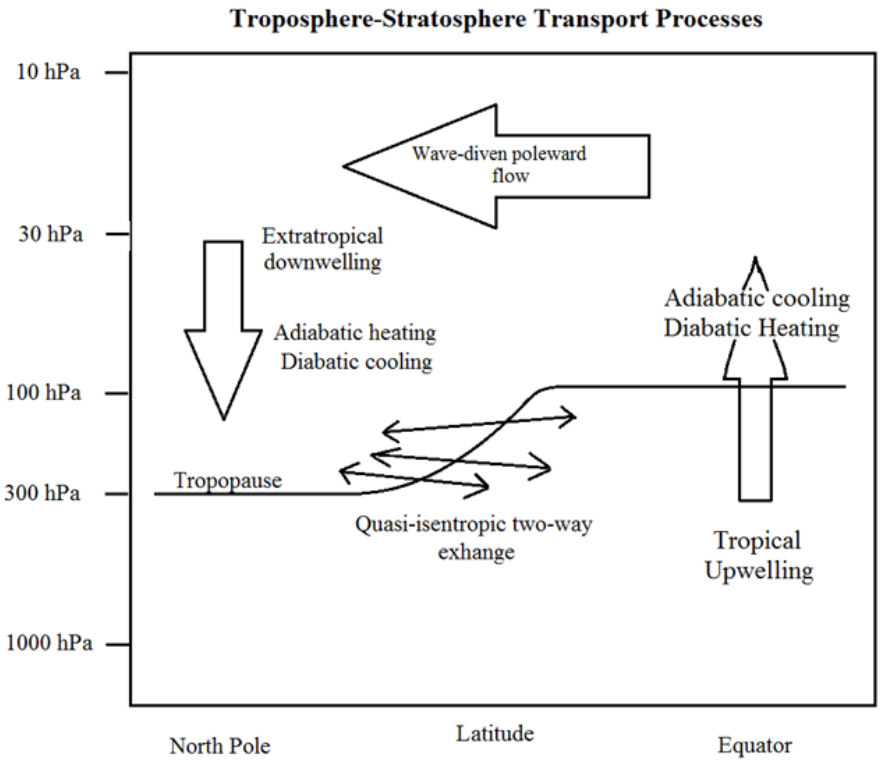

Figure 1.2: Troposphere-stratosphere dynamical transport processes. Adapted from Holton et al. [1995].

where the pumping is due to the easterly drag force exerted mainly by planetary Rossby-wave dissipation into the stratosphere. This easterly force acts together with the Coriolis torque and results in a poleward mass flow (Fig. 1.3). Mass continuity requires that the poleward flow be accompanied by upwelling in the tropics and downwelling at higher latitudes [e.g., Holton et al. 1995].

Haynes et al. [1991] used the TEM equations presented above to develop a useful approach for quantifying the pumping mechanism that drives the BDC. They used the fact that for the long time-scales involved in the BDC, the acceleration term in equation 1.9 becomes quite small. Therefore, the steady state solution of equation 1.9 $\left(\frac{\partial \overline{u}}{\partial t} \cong 0\right)$constitutes a good approximation. Rosenlof and Holton [1993] showed that the seasonal-mean is a long enough time-scale for the steady state assumption to be valid. Thus, equation 1.9 is reduced to a simple balance between the zonal

drag force \overline{G} and the Coriolis force $f_0\overline{v}^*$:

$$-f_0\overline{v}^* = \overline{G} \tag{1.13}$$

the equation 1.13 with the mass conservation equation 1.11 and requiring that $\rho_0\overline{w}^* \to 0$ as $z \to \infty$, it follows that

$$\rho_0\overline{w}^* = -\frac{\partial}{\partial y}\left(\frac{1}{f_0}\int_z^\infty \rho_0\overline{G}dz\right) \tag{1.14}$$

This equation is the expression of the *downward control principal* derived by Haynes et al. [1991]. It states that the steady extratropical upward mass flow is determined only by the zonal wave-drag force above that level.

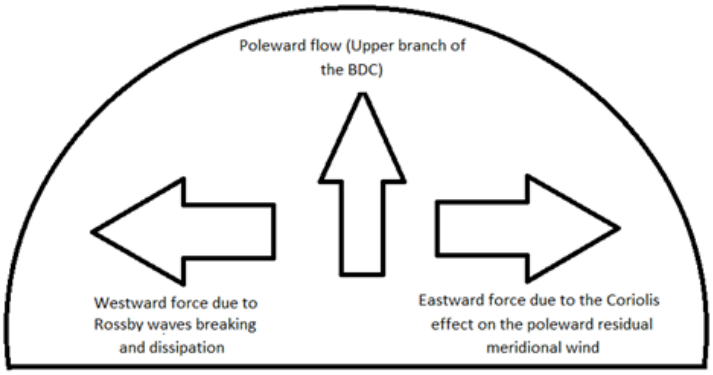

Figure 1.3: Balance of the forces responsible for the BDC

If we substitute the equation 1.14 into the equation 1.10, and we approximate the diabatic heating term $\frac{\overline{J}}{c_p}$in terms of a Newtonian relaxation proportional to the departure of temperature to its radiative equilibrium value $-\alpha_r\left(\overline{T} - \overline{T}_r\left(y,z,t\right)\right)$[e.g., Holton and Hakim 2012] we can found an expression that explicitly shows the relation between the zonally-average departure of temperature from its radiative equilibrium value in response to a zonal drag force distribution. In the case where

$\frac{\partial \overline{T}}{\partial t} = 0$:

$$\left(\overline{T} - \overline{T}_r\right) = \frac{N^2 H}{\alpha_r \rho_0 R} \frac{\partial}{\partial y} \left(\frac{1}{f_0} \int_z^\infty \rho_0 \overline{G} dz \right) \tag{1.15}$$

1.3.3 Rossby-Wave driving of the BDC

It was already noted that waves traveling upward from the troposphere to the stratosphere are responsible for the pumping mechanism that drives the BDC. The *Rossby-waves*, also called *planetary-waves*, are the type of atmospheric waves that contribute most to the pumping, especially in the extratropical NH [e.g., Shepherd 2003; Plumb 2010].

Rossby-waves are large-scale longitudinal undulations in the flow along a latitude circle that conserve their potential vorticity (PV). The potential vorticity is defined as

$$PV = \frac{1}{\rho} (f + \xi) \frac{\partial \theta}{\partial z} \tag{1.16}$$

where ξ is the vertical component of the relative vorticity

$$\xi = \frac{\partial v}{\partial x} - \frac{\partial u}{\partial y} \tag{1.17}$$

The meridional gradients of PV proportionate the restoring mechanism that drives the Rossby-waves. Rossby-wave propagation can be qualitatively understood by imagine a chain of fluid particles in a latitude circle (Fig. 1.4). In the simple case of a barotropic atmosphere $\left(\frac{\partial \theta}{\partial z} = const\right)$, the conservation of PV is reduced to the conservation of the absolute vorticity $(f + \xi)$. Then, if one fluid particle is displaced north, e.g., by the effect of topography, the planetary vorticity f of the fluid particle will increase and then must decrease in order to conserve the absolute vorticity. The induced relative circulation pushes the particle on the west hand side poleward and the one on the east hand side equatorward. Thus, the Rossby-wave vorticity pattern always propagates westward relative to the background zonal flow.

In the more realistic case where $\frac{\partial \theta}{\partial z} \neq const$, the conservation of PV is not equivalent to the conservation of absolute vorticity. Figure 1.5 shows the case of the flow crossing an ideal North-South infinite mountain range. We can suppose that the flow is adiabatic and initially with $\xi = 0$ upstream of the mountain barrier. Because

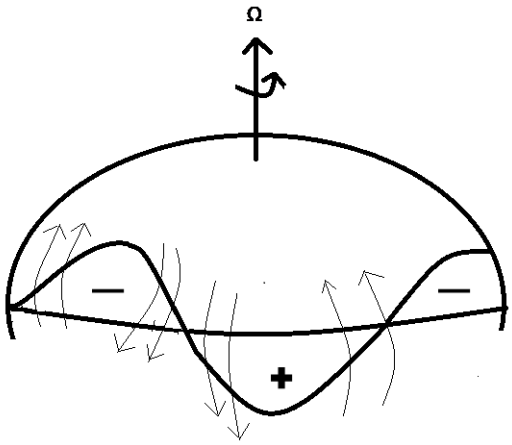

Figure 1.4: Perturbation vorticity field and induced meridional velocity of a Rossby-wave oscillating about its equilibrium latitude. Adapted from Holton and Hakim [2012].

the flow is adiabatic, it must be confined between the adiabatic surfaces $\theta_0$and $\theta_0 + \delta\theta$. \theta_{0}tends to follow the ground contour and \theta_{0}+\delta\theta is slightly deflected vertically. Then, the column of air will stretch upstream and downstream of the mountain barrier and in order to conserve potential vorticity, ξ must be positive. This cyclonic vorticity tends to deflect the column of air poleward. Flowing over the mountain barrier, the column of air must squeeze and again in order to conserve potential vorticity must acquire anticyclonic relative vorticity.

This anticylonic vorticity deflects the air column equatorward. When the air column has passed the mountain range it will be south of its original latitude so that the planetary vorticity f will be smaller and the relative vorticity must be positive. As a result of this process, a Rossby wave will be formed downstream of the mountain barrier.

1.3.4 Vertically propagating Rossby waves

Charney and Drazin [1961] deduced the conditions in which stationary planetary waves, which dominate the spectrum of Rossby waves in the stratosphere, can propagate upward into the stratosphere. They demonstrated that their vertical modes can propagate upward only with a westerly background flow weaker than a critical value, the *Rossby critical velocity* that depends on the horizontal scale of the waves.

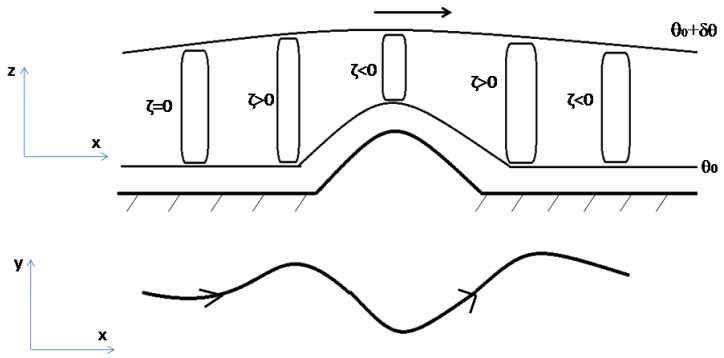

Figure 1.5: Schematic view of the generation of a Rossby-wave by a westerly flow over a topographic barrier. Adapted from Holton and Hakim [2012].

It is easily demonstrated that the zonal phase speed relative to the mean wind is

$$c - \overline{u} = \frac{-\beta}{K^2} \tag{1.18}$$

where $c = {}^{-\beta}/_{k^2}$is the westward phase speed of the wave, $\beta \equiv {}^{df}/_{dy}$is the planetary vorticity gradient, k the zonal wave number, $\overline{u}$ is the zonal velocity of the mean flow, and $K^2 = k^2 + l^2$is the total horizontal wave number squared.

From eq. 1.18 it is straightforward to see that a Rossby wave can only be stationary (i.e.: $c - \overline{u} = 0$) with a westerly mean zonal flow. In the summer hemisphere the thermal wind is directed eastward and hence, the vertical propagation of Rossby waves is inhibited. In the winter hemisphere the vertical propagation of stationary Rossby waves is possible only if the westerly flow is not too strong. Note that the stronger the zonal mean flow, the longer the waves will have to be to still be stationary. It can be demonstrated that

$$0 < \overline{u} < \beta \left[\left(k^2 + l^2 \right) + \frac{f_0^2}{4N^2H^2} \right]^{-1} \equiv U_c \tag{1.19}$$

to allow vertical propagation. Uc is the so-called Rossby critical velocity.

The westerly jet then acts like a “low pass filter” because large Rossby waves (wavenumbers 1, 2, 3) can propagate still with a strong westerly jet.

1.3.5 Rossby Wavebreaking

Throughout the previous sections, we have stated that Rossby-wave breaking impels a westward force in the zonal-mean zonal flow. Wavebreaking refers to a rapid irreversible deformation of materials contours, i.e., PV contours. Since PV is conserved in Rossby waves, isolines of potential vorticity on isentropic surfaces can be viewed approximately as material contours. The rapid deformation of these contours can be used as a fingerprint of wave breaking. Rossby waves break when their amplitudes have grown large enough that the nonlinear effects become important in the dynamical equations. As we have seen in eq. 1.17, the wave amplitude is a function of height, therefore when a wave travels upward its amplitude grows exponentially (see eq. 1.20), becomes unstable and breaks depositing its momentum.

The simplest case of wavebreaking occurs when the value of the phase speed of the wave equals the value of the background flow $\overline{u} - c_x = 0$. The area where this condition holds is called a *critical surface*.

1.3.6 Quasi-isentropic transport

The "pumping" mechanism explained above is responsible for most of the stratosphere-troposphere exchange (STE). However, a small part of the STE is due to horizontal transport along isentropic surfaces that cross the tropopause. The tropopause is the region that separates the stratosphere from the troposphere and is characterized by an increase in the static stability moving from the troposphere to the stratosphere. The tropopause behaves like a quasi-material surface with a potential temperature $\theta = 380K$. It is higher in the tropics and tilts downward and poleward, intersecting across isentropic surfaces (Fig. 1.3). The tropopause acts like a "tap" blocking STE. Nevertheless, meridional horizontal transportation along isentropes at the tropopause level can occur in some situations where the tropopause is strongly distorted by growing upper tropospheric cyclones. Such distortions are characterized by latitudinal excursions of anomalously high potential vorticity air tongues that extent equatorward from midlatitudes and are more likely to develop over the tropospheric extratropical jet.

1.4 The Ozone Layer

Most of the atmospheric ozone (O3) resides in the stratosphere between 15 and 30 km with a maximum mixing ratio near 35 km. This broad layer receives the name of *ozone layer*. Ozone, by its absorption of radiation of wavelengths less than 300 nm, is responsible for the upward increase of temperature from the tropopause to the stratopause, thus being responsible of the existence of the stratosphere itself.

Moreover, the ozone layer acts like a shield by absorbing most of the harmful ultraviolet radiation, therefore, ozone is essential for protecting the biological life on our planet.

The ozone distribution within the stratosphere largely varies both seasonally and geographically. Fig. 1.7 shows a 10-year average of total ozone column map based on the Total Ozone Mapping Spectrometer (TOMS) and Ozone Monitoring Instrument (OMI) data [Mc Peters et al. 1998, 2008]. There is a meridional increase of ozone from the tropics to high latitudes in both hemispheres, but with larger values in the extratropical NH. Mainly, the ozone varies latitudinally, although important longitudinal variations are also apparent especially in the NH where zonal maximums are found over the east coasts of Asia and North America.

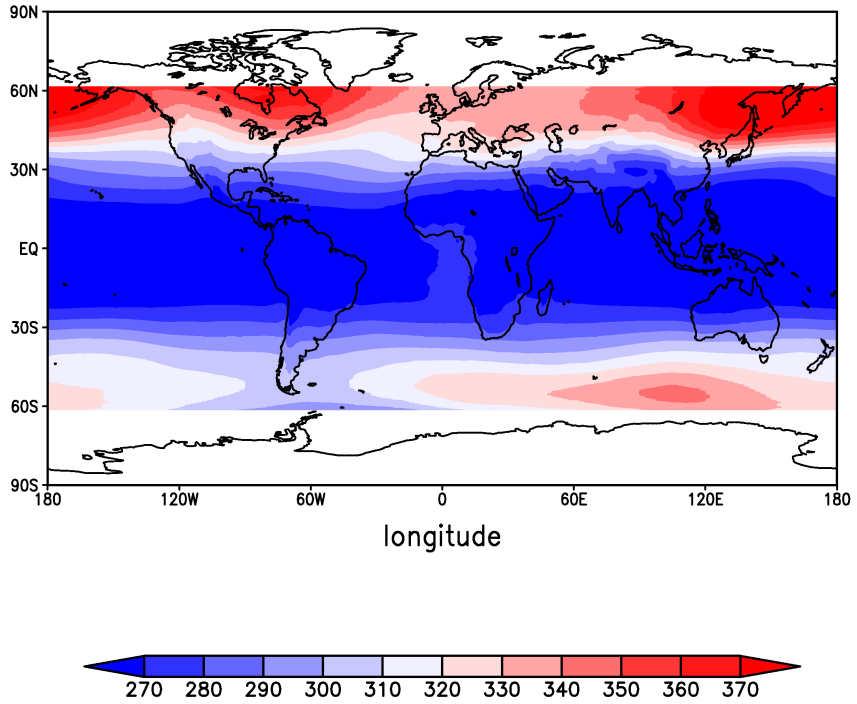

Figure 1.6: Global distribution of total ozone column (Dobson Units) based on 10 years (1997-2007) of observations with TOMS and OMI satellite instruments. Note that poleward of 60° latitude, satellite ozone retrievals lack continuous measurements due to polar night.

The ozone distribution depends on the balance between chemical production / destruction and dynamical induced transportation. Most of the ozone is photochemically produced at high altitudes over the tropics, where the ultraviolet (UV) radiation, necessary to break the oxygen molecules to form ozone, is stronger. From the tropics the ozone is slowly transported poleward and downward by the BDC. Poleward of 30° the air starts to sink and ozone is deposited in the lower stratosphere, where it can reside for long time because the UV radiation necessary for its

photodissociation is very weak.

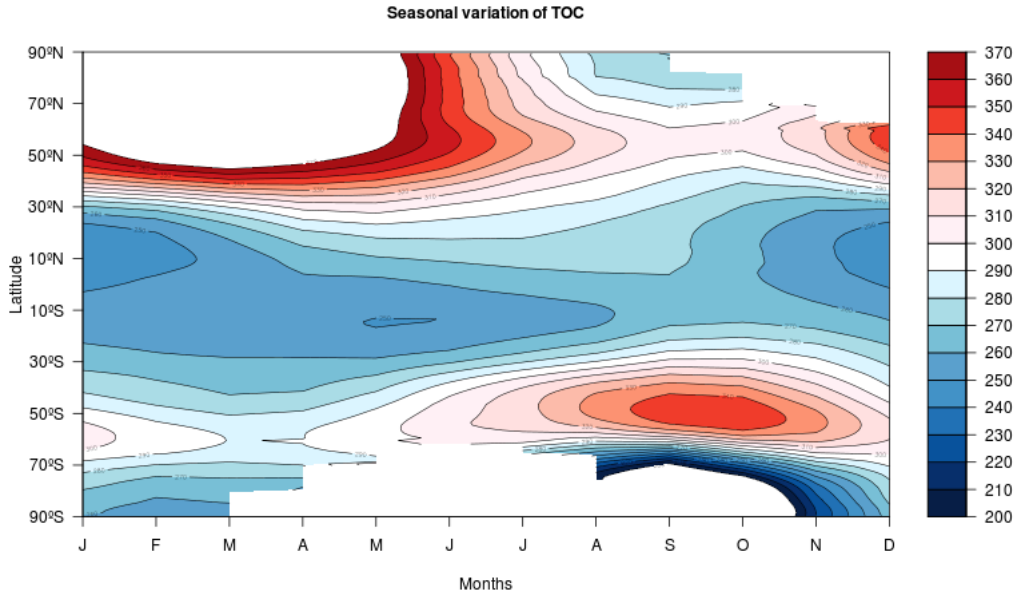

Figure 1.7: Time-latitude section showing the seasonal evolution of total ozone (Dobson Units) based on TOMS/OMI data.

The BDC largely explains the observed meridional and seasonal distribution of ozone in figures 1.7 and 1.8. The longitudinal maxima correspond with the main positions of the troughs of the stationary wave pattern of the upper stratosphere. Most of the ozone molecules in a column are confined in the lower stratosphere and its total amount is associated with variations of the tropopause height in response to synoptic and planetary scale tropospheric upper level disturbances (See Chapter 2, section 2.1.4).

1.4.1 The chemistry of the stratospheric ozone

The ozone is produced and destroyed by photochemical reactions between highly energetic UV photons and some gas species present in the stratosphere, especially the oxygen. Chapman [1930] formulated the first set of chemical reactions in an attempt to explain the existence of an ozone vertical structure.

Ozone formation starts when a highly energetic photon coming from the sun with wavelength shorter than 242 nm dissociates an oxygen molecule (O_2) resulting in two atoms of monoatomic oxygen:

$$O_2 + \hbar\nu \rightarrow 2O \tag{1.20}$$

where $\hbar$is the Planck's constant and ν is the frequency of the photon (ν =c/λ, where c is the speed of light and λ is the wavelength). Then given the high reactivity of atomic oxygen, these atoms quickly react between each other to form ozone:

$$O + O_2 + M \rightarrow O_3 + M \tag{1.21}$$

where M is another molecule probably N_2 or O_2 necessary to conserve the energy balance of the reaction.

The ozone effectively absorbs the highly energetic UV radiation. The result of this absorption is the dissociation of ozone in molecular and atomic oxygen for $\lambda < 325nm$:

$$O_3 + \hbar\lambda \rightarrow O + O_2 \tag{1.22}$$

Ozone is also destroyed through the recombination with atomic oxygen:

$$O_3 + O \rightarrow 2O_2 \tag{1.23}$$

The set of equations presented above represent the *Chapman Cycle*. Although they constitute the core of the stratospheric ozone chemistry, they are not able to explain the values of ozone observed in the stratosphere, which are quite lower than predicted by these equations alone. This is due to the action of other species such as chlorine, bromine, nitrogen and hydrogen, which act as catalysts on reactions that destroy ozone:

$$\begin{aligned} X + O_3 &\rightarrow XO + O_2 \\ XO + O &\rightarrow X + O_2 \end{aligned} \tag{1.24}$$

where X represents the catalyst (molecules containing Cl, N, Br or H). The final balance of this reaction is the destruction of one ozone molecule and the formation of two molecules of oxygen. During the process the catalyst remains unaltered, thus being able to act as catalyst again in another reaction. The source of these species is both natural and anthropogenic, for example, methane and water vapor are the principal source of HOx and NOx. ClOx comes from the oceans, biomass burning and especially from the chlorofluorocarbons (CFCs). The widespread use of CFCs in many industrial processes before their international regulation in the Montreal Protocol in 1987 has led to release enormous quantities of such compounds into the atmosphere. CFCs are highly stable in the troposphere and weakly soluble with

water, hence, they have time to be transported to the stratosphere before being removed for example by rain. Once they reach the stratosphere they are photolyzed by the sunlight and they release the chlorine atoms. These atoms then destroy ozone through the reactions 1.25 and 1.26.

$$Cl + O_3 \rightarrow ClO + O_2 \tag{1.25}$$

$$ClO + O \rightarrow Cl + O_2 \tag{1.26}$$

The result of these reactions is the reaction (1.23) plus the chlorine atom.

The photochemical processes responsible for the ozone hole are more complicated because they involve heterogeneous reactions that take place over solid and liquid surfaces inside the polar vortex. One particular case of these surfaces is the Polar Stratospheric Clouds (PSC) formed under the extremely low temperatures prevailing during winter inside the vortex. Although these clouds have been observed on both poles, they are more common in the Antarctic where the temperature is quite lower than in the Arctic.

2 Influence of the North Atlantic Oscillation on the NH total ozone column distribution

2.1 Overview

The motivation of this chapter is to examine the impact of atmospheric dynamical processes on the long-term ozone trends. In this context, we present a study which main objective is examining the correlation between one of the most prominent climatic modes of the Northern Hemisphere, the North Atlantic Oscillation (NAO), and the total ozone column (TOC), focusing our attention on the summer season when the summer NAO (SNAO) is revealed as an important source of TOC variability. Additionally, we examine the zonal asymmetry in the NAO influence on TOC, analyzing the dynamical processes that lead to this longitude-dependent pattern and their influence on the observed regional TOC trends.

This chapter is built on our paper published in the Journal of Geophysical Research Atmospheres [Ossó et al. 2012].

2.2 Introduction

Atmospheric ozone plays a crucial role in the protection of living organisms on Earth from solar ultraviolet radiation, responsible for a number of short- and mid-term negative biological effects. Several studies have demonstrated that the reduction of ozone in the atmosphere has led to an increase of solar UVB irradiance in some regions [Kerr and McElroy 1993]. On the other hand, direct and indirect interactions with the terrestrial climate system have been attributed to ozone variations, as reviewed by Pyle et al. [2005] and Forster et al. [2011]. Ozone concentration at a given location in the atmosphere depends on the balance among production, destruction, and transport processes. Photochemical and dynamical factors contribute differently to this balance depending on the latitude, altitude, and time scales, ranging from hours to decades, involved in these processes. Solar radiation also induces variations in the total ozone column (TOC) and the ozone vertical distribution from the modification of the photochemical production rates and changes in the lower

stratospheric dynamics [Hood 1997; Echer et al. 2001; Zerefos et al. 2001]. Since the early 1970s, the long-term evolution of the TOC has been driven mostly by the atmospheric concentration of ozone-depleting substances (ODSs) [World Meteorological Organization 2011]. During the 1980s and mid-1990s, statistically significant negative trends, observed from satellite and ground-based TOC measurements in the midlatitudes of both hemispheres, were particularly strong in winter and early spring [Stolarski et al. 1991; Bojkov et al. 1995]. The control of ODSs under the framework of the 1987 Montreal Protocol and subsequent revisions has slowed down their increasing trend. ODSs reached a maximum during the period 1992–1994 [World Meteorological Organization 2011] and have been decreasing since then.

Some recent studies report on the effectiveness of the Montreal Protocol and already confirm an effective global increase in total ozone values [Weatherhead and Andersen 2006; Mäder et al. 2010]. Supporting this point, several two-dimensional (2-D) and three-dimensional (3-D) chemistry-climate models (CCM) predict a decrease of ODS concentrations and a recovery of ozone levels [World Meteorological Organization 2011]. Nevertheless, because of the complex interactions among dynamical, chemical, and radiative factors controlling the evolution of the ozone layer, decreasing ODS concentration levels do not completely guarantee the recovery of the ozone to its previous levels [Intergovernmental Panel on Climate Change 2005]. Therefore, in the current scenario, in which chemical factors are progressively losing weight, it is expected that radiative and dynamical factors will have relatively more influence on the variability of short-, medium-, and long-range evolution of total ozone, especially over northern midlatitudes and the Arctic, where the ozone abundance is particularly sensitive to dynamical effects [Pyle et al. 2005]. As pointed out by Pyle et al. [2005], the dynamical feedbacks from greenhouse-gas increases could either enhance or reduce ozone abundance in some regions; currently, not even the sign of the feedback is known. Some modeling studies indicate that improving the stratospheric representation in global climate models provides a better understanding of near-surface temperature variability [Dall'Amico et al. 2010], strengthening the importance of achieving a more complete understanding of the stratosphere-troposphere coupled phenomena. On the other hand, global warming is expected to influence the behavior and geographical distribution of some climatic modes [Rind et al. 2005; Kawatani et al. 2011], such as the quasi-biennial oscillation (QBO) and the North Atlantic Oscillation (NAO), which previous studies have related to the evolution of column ozone in a wide range of temporal and spatial scales [see, e.g., Tungand Yang 1994; Appenzeller et al. 2000; Hadjinicolaou et al. 2002; Staehelin et al. 2002; Echer et al. 2004; Sitnov 2004; Harris et al. 2008]. These climate patterns can affect ozone on a broad spectrum of time scales. Therefore, to determine the influence of ODSs on TOC trends, it is fundamental to consider the potential effect of the above mentioned climatic modes in different regions and seasons.

TOC trends previously associated with ODS effects could have been overestimated or underestimated in some regions, as illustrated by Appenzeller et al. [2000], who studied the Arosa (Switzerland) and Reykjavik (Iceland) TOC series, introducing

the NAO index in a multiregression model. They found that the TOC trend associated with ODSs at Arosa was -2.4% per decade, instead of the previous value of -3.2% obtained omitting NAO information, and similarly that the TOC trend at Reykjavik was -3.8% per decade instead of the value obtained neglecting NAO, which was 0.0% [Appenzeller et al. 2000]. On average, they found that the dynamical contribution attributed to NAO effects to the long-term ozone winter trend at Arosa was approximately 25%. Similarly long-term changes in the tropopause altitude account for a similar value at Hohenpeissenberg (Germany), according to Steinbrecht et al. [1998]. Hood et al. [1999] attributed 25%–40% of the TOC variations in late winter to changes in Rossby wave breaking, in agreement with the 25% for Hohenpeissenberg (Germany) record in February estimated by Steinbrecht et al. [2001]. Knudsen and Andersen [2001] found similar rates (35%) during the April–May period. Moreover, recent work indicates similar estimates for the dynamical contribution to TOC changes, providing rates of about 1/3 or higher [Harris et al. 2008; Hood and Soukharev 2005; Rieder et al. 2010a, 2011; World Meteorological Organization 2007; Wohltmann et al. 2007]. The pioneering work of Orsolini and Doblas-Reyes [2003] showed that 65% of the TOC variability in spring could be explained by four climate patterns originating in the troposphere. Their results confirmed the dominant role of the NAO, but they also pointed out that other leading patterns (especially the European blocking pattern) should not be neglected over the Euro-Atlantic sector. In addition, the NAO signal is also clearly visible in the low-ozone episodes, more frequent in the high phase of the NAO [Orsolini and Limpasuvan 2001]. Rieder et al. [2010b, 2011], analyzing TOC timeseries of various European long-term ground-based stations, highlighted that also moderate NAO events have a significant effect on the TOC. They also showed that the NAO signal is reflected in the ozone extremes without always being visible in the ozone mean values.

Assessing the contribution of changes in atmospheric dynamics to long-term ozone trends is therefore of fundamental importance, particularly in a future scenario in which the effect of chemical factors may be limited as a result of the Montreal Protocol's effectiveness. In this context, we present a study whose main objective is examining the correlation between one of the most prominent climatic modes of the Northern Hemisphere, the North Atlantic Oscillation, and the total ozone column, focusing our attention on the summer season when the summer NAO (SNAO) is revealed as an important source of TOC variability. Additionally, we examine the zonal asymmetry in the NAO influence on the TOC, analyzing the dynamical processes that lead to this longitude-dependent pattern and their influence on the observed regional TOC trends [Peters et al. 2008]. The analysis has been done in low latitudes and midlatitudes of the Northern Hemisphere with a 1.00° x 1.25° latitude-longitude grid resolution, describing the spatial structure of the correlation field in both winter and summer and also calculating the correlation between NAO and thermal tropopause pressure and geopotential heights at 200 and 500 hPa.

2.3 The North Atlantic Oscillation

2.3.1 What it is and what it does

The NAO is primarily a north-south atmospheric mass oscillation over the North Atlantic region. It is characterized by simultaneous out-of-phase pressure or geopotential height anomalies over the subtropical Atlantic and the Arctic and by changes in the intensity and position of the jet streams (e.g., Hurrel et al. [2003]). The NAO constitutes the dominant mode of atmospheric variability over the middle and high latitudes of the NH. Indeed, at interannual timescales, it determines the climate variability from the east coast of the United States to Siberia and from the Arctic Ocean to the subtropical Atlantic [Hurrell et al. 2003].

The NAO is said to be in its positive phase when the jets streams are displaced poleward of their normal positions and the sea level pressure (SLP) over the Arctic and over the subtropical Atlantic are higher and lower than normal respectively. This pattern forces a northward shift of the winter storm tracks in the Atlantic resulting in warm and wet winters in Northern Europe and eastern US and dry and cold winters in the Mediterranean area and in northeastern Canada and Greenland (e.g., Hurrel and van Loon [1997], Dickson et al. [2000]). In contrast, the negative phase is characterized by an equatorward shift of the jet streams and by anomalous high pressures over the Arctic and anomalous low pressures over the subtropical Atlantic. It results in fewer and weaker winter storms crossing in a more west-east pathway than in the positive phase. This configuration brings moist air to the Mediterranean and cold and dry air to Northern Europe [Hurrel et al. 1995].

Nowadays, the most used technique to describe the spatial signature of the NAO is the EOF or principal component analysis (see e.g., Wilks [2006] for a detailed description of this technique). In this approach, the spatial pattern of the NAO is identified from the eigenvectors of the cross-covariance matrix calculated from the time variations of the SLP anomalies or other climate variable over the North Atlantic region. The NAO emerges as the leading EOF throughout the year and explains more than one third of the total variance of the SLP over the Atlantic during winter season (Fig. 2.1) (see e.g., Hurrel et al. [2003]).

The temporal evolution of the NAO is commonly characterized by the NAO-Index. Many indices have been proposed to describe the temporal evolution of the NAO (see Stephenson et al. [2003] for a description of some of these indices). Modern indices are based on the difference in surface pressure anomalies between various northern and southern locations over the Atlantic region. For example, Hurrel et al. [1995a] defined the NAO-Index as the difference between sea level pressure (SLP) anomalies at Lisbon, Portugal and the Stykkisholmur, Iceland. In this approach the SLP is usually measured at fixed ground stations and their data record extends back to 1864 constituting a quite long and simple data set of the NAO. Nevertheless, as pointed out by Hurrel et al. [1995], this definition has some important limitations:

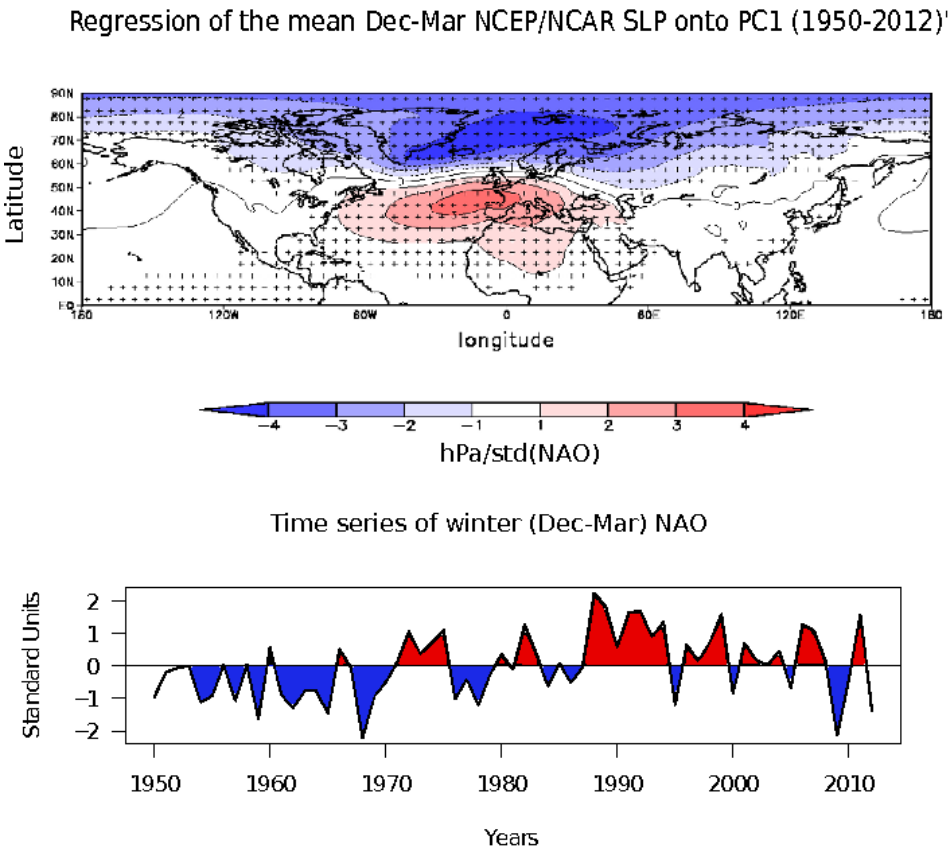

Figure 2.1: *Top panel*: Spatial pattern of the winter NAO displayed by regressing Dec-Mar mean SLP anomalies upon the standardized principal component time series of the leading EOF for the period (1950-2012). The leading EOF is defined from the covariance matrix of the Dec-Mar mean gridded SLP anomalies in the domain (20ºN - 80ºN; 90ºW - 40ºE) and explains about 50% of the total variance of the original data. SLP anomalies are based on the NCEP/NCAR dataset [Kalnay et al. 1996]. Thus, the top plot represents pressure anomalies in hPa for one standard deviation of the NAO time series. Regression coefficients statistically significant at the 95% threshold are marked with black dots. *Bottom panel*: Normalized time series of the winter NAO built projecting the leading EOF of Dec-Mar mean SLP anomalies onto the NCEP/NCAR Dec-Mar mean gridded SLP anomalies for the period 1950-2012.

- First, "the stations are fixed in space and hence they do not track the movement of the NAO centers of action through the annual cycle".
- Secondly, "the station-based pressure measurements are noisy due to small-scale and transient phenomena unrelated to the NAO".

A different approach is to define the NAO-Index using the EOF technique. In this approach, the NAO-Index is defined as the principal component time series of the leading EOF of gridded SLP anomalies (in this work the spatial patterns obtained

from EOF analysis are refer as the "EOFs" and the time series that describe the evolution through time of these patterns as "Principal Components").

It must be underlined, that the EOF method breaks the original field into "data modes". These modes are constrained to explain the maximum amount of variability of the original data but they do not necessarily represent "physical modes". Thompson and Wallace [1998, 2000] presented evidence that the NAO should be viewed as the regional manifestation of a larger pattern than the NAO that they called the *Northern annular mode* (NAM). This pattern is equivalent to the *Southern annular mode* (SAM). It describes the meridional atmospheric mass oscillation between the entire Arctic Circle and a zonal ring at midlatitudes with centers of action over the North Atlantic and the North Pacific oceans. The NAM is characterized by a deep and nearly barotropic structure, with zonal wind perturbations of opposite sign along~ 55º and~ 35º latitudes [Thompson et al. 2003]. It is defined as the leading EOF of winter SLP data over the NH (20º-90º) and its signature is also evident in the leading EOFs of geopotential heights and zonal winds from the surface up to 0.3 hPa within the stratosphere [Baldwin and Dunkerton 2001]. The NAM spatial pattern closely resembles the spatial pattern of the NAO except for larger amplitude anomalies over the Northern Pacific area. The NAM-index, calculated as the principal components of the leading EOF, is strongly correlated with the NAO-Index (r=0.95) (e.g., Hurrel et al. [2003]). The view of the NAO as a regional manifestation of the NAM was, however, not universally accepted. Some authors (e.g., Deser [2000]) supported the so-called "regional perspective" where the NAM is thought to be a statistical artifact of locally occurring dynamics (see e.g., Thompson et al. [2003] for a detailed review of this issues).

The NAO-Index used in this study corresponds to the principal components of the leading EOF of the monthly gridded SLP anomalies over the North Atlantic (20º-70º; 90ºW-40ºE), as described by Hurrell et al. [1995] and Folland et al. [2009]. The SNAO has a smaller scale than its winter counterpart and its spatial pattern is clearer from the EOF calculated over this region than over the entire hemisphere [Folland et al. 2009]. For this reason, we will refer to the NAO/NAM just as NAO.

2.3.2 The Summer North Atlantic Oscillation

The largest climate impacts of the NAO are observed during winter months. This fact explains why most of the NAO related studies focus in this season. However, recent work [e.g., Folland et al. 2009; Bladé et al. 2011] showed that during the summer months, the NAO substantially affects the variability patterns of precipitation, temperature, and cloudiness. Folland et al. [2009] defined the SNAO as the leading EOF of the extratropical North Atlantic SLP during high summer (July-August). They showed that during summer months, the dipole that constitutes the NAO moves northward, tilt to the west and decrease its extension and intensity compared with the winter season. Fig. 2.2 displays the spatial pattern and index of the SNAO for the period 1950-2012 for the NCEP/NCAR SLP dataset.

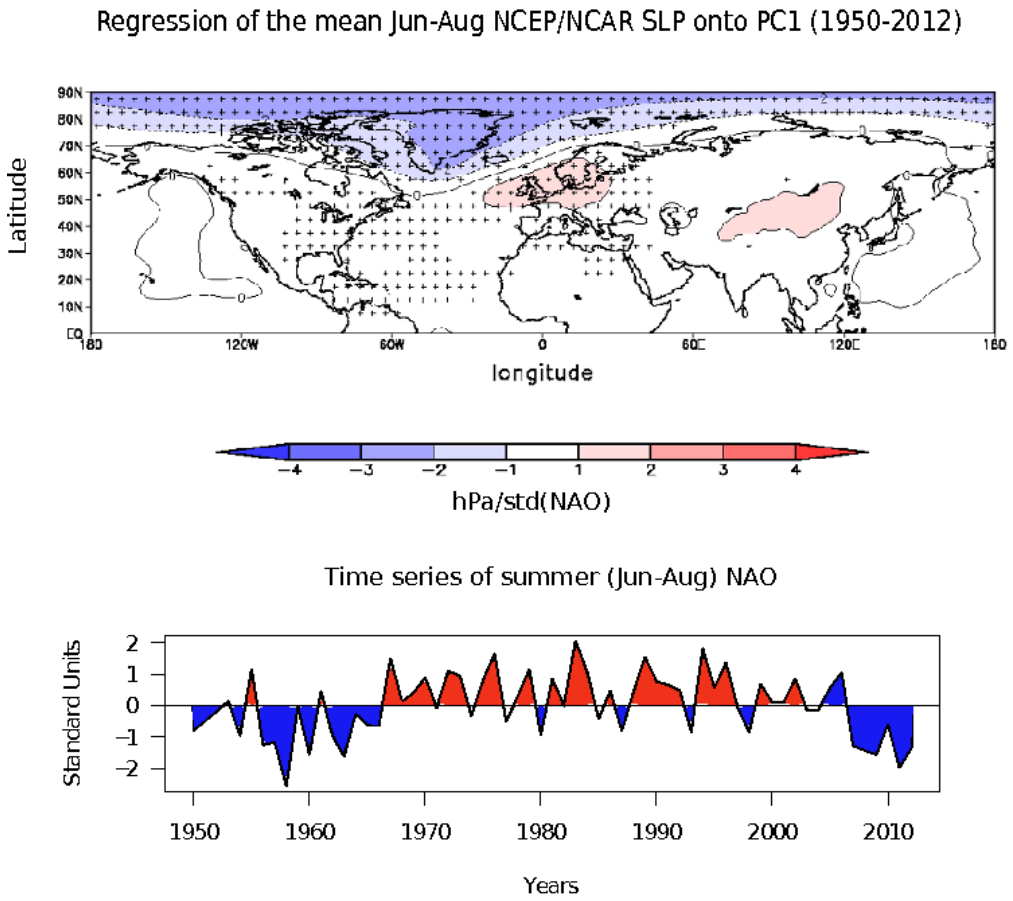

Figure 2.2: *Top panel*: Spatial pattern of the summer NAO displayed by regressing Jun-Aug mean SLP anomalies upon the standardized principal component time series of the leading EOF for the period (1950-2012). The leading EOF is defined from the covariance matrix of the Jun-Aug mean gridded SLP anomalies in the domain (20ºN - 80ºN; 90ºW - 40ºE) and explains about 50% of the total variance of the original data. SLP anomalies are based on the NCEP/NCAR dataset [Kalnay et al. 1996]. Thus, the top plot represents pressure anomalies in hPa for one standard deviation of the NAO time series. Regression coefficients statistically significant at the 95% threshold are marked with black dots. *Bottom panel*: Normalized time series of the mean Jun-Aug NAO built projecting the leading EOF of Jun-Aug mean SLP anomalies onto the NCEP/NCAR Jun-Aug mean gridded SLP anomalies for the period 1950-2012.

2.3.3 A dynamical mechanism for the NAO/NAM

There is wide agreement that the NAO/NAM arises from the intrinsic internal nonlinear dynamics of the atmosphere. The time series of the NAO/NAM-Index vary without any preferred time scale and resemble a red-noise process with a decorrela-

tion timescale[1] of about 10 days in the troposphere and of the order of several weeks in the stratosphere (e.g., Thompson et al. [2003]).

As aforementioned, the NAO/NAM is characterized by fluctuations in the intensity of tropospheric westerly winds between the subtropics and high latitudes. The mechanism driving these fluctuations can be qualitatively understood from the zonal-mean zonal momentum equation introduced in chapter 1:

$$\frac{\partial \overline{u}}{\partial t} = f_0 \overline{v} - \frac{\partial \left(\overline{u'v'}\right)}{\partial y} \tag{2.1}$$

where we have neglected the $\overline{X}$ term.

From eq. 2.1 it is clear that the variations of the vertically averaged zonal-mean zonal wind are driven by the convergence of eddy momentum fluxes. Therefore, changes in the zonal flow, and thus in the tropospheric NAM Index, must be forced by variations of momentum flux, which is transported mainly by synoptic scale eddies around 45º (Fig. 2.3) [e.g., Thompson et al. 2003].

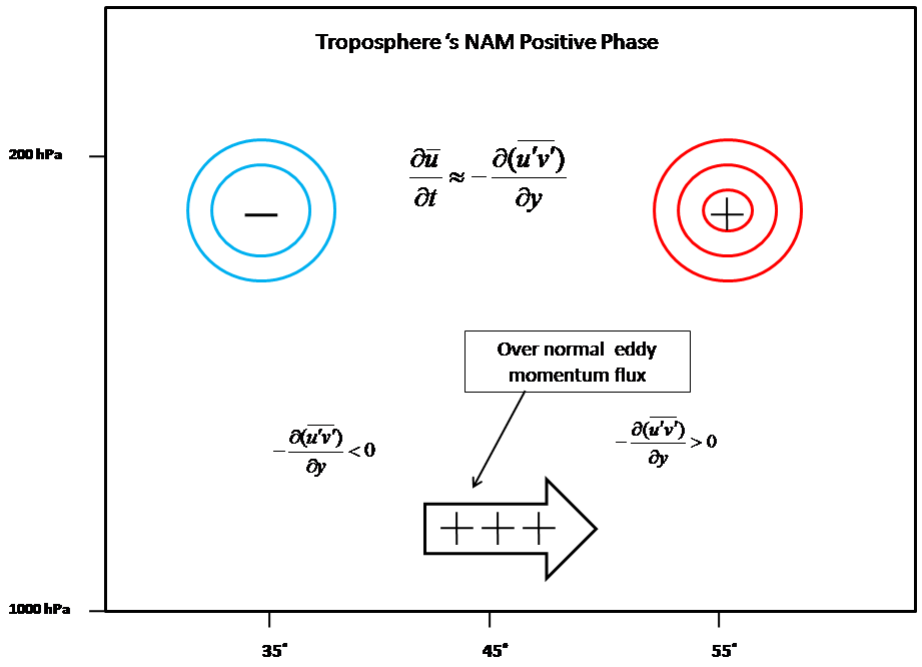

Figure 2.3: Schematic picture of the anomalous eddy momentum flux driving the tropospheric component of the NAM. Concentric circles represent the zonal wind anomalies associated with the positive phase of the NAM.

[1]Number of lags that it takes for the autocorrelation function to reach zero correlation.

The longer variability timescales of the stratosphere's NAM component suggest that different dynamic mechanisms are involved. We can understand stratospheric NAM-like variability from the TEM zonal-mean zonal momentum equation introduced in chapter 1:

$$\frac{\partial \overline{u}}{\partial t} - f_0 \overline{v} = \overline{G} \tag{2.2}$$

where $\overline{G}$ is the zonal-mean zonal drag force impel to the zonal-mean zonal flow mainly by planetary wave breaking into the stratosphere. From eq. 2.2 we can deduce that the vertical average changes in the zonal-mean zonal flow must be driven by variations on the zonal-mean zonal drag force $\overline{G}$ and hence by anomalous planetary wave breaking into the stratosphere.

2.3.4 The NAO Troposphere-Stratosphere connection and TOC

The NAO impacts on the troposphere-stratosphere coupling through two superposed mechanisms:

1. Relatively slow coupling (~ a few weeks) occurs through interactions between planetary-waves and the zonal-mean flow. The positive NAO phase is associated with enhanced equatorward refraction of upward propagating planetary-waves [Ambaum and Hoskins 2002]. Consequently few waves break into the stratosphere and the zonal flow becomes stronger than normal. The strong stratospheric zonal flow, on the other hand, changes the background conditions for wave propagation in such a way that the phase of the zonal-mean flow anomalies propagates poleward and downward, eventually reaching the lower troposphere. Then, downward propagating anomalies reinforce the tropospheric westerly flow and hence the NAO/NAM positive phase [e.g., Haynes et al. 2005]. Note that the NAO troposphere-stratosphere connection is bidirectional, i.e., the tropospheric component of the NAO influences the stratospheric one and vice-versa (Fig. 2.4).

2. Effectively instantaneous coupling occurs via hydrostatic and geostrophic adjustment of the troposphere-stratosphere potential vorticity (PV) distributions. As discussed in Hoskins et al. [1985] the isentropic surfaces tend to bend towards/against a positive/negative PV anomaly. The occurrence of an upper level PV anomaly, for example by the passage of a tropospheric low (PV>0)/high (PV<0) pressure system leads to a lower/higher tropopause. Positive/negative PV anomalies then stretch/squeeze the columns of stratospheric air, and hence increase/decrease the total mass and similarly the TOC (Fig. 2.5).

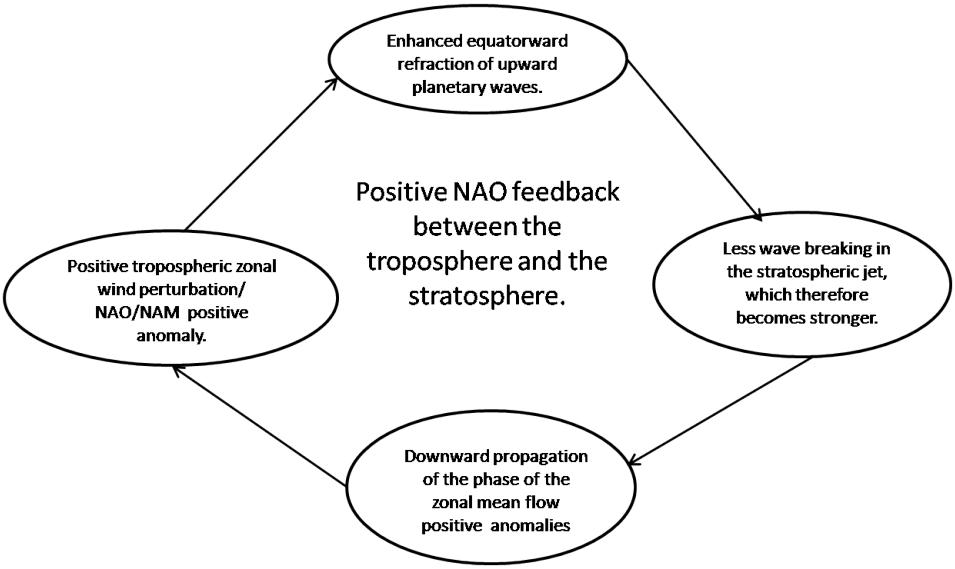

Figure 2.4: Diagram of the positive NAO feedback between the troposphere and the stratosphere.

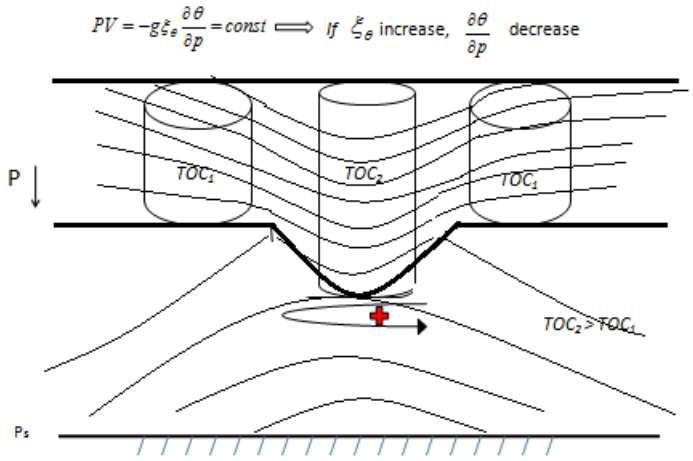

Figure 2.5: Stretching of a column of stratospheric air associated with a tropospheric positive vorticity anomaly. The thick lines represent the tropopause and an arbitrary level into the stratosphere. Thin lines represent potential temperature surfaces. Note that potential temperature surfaces are bent towards the positive vorticity anomaly.

Ambaum and Hoskins [2002] presented the most comprehensive study to date about the effects of the winter NAO on troposphere-stratosphere connections. The connections they showed involve the two mechanisms introduced above. First, they showed that the NAO positive phase in the troposphere is associated with lower than normal tropopause height above the Icelandic low. The low tropopause is associated with higher than normal values of TOC over this area. Moreover, the positive NAO phase is associated with stronger than usual stratospheric polar vortex. Then, the associated positive vorticity anomaly results in a higher than usual tropopause and lower TOC values over the North Pole. A strong polar vortex, in the other hand, acts like a shield refracting vertically propagating planetary waves. Therefore it is less susceptible to be disturbed and becomes even more intense. Finally, the strong polar vortex changes the background conditions for wave propagation in such a way that the phase of the stratospheric zonal flow anomalies propagates poleward and downward and eventually reaches the lower troposphere reinforcing the westerly circulation. Therefore, the NAO positive phase is reinforced closing the "feedback loop".

2.3.5 The NAO response to climate change

Over the past five decades the winter NAO-Index based on observations has exhibited a statistically significant upward trend [Thompson et al. 2000, Gillet et al. 2003]. This trend has been attributed to a range of different forcings. These include increases in greenhouse gas concentrations, stratospheric ozone depletion, tropospheric sulfate aerosols, and changes in solar irradiation. Although all of them can play a role, there is a large disagreement about their relative importance [Gillet et al. 2003 and reference therein].

The influence of increasing greenhouse gas concentrations on the NAO has been analyzed in all of the major climate models. Most of them have shown an upward trend in the NAO although weaker than the observed [Gillet et al. 2003]. Folland et al. [2009] using two Hadley Center climate models forced with increasing levels of atmospheric CO2 found that the changes in circulation were equivalent to an increasingly positive phase of the SNAO.

Different authors proposed a mechanism that might explain the link between greenhouse gases and the NAO [e.g., Shindell et al. 1990; Hartmann et al. 2002]. The basic idea is the following: ¬The main effect of increasing greenhouse gas concentrations is warming the troposphere and cooling the stratosphere and most of the GCMs predict an enhanced warming at tropopause levels in the tropics. Since the tropopause slopes down from the tropics to the poles, an enhanced warming in the tropical upper troposphere together with the cooling of the lower stratosphere will increase the meridional temperature gradient in the upper troposphere - lower stratosphere. This in turn is expected to enhance the zonal wind in the mid-latitude tropopause region to maintain the thermal-wind balance and then, through the planetary wave – mean flow feedback mechanism showed above (Fig. 2.4), to strength

the stratospheric polar vortex. Finally the stratospheric zonal wind anomalies might propagate downward to the lower troposphere reinforcing the positive phase of the NAO.

2.4 Data and Methodology

Monthly mean TOC values have been retrieved from the Total Ozone Mapping Spectrometer (TOMS) on the Nimbus-7 (1979-1993) and Earth Probe (1996-2005) satellites, and the Ozone Monitoring Instrument (OMI) (from 2004 to 2009), on the Aura satellite of the Earth Observing System's (EOS) series [McPeters, 1996]. The data used were derived from TOMS version 8 and OMI-TOMS collection 3, both based on the same algorithm, to ensure continuity and homogeneity of the data series. TOMS data have a maximum uncertainty of 3% [Bhartia, 2002]. The years 1992 and 1993 have been excluded from the data series to eliminate the influence of the 1991 eruption of Mt. Pinatubo which injected huge amounts of sulfur dioxide in the stratosphere [Daniel et al. 1995; Schoeberl et al. 1993]. From 1994 to 1996, the mission was not operative so these years are not available either. Therefore the final data set considered in the present work ranges from 1980 to 2009, excluding the 1992 to 1996 period (26 years). The spatial resolutions of the two data sets OMI (1.00^{o} x 1.00^{o}) and TOMS (1.25^{o} x 1.00^{o}) are different, so OMI data have been interpolated to the original TOMS grid to homogenize the series.

The monthly mean NAO index was provided by the Climate Analysis Section website of the National Center for Atmospheric Research (NCAR) [Hurrell, 1995] and they are quite similar to the ones we derived from NCAR/NCEP SLP data showed in Fig. 2.1 and Fig. 2.2 except for the longer time-period used in those figures.

The geographical domain considered is the Northern Hemisphere latitudes below 60^{o}. Satellite ozone retrievals at higher latitudes lack continuous measurements in wintertime so correlation computations are not reliable.

The linear correlation field between total ozone and NAO index time series has been computed at each grid point for extended winter (December to March) and high summer (July-August) seasons in 1980-2009, excluding the period 1992 to 1996 as explained above. Linear correlation fields for June, July, August and September have also been computed separately (see Ossó et al. [2011] Fig. A1). We test the correlation statistical significance at a 95% significance level using a two-sided nonparametric permutation test (see, for example, Wilks [2006]). Ozone data time series ¬used in this analysis are not well described by a Gaussian distribution, so classical statistical methods are not appropriate, as it was also pointed out by Rieder et al. [2010a]. Nonparametric permutation tests are more adequate in this context because no assumptions regarding an underlying parametric distribution for the data for the test statistic are necessary [Wilks, 2006]. 99% and 90% significant correlations for winter and high summer seasons have also been calculated in order

to provide sensitivity analyses (see Ossó et al. [2011] Fig. A2 and Fig. A3). p-value contour maps for both seasons are given in Ossó et al. [2011] (Appendix A, Fig. A4). Spatial correlation was neglected in the statistical analysis, since the test was performed on grid-cell basis.

Additionally, seasonal correlations between the NAO index and the thermal tropopause pressure, and the geopotential heights at 200 and 500 hPa have been calculated. Monthly mean values of thermal tropopause pressures have been derived from the National Centers for Environmental Prediction (NCEP)/NCAR reanalysis [Kalnay et al. 1996] and monthly average geopotential heights from the second reanalysis of NCEP/Department of Energy (DOE), an enhanced version of the first reanalysis including satellite data and corrections of the parameterizations of physical processes [Kanamitsu et al. 2002]. Table 2.1 summarizes the temporal/spatial characteristics of the datasets employed in this study, as well as relevant references and online sources for data and documentation.

	Temporal resolution	Spatial resolution	Data source	Reference
TOC(TOMS)	Monthly	1.0° lat x 1.25° lon	http://ozoneaq.gsfc.nasa.gov	*McPeters et al.* [1998]
TOC(OMI)	Monthly	1.0° lat x 1.0° lon	http://ozoneaq.gsfc.nasa.gov	*McPeters et al.* [2008]
NAO	Monthly	---	http://www.cgd.ucar.edu/cas/jhurrell/indices.html	*Hurrell* [1995]
TP	Monthly	2.5° lat x 2.5° lon	ftp://ftp.cdc.noaa.gov/Datasets/ncep.reanalysis.derived/tropopause/	*Kalnay et al.* [1996]
HGT	Monthly	2.5° lat x 2.5° lon	http://www.esrl.noaa.gov/psd/data/gridded/data.ncep.reanalysis2.pressure.html	*Kanamitsu et al.* [2002]

Table 2.1: Description of the datasets used in this study (a) (TOC=total ozone column; NAO=North Atlantic Oscillation; TP=thermal tropopause pressure; HGT=geopotential height).

2.5 Results

2.5.1 Winter NAO and TOC

Fig. 2.6 shows the linear correlation field between the NAO index and TOC during winter season (December to March) – 95% significance level areas are shown with dots. Three zones between 40º and 60º are clearly anticorrelated. The first of them is over Western Europe, where the NAO index accounts for up to 30% of the TOC seasonal variability. The second zone is over the eastern North American coast with a similar negative correlation, though at a slightly lower latitude, can be found. The third zone is over North-East Asia, where the explained variance, computed as the squared linear correlation coefficient (r^2), reaches 60%. This high value might be attributed to a stronger polar vortex penetration to lower latitudes in these longitudes during positive NAO years (see section 2.2.4.), which implies the destruction of massive amounts of ozone through catalytic reactions and also an increase of the tropopause height [Ambaum and Hoskins, 2002] and with the transfer of wave energy downstream towards Siberia that reinforces the surface anticyclone that contribute to a higher tropopause and hence a lower TOC [Sung et al. 2011].

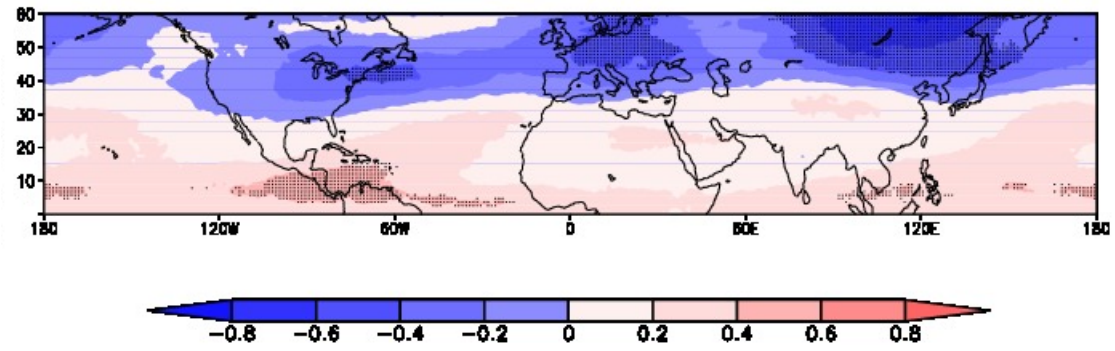

Figure 2.6: Linear correlation field between the NAO index and TOC during wintertime (Dec-Mar); the areas with a 95% significance level are indicated by dots.

The spatial pattern of the correlation field between the NAO and TOC presented over Western Europe is similar to the correlation found by Appenzeller et al. [2000] between the NAO and the tropopause height. However, the TOC variability explained by the NAO is lower than would be expected from a simple direct relation among NAO – tropopause height – TOC. This could be explained by the intensification of the meridional transport of ozone-rich tropical air towards mid-latitudes, e.g. by the Brewer-Dobson circulation [Salby and Callaghan, 2005] in years with

positive NAO which could partly balance the effect of the increase of the tropopause height upon TOC over Western Europe.

With regard to positive correlated areas, the most remarkable feature is a local maximum centered over Central America. This could be related to positive phases of the NAO amplified by some degree by the presence of the El Niño-Southern Oscillation (ENSO) and its associated increment in convection and subsequent average decrease of the tropopause height. High resolution simulations of coupled atmosphere-ocean models of the European Centre/Hamburg Model (ECHAM /OPYC) [Latif, 2001; Timmermann et al. 1999; Wanner et al. 2001] suggest possible links between the ENSO and the NAO through the interaction between the ocean and the atmosphere supporting this hypothesis.

Fig.2.7 shows the 99% and 90% significant correlations plots. The hypothesis test performed at 99% level reduces the extension of the significant correlated areas as expected. Despite most of the areas described above are still significant, positive correlated areas over Central America are no longer significant, showing that correlations obtained at 95% and 90% confidence levels must be interpreted carefully on this region.

The results presented for winter indicate that the NAO variability is able to explain to large extent the TOC behavior, through the interactions upon tropopause pressure and TOC, and through the interaction between the NAO and the arctic polar vortex. Stronger meridional stratospheric circulation (BDC) transporting ozone from the tropics to higher latitudes in the NAO positive phase can also play a role on the observed correlated fields. Further insight can be obtained by examining the correlation distribution between the NAO and tropopause pressure (Fig. 2.8a) which reproduces similar spatial features as Fig. 2.6, particularly for negatively correlated local minima, supporting a clear link among NAO, tropopause pressure and TOC.

The NAO signal can also be observed in correlation fields with geopotential heights, which again exhibit common features with the Fig. 2.6 and Fig. 2.8a. The correlations between the NAO index and the geopotential height at 200 and 500 hPa are shown in Fig. 2.8b and 2.8c, respectively. Both correlation fields show approximately the three zones previously described where the TOC was in opposite phase with the NAO – however note that now the correlation is positive. The zones over North-East Asia and Western Europe are the most intense, this latter extending, with weaker correlation, to the east coast of North America.

2.5.2 Summer NAO and TOC

Fig. 2.9 shows the correlation between the SNAO in high summer season (July to August) and TOC (panel a) and the correlation between the SNAO and the geopotential field at 200 hPa (panel b). Fig. 2.9a depicts clearly two relative maxima

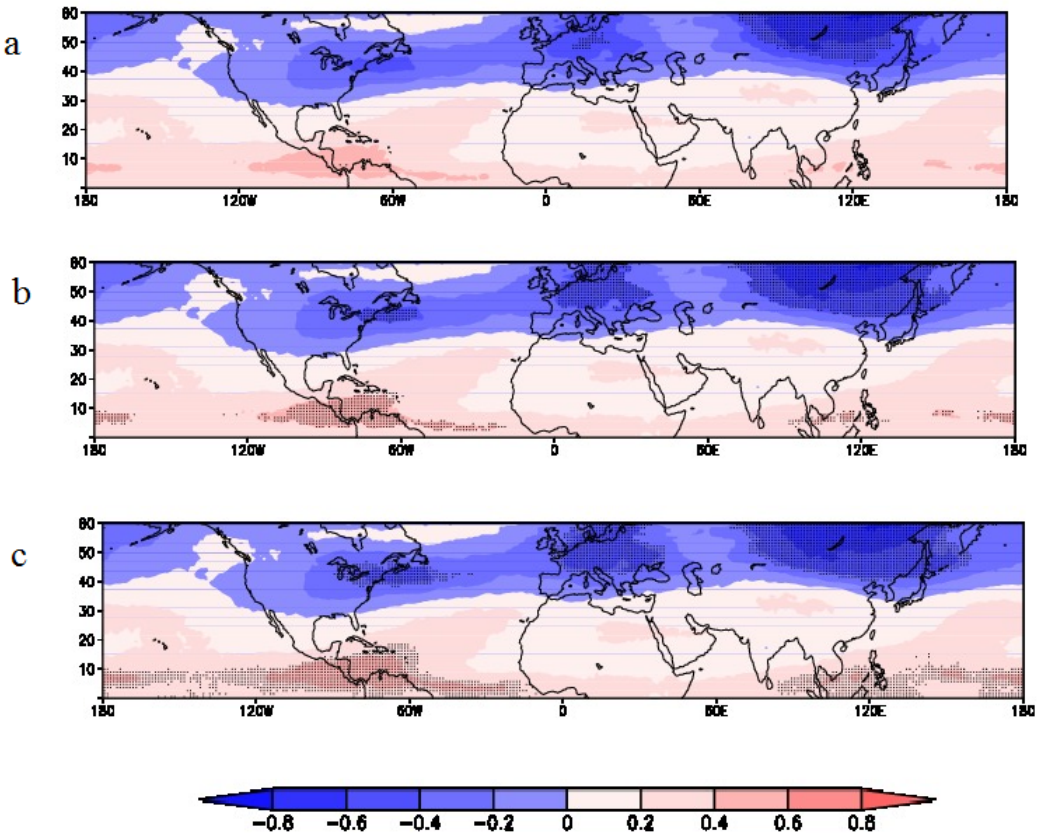

Figure 2.7: Linear correlation field between the NAO index and TOC during wintertime (Dec-Mar) for **(a)** 99% significance level, **(b)** 95% significance level, and **(c)** 90% significance level.

(positive correlation) over Greece and West Portugal. The negative correlation areas of the SNAO on TOC over Europe move northwards in comparison with winter months. Over Southern Europe and Mediterranean Sea, including the significant area over Greece, the correlation pattern shows a reversal from winter to high summer seasons. This inverse behavior of the SNAO is also observed in other fields such as precipitation, where positive SNAO values imply a rainfall increase over the Mediterranean region [Bladé et al. 2011]. The two positive correlation centers of SNAO-TOC over Greece and west of Portugal are associated with two relative geopotential lows centered at 250 hPa that are highly correlated with positive SNAO years. Fig. 2.10 shows the composite geopotential anomalies fields of the years between 1979-2009 with a SNAO index plus one standard deviation above its long term mean value (panel a) and minus one standard deviation below its long term mean value (panel b) at 200 hPa in the European region. Long-term mean values were

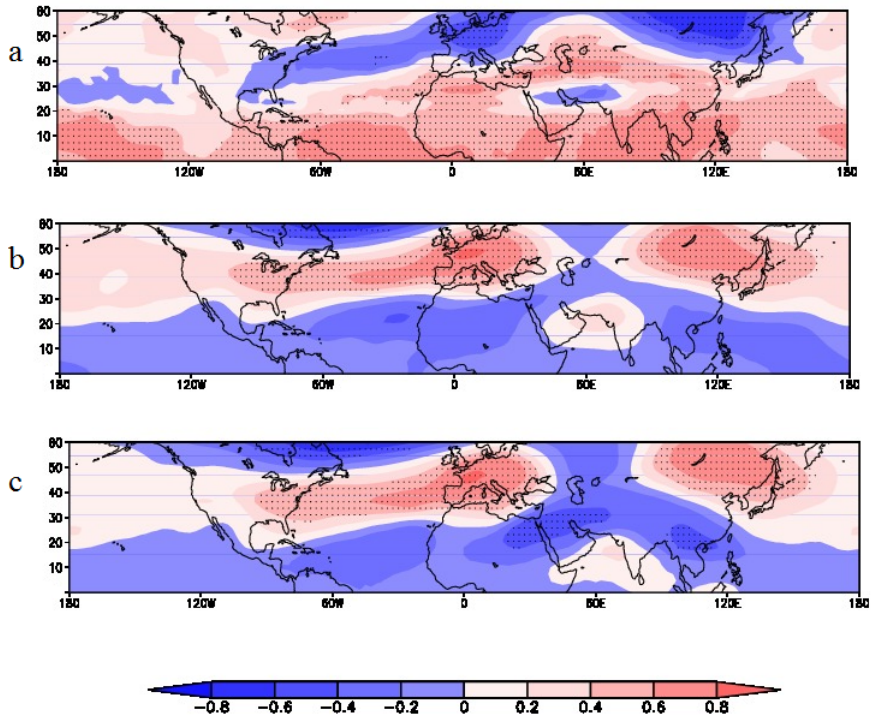

Figure 2.8: Linear correlation between the NAO index and **(a)** the thermal tropopause pressure (hPa) and geopotential heights (meters) at **(b)** 200 hPa and **(c)** 500hPa during wintertime (Dec-Mar); the areas with a 95% significance level are indicated by dots.

calculated using the 1949-2010 period. Fig. 2.10a clearly shows a tripole pattern with negative geopotential anomalies over Greece and West Portugal and a positive geopotential anomaly at higher latitudes (45ºN-60ºN). In Fig. 2.10b the opposite pattern is shown. Deeper insight about these negative geopotential anomalies can be achieved by representing the height-latitude cross-section composite of the geopotential anomaly over Greece (Fig.2.11). The geopotential anomaly extends from 600 to 200 hPa with its center located around 250 hPa.

Another remarkable feature of Fig.2.9 is a maximum (positive correlation) over South-West US. Folland et al. [2009] found a weak but significant correlation between the SNAO and the SST in the Tropical Pacific. This suggests that the SNAO phase is to some extend influenced and/or related to the ENSO phase. An increased convection would lead to a lower tropopause height and a higher TOC. Moreover, the tropical cyclone season is more active during positive phases of ENSO [Lander 1994; Emanuel 2007; Corral et al. 2010]. The successive passage of deep depressions could lead to an average decrease of the tropopause height, thus increasing TOC.

Fig. 2.9 also shows the statistically significant dipole pattern with a positive correlation center over the North Pacific Ocean and a negative correlation over North-West Canada. Complementary NCEP reanalysis data indicate that positive SNAO years are correlated with a negative geopotential height anomaly over the North Eastern Pacific and with a positive anomaly over Western Canada that are spatially coincident with the dipole pattern mentioned above (Fig. 2.9b). This train of teleconnections including the two relative upper level lows is strongest at upper levels (~ 200hPa) and absent in the surface and their meridional extent seem to coincide with the summer upper level jet.

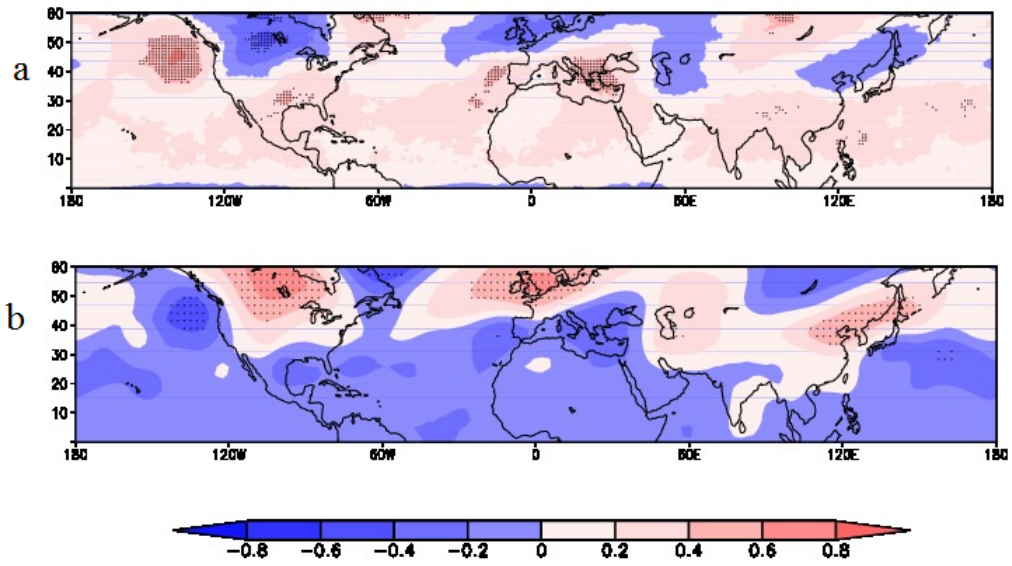

Figure 2.9: (a) Linear correlation field between the SNAO index and TOC during high summer (Jul-Aug); **(b)** linear correlations between SNAO and geopotential height (meters) at 200 hPa. The areas with a 95% significance level are indicated with dots.

Watanabe [2004] called the similar winter circumglobal wave pattern the *NAO downstream extension* and suggest that this downstream extension is due by quasi-stationary Rossby waves excited by a vorticity source associated with the NAO and meridionally trapped by the large vorticity gradients within the jet stream. Bladé et al. [2012] found a similar circumglobal wave pattern than in Fig. 2.9b. They suggested that this pattern could be the summer counterpart of the NAO downstream extension of Watanabe [2004]. Hence, the SNAO would excite a quasi-stationary

Rossby wave that will get trapped by the large vorticity gradients of the summer jet stream.

The hypothesis test performed at 99% level reduces the extension of the significant correlations areas. Positive correlated areas over South-West US and West Portugal are no longer significant. Anyway we consider that the positive correlation over West Portugal is still consistent because the correlation coefficient value is between 0.4 and 0.6 and other analysis such as the anomalies plot (Fig. 2.10) support the physical background for the existence of this correlation.

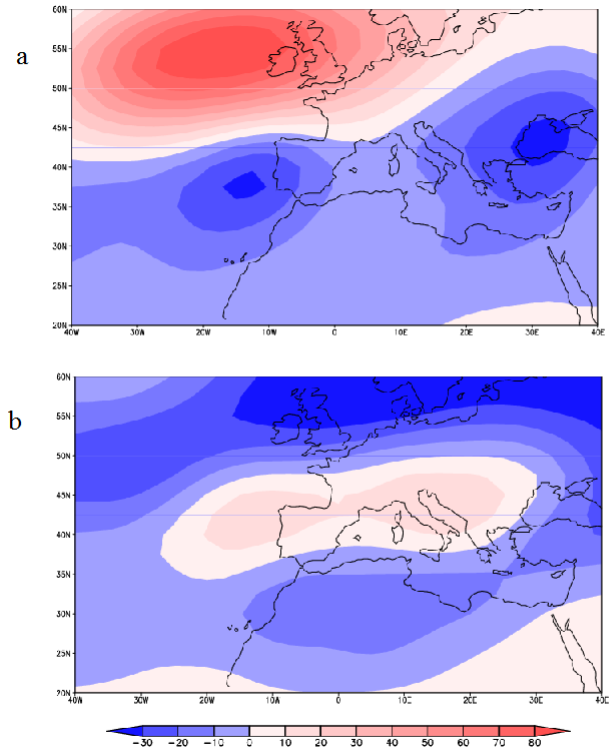

Figure 2.10: Composite anomalies of geopotential height at 200 hPa in the period 1979-2009 over the European region for SNAO (a) plus one standard deviation (SD) above its long-term mean and (b) minus on SD below its long-term mean. The long term mean was calculated using the 1949-2010 period. Image provided by the NOAA/ESRL Physical Sciences Division, Boulder, Colorado (www.esrl.noaa.gov/psd/).

Folland et al. [2009] showed that July and August SNAO indices are similar while that of June is substantially different from those in July and August. For this reason, they recommend to use the high summer definition of SNAO. We calculated the monthly SNAO-TOC correlation maps (June to September) to provide valuable

insight in the seasonal TOC variability (Fig. 2.12). The SNAO-TOC correlation pattern explained above seems to be strengthened in July where the picture clearly shows the two local positive correlations over Greece and West Portugal and extended positive correlation areas across the North Atlantic Ocean. In August, the two local positive correlations mentioned above are weaker than in July and the dipole pattern mentioned above over the North Pacific Ocean and North Canada is apparent.

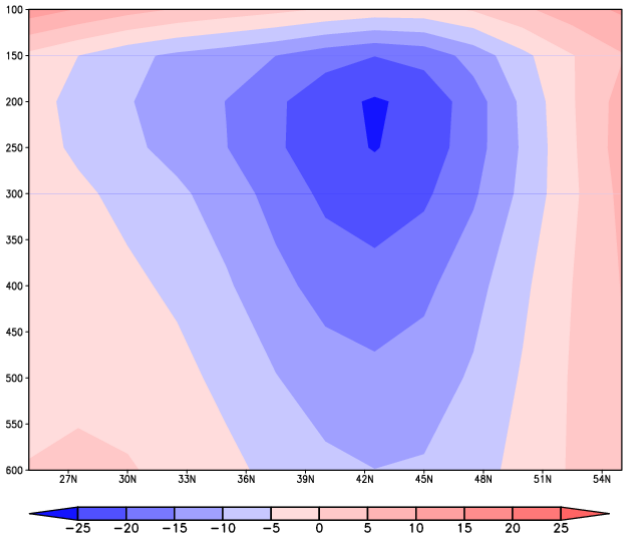

Figure 2.11: Height-latitude cross section composite of geopotential height anomaly (m) for the period 1979-2009 with a SNAO index plus one standard deviation above its long-term mean. Image provided by the NOAA/ESRL Physical Sciences Division, Boulder, Colorado (www.esrl.noaa.gov/psd/).

2.6 Conclusions

The correlation between the NAO and TOC has been studied for the Northern Hemisphere during 26 years for the high summer and winter seasons. The results indicate that the influence of the NAO on TOC is fundamental to understand the TOC interannual variability at a regional scale. This link is caused through troposphere – stratosphere interactions, where the tropopause pressure plays a vital role. The NAO has an effect not only on the climatic conditions of the troposphere but also influences substantially the lower stratosphere. The variation caused on the thermal tropopause pressure is instrumental in controlling TOC values.

In a global climate change scenario, the evolution of circulation patterns (e.g., the NAO) and other expected variations such as changes in the lower stratosphere tem-

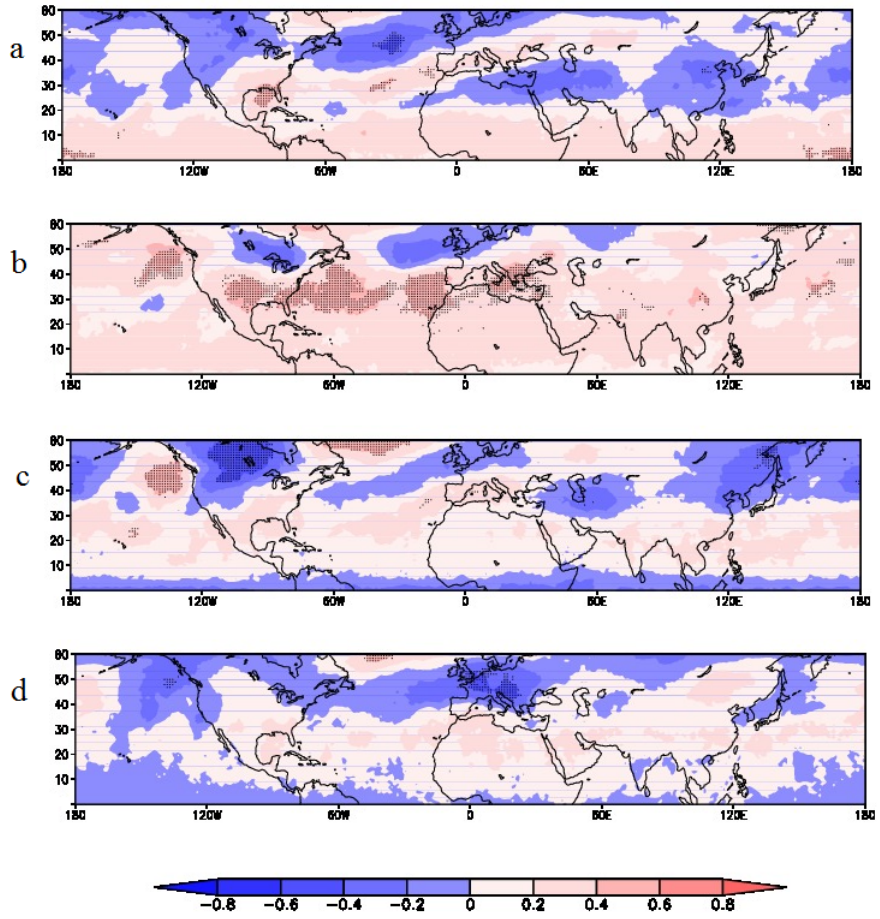

Figure 2.12: Monthly linear correlation fields between the SNAO index and TOC for **(a)** June, **(b)** July, **(c)** August, and **(d)** September.

perature, indicate a situation where the understanding of the complex troposphere – stratosphere interactions is fundamental to forecast the evolution of the TOC.

In this context, our study reveals some important regional and seasonal features of the connection between TOC and the NAO and especially the SNAO. During winter, TOC variability associated with the NAO is particularly important over Northern Europe, the US East Coast and Canada explaining up to 30% in TOC variance for this region. Further the explained variance reaches up to 60% over North Eastern Asia. One central finding of this work is the inverse relation over Southern Europe between the winter NAO and summer NAO (SNAO) on TOC values. A positive SNAO produces a retrograde circulation over the Eastern Mediterranean favoring the generation of two relatively small low pressure systems at 200 hPa over the central

Mediterranean and west of Iberian Peninsula positively correlated with TOC values, as shown in this work.

3 Is the impact of the climate change on the stratosphere supported by observations?

3.1 Overview

The aim of this chapter is to examine the evidence for observed trends in the stratospheric overturning circulation using a suite of currently available stratospheric temperature data. Trends are inferred from a range of observational data (NOAA-SSU, MetOffice-SSU, MSU TLS, RATPAC and RICH radiosondes) and two primary reanalysis products (ERA-Interim and MERRA). Finally trends derived from observations are compared with trends from a suit of Climate-Chemistry models.This chapter is built on Ossó et al. [2014].

3.2 Stratospheric Cooling

The climate of the stratosphere is changing due to natural and anthropogenic processes. These processes are inducing changes in the stratospheric composition, temperature and circulation [e.g., Forster et al. 2011 and reference therein].

One of the main impacts of climate change on the stratosphere is the stratospheric cooling. The stratosphere is cooling due to the radiative effects associated with ozone depletion and increased concentration of some greenhouse gases (GHGs) such as CO2 [Ramaswamy 2001; Shine et al. 2003; Randel et al. 2009]. The relative contribution of the ozone loss and the GHGs to this cooling phenomenon depends on the altitude, latitude and season. Globally, it is thought that ozone depletion is the main driving force of the lower-stratosphere cooling. On the contrary, both ozone depletion and GHGs concentration increase have similar contributions to the cooling of the middle and upper stratosphere [Shine et al. 2003].

Whether a GHG warms or cools the stratosphere depends on the opacity of the troposphere to the particular absorption wavelengths of the gas [e.g., Clough and Iacono 1995]. The troposphere is highly opaque to the wavelength absorption bands of GHGs such as CO2 and H2O. Most of their main band (15000 nm) is absorbed at quite low altitudes in the troposphere. As schematically shown in figure 3.1, most of

the upwelling radiation reaching the lower stratosphere comes from the cold upper troposphere. Because of the different emission temperatures between the upper troposphere and the stratosphere, when CO2 concentration increases, the radiation absorbed by stratospheric CO2 increases less than its emission. Therefore, in the stratosphere the CO2 emits more radiation than absorbs leading to a cooling at all heights.

Other GHGs such as O3 and CFCs have a weaker impact than CO2 because their absorption in the troposphere is smaller. They do not completely block the radiation from the surface in their wavelength absorption bands and can still absorb energy in the stratosphere and heat this region [Ramaswamy et al. 2001].

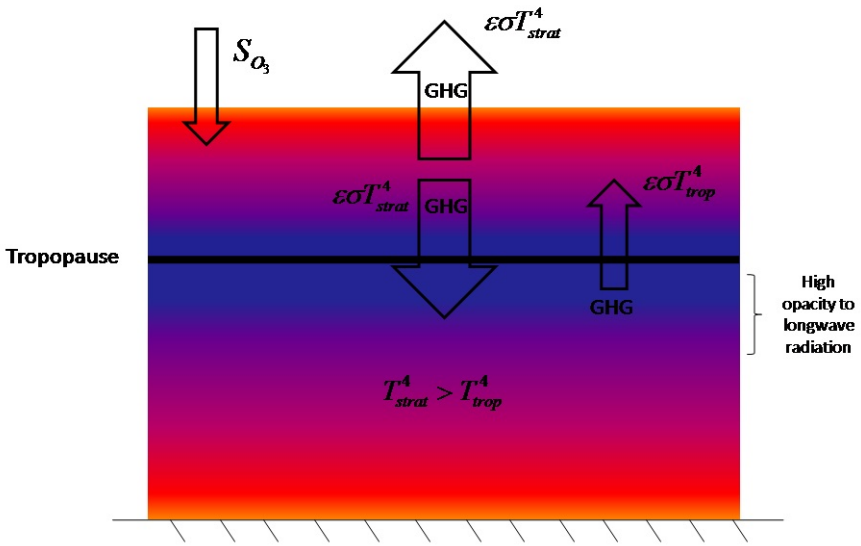

Figure 3.1: Schematic picture showing how CO2 contributes to radiatively cool the stratosphere. Red and blue color represents temperatures, represents the radiative heating by O3, is the radiation emitted by tropospheric CO2 and is the radiation emitted by stratospheric CO2.

3.3 How well constrained are the stratospheric temperature trends?

Stratospheric temperature time series derived from observations are characterized by large variability on multiple timescales and long-term trends [Forster et al. 2011]. The evolution of stratospheric temperatures is driven by both natural and anthropogenic forcings. The main natural forcings are the solar cycle, the ENSO and

explosive volcanic eruptions, while the anthropogenic forcings are the emissions of ozone-depleting-substances (ODS) and GHGs. To understand and predict the evolution of stratospheric temperatures, it is fundamental to identify and quantify the relative effects of these forcings. This task can be undertaken by comparing the observed and simulated evolution of stratospheric temperatures.

Several studies based on observations have examined the long-term evolution of stratospheric temperatures [e.g., Nash and Forrester 1986; Ramaswamy 2001; Shine et al. 2003; Ramaswamy et al. 2006; Randel et al. 2009; Gillett et al. 2010]. These studies consistently show that global-mean stratospheric cooling has occurred at all heights. Moreover, they show that the time evolution of this cooling is not linear. It took place as two downward steps following the transient warming associated with the volcanic eruptions of "El Chichón" (1982) and Mt. Pinatubo (1991). These volcanic eruptions injected enormous quantities of aerosols into the stratosphere that have two opposite effects on stratospheric temperatures:

1. They heat the stratosphere by absorbing longwave radiation.

2. They indirectly contribute to cool the stratosphere by destroying ozone through heterogeneous chemical reactions over their surface.

Ramaswamy [2006] suggested that the overall long-term cooling is driven by the human emissions of GHGs while the impact of the natural forcings is to modulate the temporal evolution of the cooling. Thompson and Solomon [2009] suggested that the two downward steps are consistent with the superposition of the transient warming due to the aerosol release by volcanic eruption, the combined effects of long-term stratospheric cooling and the transient cooling effect due to enhanced ozone loss after these volcanic eruptions. These findings have been supported by simulations performed with Climate-Chemistry Models (CCMs) forced with increased GHG concentration [SPARC CCMVal 2010].

In 2012, the National Oceanic and Atmospheric Administration (NOAA) Center for Satellite Applications and Research (STAR) group published a new version of the Stratospheric Sounding Units (SSU) dataset [Wang et al. 2012]. The original SSU dataset was published by scientists of the UK Met Office [Nash and Forrester 1986; Nash 1988), and then revised to take into account long-term increase in atmospheric CO2 [Shine et al. 2008] (see section 3.3 for a detailed explanation of SSU datasets). Thompson et al. [2012] showed that the NOAA-SSU data set provides a strikingly different picture of stratospheric temperature trends during the period (1979-2005) when compared with the original MetOffice-SSU data set. Moreover, they showed that there are also large discrepancies on the long-term trends between the two SSU data sets and the ones derived from a suit of state of the art coupled atmosphere-ocean global circulation models (AOGCMs) from the Coupled Model Intercomparison Project Phase 5 (CMIP5) and CCMs from the CCMVal2 archive

[SPARC 2010]. These discrepancies are not only apparent in the global-mean but also in the latitudinal structure of the trends. Figure 3.2 reproduces the figure 3 shown by Thompson et al. [2012]. This figure shows the meridional structure of zonal-mean stratospheric temperature trends between 1979 and 2005. Trends are displayed for four altitude ranges from observations (NOAA-SSU, MetOffice-SSU and MSU4) and a suit of CCM runs available through the CCMVal2 archive. CCM runs are transformed to SSU and MSU4 time series using the appropriated weighting functions (Fig. 3.3). Figure 3.2 shows that the meridional trend structure of NOAA-SSU and MetOffice-SSU largely differ. Moreover the CCM runs do reproduce neither the NOAA-SSU nor the MetOffice-SSU meridional trend structure. Interestingly, the trends of the NOAA-SSU are characterized by larger cooling in the tropics than in the extratropics consistently with an acceleration of the BDC.

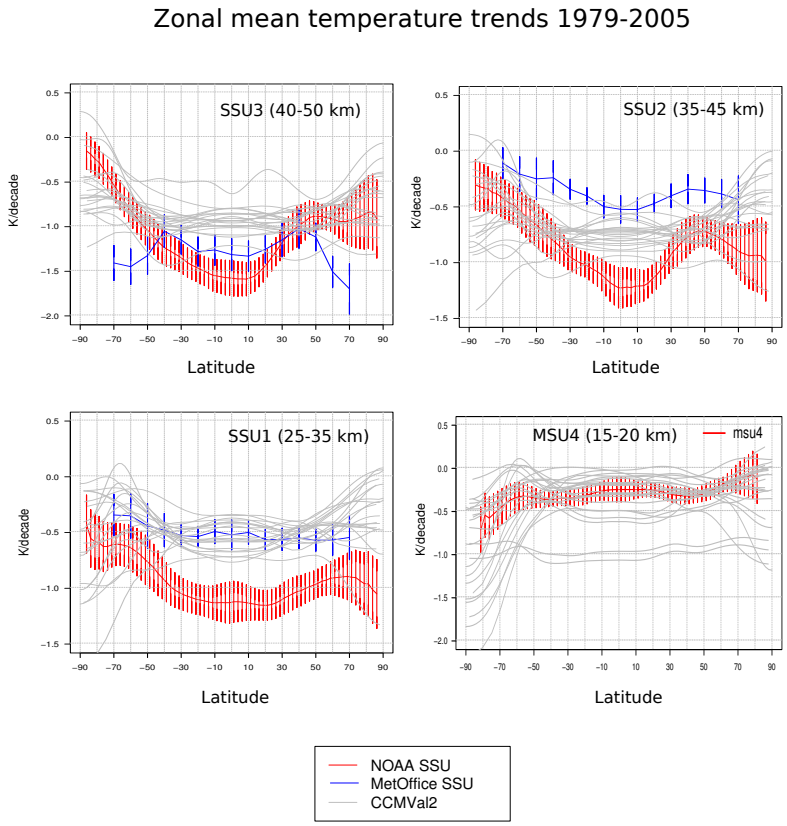

Figure 3.2: Meridional structure of zonal-mean stratospheric temperature trends during the period 1979-2005. Trends are shown for altitude ranges, data sets and model runs as indicated. Vertical error bars indicate the 95% confidence levels. Model runs were transformed to SSU and MSU4 time series using the appropriate instrument weighting functions. Figure adapted from Thompson et al. [2012].

3.4 How Robust are trends in the Brewer-Dobson Circulation derived from observed stratospheric temperatures?

3.4.1 Introduction

The BDC plays a key role in determining the long-term mean climate of the stratosphere. Recent studies suggest that stratospheric climate change may also play a prominent role in long-term variations of the BDC. General circulation models (GCMs) forced with in¬creasing GHG concentrations robustly predict an ac¬celeration of the BDC upward mass flux in the tropics in the 21st century [e.g., Rind et al. 1998; Butchart and Scaife 2001; Sigmond et al. 2004; Butchard et al. 2006].

A strengthening of the upward mass flux in the 21st century is also predicted by many recent coupled CCMs [e.g., McLandress and Shepherd 2009; Butchard et al. 2010; Lin and Fu 2013]. The strengthening of the BDC under increasing GHG concentration scenarios is considered one of the most robust responses found in the cur-rent generation of CCMs [SPARC CCMVal 2010; Forster et al. 2011 and reference therein]. The simulated trend in the BDC has raised interest in stratospheric climate change, and highlights the critical need for high-quality observations to test the predictions of model simulations.

The simulated increases in the tropical upward mass flux associated with the BDC are believed to be due to changes in the penetration of tropospheric wave forcing into the stratosphere under climate change. However, the mechanisms for such changes remain unclear. Butchart et al. [2010], using a large number of model simulations with comparable emission scenarios, found an increase in the annual-mean tropical upwelling in the lower stratosphere of about 2%/decade throughout the 21st century, of which ~60% is due to parameterized orographic gravity wave drag. Increases in orographic wave drag in the lower stratosphere are considered a robust model response to climate change that results from the eastward acceleration of the subtropical jets [Li et al. 2008; McLandress and Shepherd 2009; Butchart et al. 2010]. Other studies suggest that ~60% of the net upward mass flux trend is a consequence of increased planetary wave drag [McLandress and Shepherd 2009]. Calvo and Garcia [2009] concluded that enhanced dissipation of quasi-stationary planetary waves forced by increased tropical convection is responsible for the upwelling trends.

If the simulated strengthening of the BDC were to occur, it would dramatically change the distribution of chemical species in the stratosphere. Ozone would decrease in the tropics and increase at midlatitudes in the lower stratosphere. Shepherd [2008] showed a super-recovery of total ozone in the NH midlatitudes and a decrease in the tropics due to changes in the lower stratospheric ozone concentration in the second half of the 21st century as a consequence of a strengthening BDC. Stratospheric ozone redistribution would also affect tropo¬spheric ozone by changing the

penetration of ultraviolet radiation into the troposphere, thus potentially affecting photolysis rates [Hegglin and Shepherd 2009; WMO 2011], as well as changing stratosphere to troposphere transport of ozone at mid to high latitudes.

Observational support for the simulated strengthening of the BDC remains unclear [Butchard 2014]. The strength of the BDC is characterized in many modeling and reanalysis based studies in terms of tropical upwelling or meridional mass transport. In practice, both quantities are very difficult to diagnose directly from meteorological observations [Seviour et al. 2012; Butchard 2014]. As such, many observational studies of trends in the BDC rely on indirect measurements of the strength of the BDC. Engel et al. [2009] analyzed balloon-borne measurements of stratospheric trace gases and argued that the resulting trends in the mean age of air in the stratosphere do not support any significant long-term trend in the NH branch of the BDC over the past ~30 years. Their results differ from model simulations that predict decreasing trends of the stratospheric mean age [Austin et al. 2006; Austin et al. 2007; Garcia et al. 2007; Garcia and Randel 2008], albeit the simulated trends are within the error bars of the Engel et al. [2009] results. Cook and Roscoe [2009] concluded that there is no significant trend in the BDC over the Southern Hemisphere since 1990 based on NOy measurements over Antarctica. Thompson and Solomon [2009] analyzed the meridional structure of ozone column and lower-stratosphere temperatures from observations and concluded that the meridional structure of the ozone trends is consistent with a strengthening of the BDC since the late 1970s. Lin et al. [2009] found increasing extratropical temperatures in the SH, indicative of a strengthening of the BDC. Fu et al. [2010] presented evidence that the seasonality of tropical lower-stratospheric temperature trends is a consequence of changes in the BDC driven by extratropical wave forcing.

Reanalysis fields have also been used to diagnose the strength of the BDC over the last decades. Iwasaki et al. [2009], analyzing the BDC from five reanalysis (JRA-25, ERA-40, ERA-Interim, NCEP/NCAR and NCEP/DOE), concluded that, although the climatological mean states are consistently captured by reanalysis, the yearly trends are not reliable due to the large discrepancies between results derived from the different reanalysis. Seviour et al. [2012], using ERA-Interim reanalysis, showed a decrease in the upwelling mass flux in contrast to the increase projected by models, even though the reanalysis reproduced the major features of the BDC. On the other hand, Garny et al. [2010] found agreement between modeled tropical upwelling and its wave forcing and that in the ERA-Interim analysis.

Since the BDC is associated with large-scale variations in vertical motion, temperature measurements can also be used to infer changes in the strength of the BDC. Young et al. [2012] provided the most comprehensive study to date of observationally based trends in the BDC using both Microwave Sounding Unit (MSU) and Stratospheric Sounding Unit (SSU) observational stratospheric temperature data. The authors exploited the relationship between tropical and extratropical temperatures and the interannual variation in circulation's strength [Ueyama and Wallace 2010; Young et al. 2011] to empirically derive a temperature-based BDC Index (BDCI)

over 1979-2005. Their results are consistent with a strengthening of the NH branch of the BDC during December throughout the depth of the stratosphere, and with a significant strengthening of the SH branch of the BDC during August from the MSU Total Lower Stratosphere (TLS) level to the mid-stratosphere SSU-26 level. They also found a significant weakening of the NH BDC branch during March that is consistent with a change in the seasonal cycle of the circulation.

The results showed by Young et al. [2012] above the lower stratosphere are based entirely on a version of the SSU data produced by the UK Met Office. As stated in section 3.2, in 2012, the National Oceanic and Atmospheric Administration (NOAA) Center for Satellite Applications and Research (STAR) group published a new version of the SSU dataset [Wang et al. 2012]. As stated in section 3.2, stratospheric temperature trends derived from the NOAA-SSU and the previous MetOffice-SSU datasets yield strikingly different results [Wang et al. 2012 and Thompson et al. 2012]. This is true not only in terms of the global-mean trends, but also in terms of the latitudinal structure of the trends. The marked differences between the Met Office and NOAA versions of the SSU data suggest that the observed trends in the BDC will differ widely from one SSU dataset to another.

The purpose of this chapter is to revisit the observational evidence of the strengthening of the BDC over the past few decades using the suite of currently available temperature measurements. We will examine trends in the BDC as inferred from a range of observational data sets (NOAA-SSU, MetOffice-SSU, MSU TLS, RATPAC and RICH radiosonde) and two meteorological reanalyses (ERA-Interim and MERRA).

3.4.2 Data

3.4.2.1 Satellite data

We analyze satellite brightness temperature data from the MSU and SSU instruments, both of which are part of a series of consecutive NOAA operational polar-orbiting satellites. We use lower stratospheric data processed by the Remote Sensing Systems (RSS) [Mears and Wentz 2009], combining channel 4 from MSU (MSU4) and channel 9 from the Advanced Microwave Sounding Unit (AMSU). The monthly mean brightness temperature is provided on a 2.5° x 2.5° horizontal grid spanning from 82.5° S to 82.5° N over the period 1979-2005. MSU4 provides global coverage of temperature in an atmospheric layer between roughly 13 and 22 km, covering mainly the lower stratosphere in the extratropics but also part of the upper troposphere in the tropics (Figure 3.3).

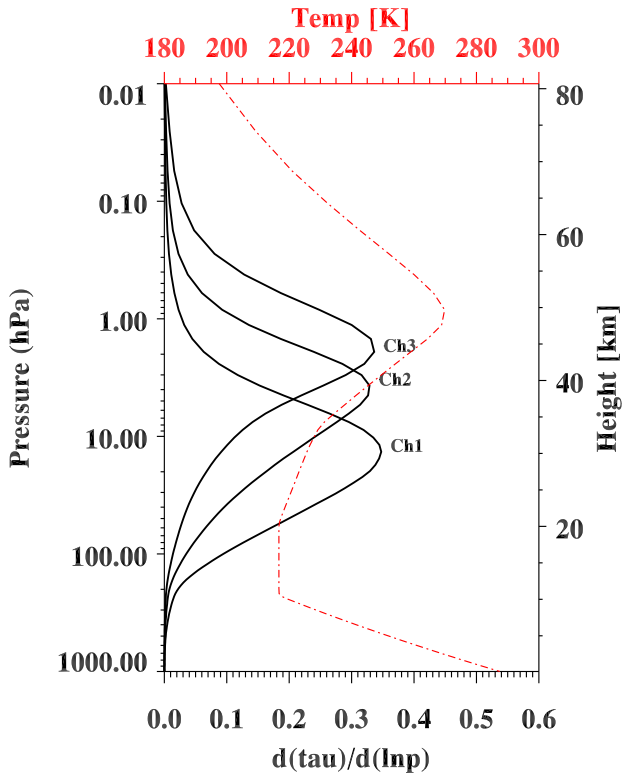

Figure 3.3: Weighting functions for MSU4 and the SSU channels. SSU 25, SSU 26 and SSU 27 correspond to the three SSU channels analyzed on this study. The weighting function describes the relative contribution that the radiation of a particular layer makes to the total radiation received above the atmosphere by the satellite. Figure courtesy of Remote Sensing Systems (reproduced with permission).

Channels 1, 2 and 3 of the SSU data set have their weighting functions centered at approximately 30, 40 and 45 km (Figure 3.3), respectively, and have been used to analyze the temperature in the mid and upper stratosphere. The SSU instrument consists of a pressure-modulated radiometer that senses temperature in the infrared CO2 band of 15 µm. The SSU data are the only long time period near-global coverage source for temperature in the middle and upper stratosphere; the data is available from 1979 to 2005. As stated in section 3.2, the temperatures derived from the different SSU channels have been analyzed in previous studies to assess stratospheric temperature trends (cited above). However, the use of the SSU data for climate studies requires consideration of specific calibration issues. These issues include: 1) gas leaking has occurred in all SSU pressure cells over time, causing changes in the altitude being measured by the instrument, 2) at high altitudes, the diurnal and semidiurnal tidal variations become large, and thus satellite orbital drift and orbital changes between the different satellite missions can lead to large biases in temperature, 3) long term changes in carbon dioxide concentrations have led to an upward drift of the satellite weighting functions with time [Shine et al. 2008],

and 4) some consecutive satellite missions do not have overlapping data to facilitate the merging of the radiances.

Here we use two SSU temperature datasets that have been processed independently. The first dataset consists of corrected SSU brightness temperatures derived from the pioneering work conducted by scientists of the UK Met Office [Nash and Forrester 1986; Nash 1988], and then revised to take into account long-term increases in atmospheric CO2 [Shine et al. 2008]. The Met Office SSU temperature data are available as monthly zonal mean anomalies on a 10° latitude grid covering from 70° S to 70° N. The data is hereafter referred to as 'MetOffice SSU'. The second dataset consists of recently reprocessed SSU radiances by the NOAA STAR group. The data are available on a 2.5°x2.5° horizontal grid covering from -87.5° S to 87.5° N for the period 1979-2005. Details of the data processing are provided by Wang et al. [2012]. The NOAA temperature product is hereafter referred to as 'NOAA SSU'.

3.4.2.2 Reanalysis datasets

We also analyze temperature data from two meteorological reanalyses: ERA-Interim [Dee et al. 2011] and the Modern-Era Retrospective for Research and Applications (MERRA) [Rienecker et al. 2011]. The European Centre for Medium-Range Weather Forecasts (ECMWF) ERA-Interim dataset incorporates observations from radiosondes, balloons, dropsondes, aircraft and satellites such as MSU and SSU that are assimilated with the 4D-Var ECMWF Integrated Forecast System (IFS) model [Seviour et al. 2012; Simmons et al. 2007]. Ozone column and profile retrievals are assimilated in the reanalysis [Dragani 2010], but they are only used in the radiation scheme [Seviour et al. 2012]. Ozone assimilation causes large and unrealistic changes in temperature and winds near the top of the model, where the flow is not well constrained by observations [Dee et al. 2011]. Those problems are temporally solved modifying the analysis scheme to prevent any direct influence of ozone on the dynamic fields, so the ozone assimilations only modify the ozone field itself. We use the version provided from 1979 onwards at 6 hourly temporal resolutions on a 1.5° x 1.5° horizontal grid at 37 discrete pressure levels with a model top at 1 mb.

The National Aeronautics and Space Administration (NASA) MERRA reanalysis was generated with version 5.2.0 of the Goddard Earth Observing System (GEOS) atmospheric model and data assimilation system (DAS) [Rienecker et al. 2008]. MERRA, like ERA-Interim, incorporates observations from radiosondes, balloons, dropsondes, aircraft, buoys and satellite data that are assimilated with a 3D-VAR analysis algorithm based on the Gridpoint Statistical Interpolation scheme (GSI) [Wu et al. 2002; Derber et al. 2003; Purser et al. 2003 a,b]. MERRA processes the satellite radiances of the SSU instrument with a specific algorithm to take into account the leaking problems with the CO2 pressure cells but the effect of the sensitivity of the SSU weighting functions to changes in atmospheric CO2 is not corrected. We use the version provided from 1979 onwards at 6 hourly temporal

resolutions on a 0.5° x 0.5° horizontal grid at 22 discrete pressure levels with a model top at 0.1 mb.

3.4.2.3 Radiosondes

We use two related radiosonde products to assess trends in the lower stratosphere. The Radiosonde Atmospheric Temperature Products for Assessing Climate B (RATPAC-B) [Free et al. 2005] provides monthly mean temperature anomalies at 13 pressure levels from surface to 30 mbar for 85 globally distributed stations. The monthly means from 1958 to 1997 were adjusted by a team of climate scientists using a multifactor analysis without satellite data as references with minimal use of neighbour station comparisons (see Free et al. [2005] and reference therein). The dataset was extended with the Integrated Global Radiosonde Archive (IGRA) [Durre et al. 2006] from 1997 onward without any adjustment for inhomogeneities. Free et al. [2005] calculated an uncertainty in global mean trends from 1979 to 2004 of less than 0.15 K/decade in the stratosphere at individual pressure levels. The 00Z and 12Z combined observations were binned into 10°-wide latitude bands to determine zonal mean temperature anomalies and subsequently the global weighted mean anomalies.

The second dataset is the Radiosonde Innovation Composite Homogenization product (RICH) [Haimberger et al. 2012]. RICH is built using more than 1000 daily station records from the global radiosonde network and it constructs the reference series for homogenization from composites of neighboring radiosonde station temperature anomalies. Therefore its homogenization estimates are independent of the satellite data. RICH provides homogenized temperature anomalies at 10 discrete pressure levels ranging from 850 mb to 30 mb for the period 1958 -2012 on a 5º x 5º horizontal grid resolution.

We use radiosonde data at 100, 70, 50 and 30 mb, i.e., the levels that lie within the vertical range of MSU and SSU1 instruments.

3.4.3 Inferring trends in the BDC from temperatures

As show in Chapter 1, the BDC can be approximated from the transformed Eulerian mean (TEM) residual circulation, which provides an estimate of large-scale atmospheric transport. The linearized version of the TEM thermodynamic energy equation (equation 1.10, chapter 1) relates the stratospheric temperature tendency to the vertical motion due to the BDC:

$$\frac{\partial \overline{T}}{\partial t} = -\alpha_r \left(\overline{T} - \overline{T}_r \right) - \overline{w}^* S \tag{3.1}$$

where $\frac{\partial \overline{T}}{\partial t}$ is the local temperature tendency; the diabatic term $\frac{\overline{J}}{c_p}$ has been approximated in terms of a Newtonian relaxation proportional to the departure of temperature to its radiative equilibrium value $-\alpha_r \left(\overline{T} - \overline{T}_r\right)$ with a time scale $1/\alpha_r$(see equation 1.15 chapter 1); $\overline{w}^* S$ denotes the adiabatic cooling (warming) associated with the upward (downward) flow with residual vertical velocity $\overline{w}$ and $S = N^2 H R^{-1}$is the static stability parameter.

As demonstrated by Yulaeva et al. [1994], the BDC is clearly apparent in the out-of-phase seasonal cycle between extratropical and tropical mean temperatures. They also showed that the month-to-month temperature changes in the tropics and extratropics are significantly anticorrelated, indicating compensation between compressional warming and expansional cooling Moreover, they suggested that the observed out-of-phase seasonal cycles in the lower stratosphere temperature between the tropics and extratropics are controlled by the strength of the extratropical wave driving and hence by the BDC.

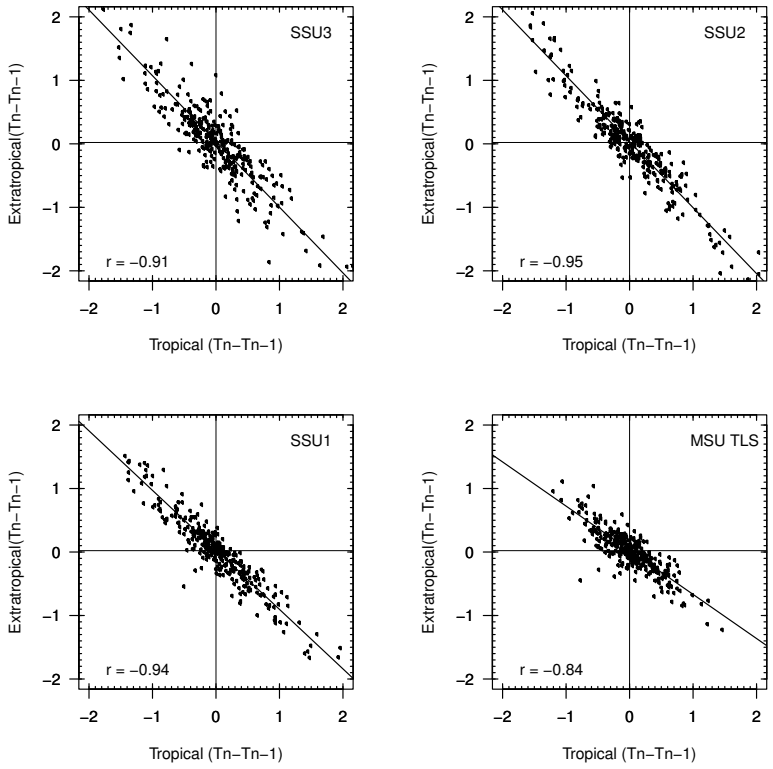

Figure 3.4: Scatterplot of the month to month change in temperature anomalies for the tropics (20ºS-20ºN) against extratropics (poleward of 30ºS and 30ºN) for the MSU4 (MSU TLS) and the three NOAA-SSU channels. Correlation coefficients are also given. Years 1982, 1991 and 1992 have been excluded to avoid the potential influence of the El Chichon and Mt Pinatubo eruptions.

Young et al. [2011] used the Met Office SSU data to extend the analysis of Yulaeva et al. [1994] into the middle and upper stratosphere. They demonstrated that the out of phase relationship between tropical and extratropical stratospheric temperatures (which is indicative of variability in the BDC) also extends to the middle and upper stratosphere. Figure 3.4 shows a scatterplot of the month to month change in temperature anomalies for the tropics (20ºS-20ºN) against extratropics (poleward of 30ºN and 30ºS) for the MSU4 (MSU TLS) and the three NOAA-SSU channels during 1979-2005. This figure clearly shows that tropical and extratropical temperatures are strongly anticorrelated throughout the stratosphere.

The BDC has a very weak signature in the tendency in global-mean temperatures, since regions of rising motion and adiabatic cooling are compensated by regions of sinking motion and adiabatic warming [Yulaeva et al. 1994 and Rosenlof 1995]. Hence, trends in the BDC should be most clear not in global-mean stratospheric temperature trends, but rather in the horizontal structure of the temperature trends. For this reason, we examine all temperature trends as "departures" from the global-mean, that is:

$$Trend(T^*) = Trend\,(T_{zonal} - T_{global}) \tag{3.2}$$

Where Tzonal is the zonal-mean temperature anomaly and Tglobal is the weighted global mean temperature anomalies. Presumably, trends in the departure temperature field are not strongly affected by trends due to well-mixed greenhouse gases, although any forcing that includes a latitudinal gradient (e.g., the ozone hole or the meridional gradient of the GHG heating rates) will project onto T*.

To gain further insight, we calculate trends for a temperature based BDC index (BDCI) defined as the cosine-weighted extratropical mean temperature anomalies of a given hemisphere minus the cosine-weighted tropical mean temperature anomalies for each month.

$$BDCI = T_{extr} - T_{trop} \tag{3.3}$$

Positive trends in the BDCI indicate warming in the extratropics juxtaposed against cooling in the tropics that may indicate an acceleration of the BDC [Young et al. 2012].

To test the ability of the BDCI to capture the evolution of the BDC we use the outputs of the Whole Atmosphere Community Climate Model (WACCM) [Garcia et al. 2007, and references therein) to compare trends in the temperature-based BDCI (from here after BDCI_T) with trends in a newly defined BDCI based on the TEM residual vertical velocities (W^*) that we assume, as a hypothesis, represents the "real" BDC.

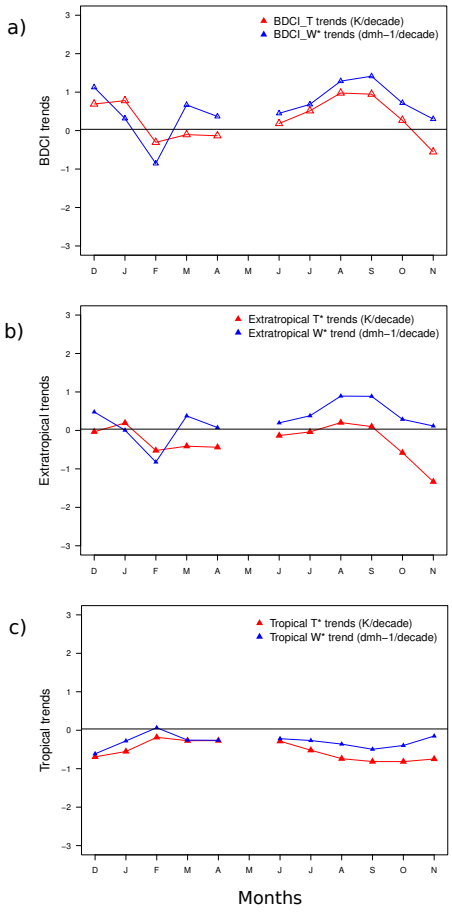

Figure 3.5: **(a)** Seasonal BDCI_T trends and BDCI_W* trends at 70 mb for the WACCM model (the sign of W^*has been reversed to facilitate comparison). **(b)** Seasonal extratropical T^* trends and W^* trends at 70 mb for the WACCM model. **(c)** Seasonal tropical T^* trends and W^* trends at 70 mb for the WACCM model. Note that from December to April the BDCI_T trends are computed for the NH and from June to November for the SH. May has been excluded to the analysis because extratropical temperatures are well correlated with the tropical ones neither in the NH nor in the SH.

$$BDCI\_W^* = W^*_{extr} - W^*_{trop} \tag{3.4}$$

where W^*_{extr} is the extratropical (from 40º to 80º in the NH or in the SH depending on the month) W^*cos-weighted mean and $W^*_{trop}$the tropical (-20º to 20º) W^*cos-weighted mean.

Figure 3.5 shows the trends in BDCI_W* and BDCI for each month at 70 mb. Note that a positive trend in the BDC mass flux would lead to a negative trend in the BDC_W* (increased downwelling in the extratropics linked with increased upwelling in the tropics) and a positive trend in the temperature based BDCI. According to Fig. 3.5 (note that the sign of W* has been reversed to facilitate comparison with BDCI), trends in the BDCI_W* and BDCI match reasonably well from June to September in the SH and during December and somewhat in January and February in the NH, hence suggesting that at least during these months the BDCI should be suitable to infer trends in the BDC. On the contrary, the indices do not match during November in the SH and during March-April in the NH and, hence the BDCI seems inadequate to infer trends in the BDC. Note that the months where the BDCI_W* and BDCI are not juxtaposed coincide with the timing of maximum ozone depletion in the SH (October- November) and in the extratropical NH (March-April). We can test that comparing trends for the extratropical temperature means versus the trends for the extratropical W* mean (Fig. 3.5b) and the corresponding for the tropics (Fig. 3.5c). Figure 3.5c shows that the trends in the temperature and W* means are quite similar in the tropics but they are not in the extratropics. These results suggest that the BDCI have to be interpreted carefully during months with strong ozone depletion at high latitudes.

Trends for temperature time series and for the BDCI were calculated using least-square linear regression applied to monthly-mean binned temperature data over the period 1979-2005. Years 1982, 1991 and 1992 are excluded from the analysis to avoid potential influences on the trends due to the transient warming after the El Chichón and Pinatubo eruptions in 1982 and 1991, respectively. Year 2002 has also been removed to avoid the influence of the September major stratospheric warming event in the SH [Newman and Nash 2005]. The significance of the trends was assessed using the methodology outlined by Santer et al. [2001] that accounts for the autocorrelation of the series.

3.4.4 Results

3.4.4.1 Temperature trends in satellite data

Figure 3.6 displays the zonal-mean temperature trends as a function of month and latitude for the four layers sampled by the MSU4 and the SSU instruments. The left column shows results for the NOAA-SSU data; the right column results for the MetOffice-SSU data and the bottom plot, the corresponding MSU4 trends. Trends are determined using the *departure* of local zonal-mean temperatures from the global-mean, T* that, as discussed in Section 3, are to first order linearly independent of changes in well-mixed greenhouse gas concentrations, and primarily reflect changes due to either 1) dynamics and/or 2) spatially inhomogeneous radiative forcing, such as that due to the ozone hole.

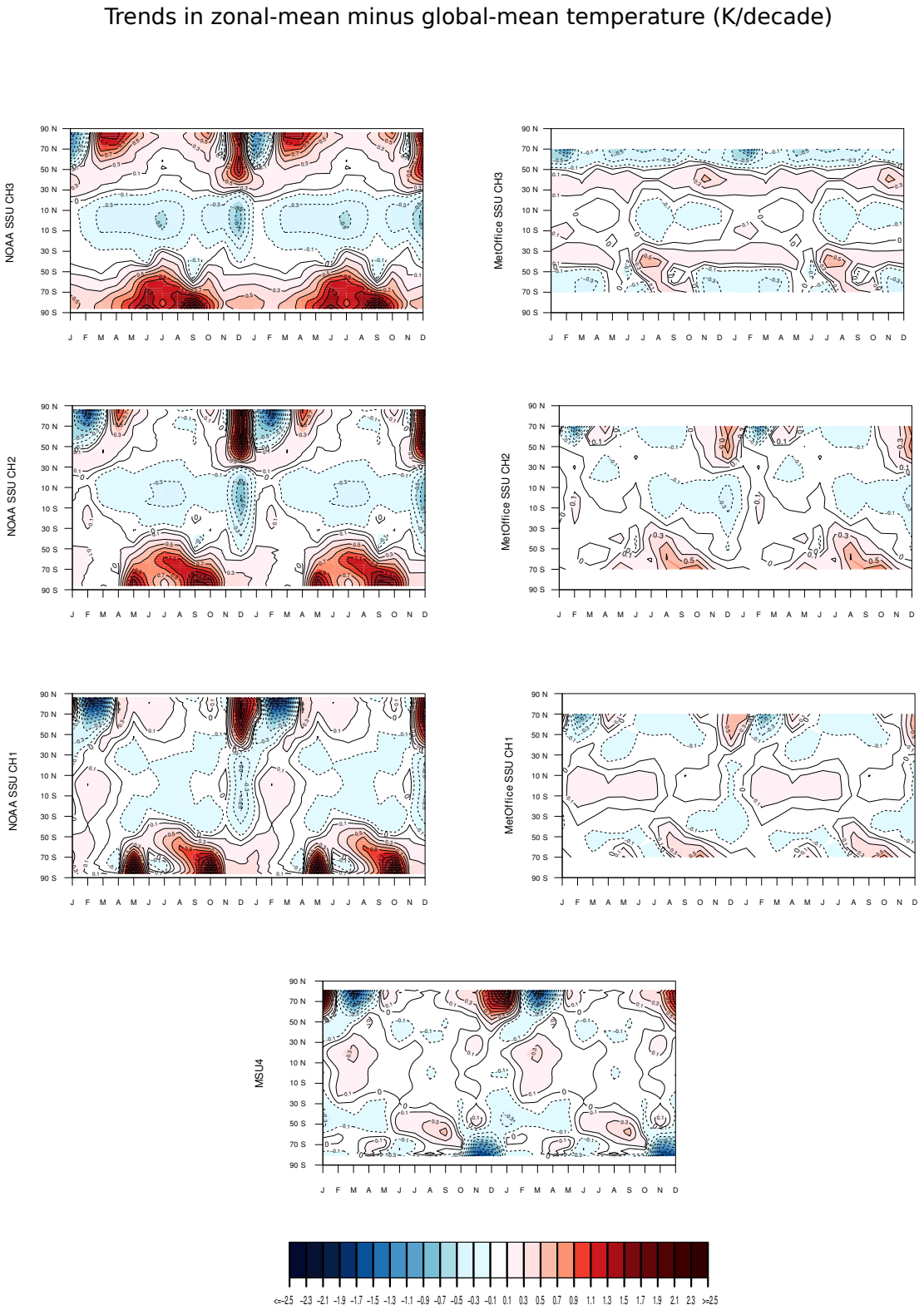

Figure 3.6: Zonal-mean T* trends as a function of month and latitude for the four layers sampled by the MSU4 and the NOAA and MetOffice SSU products. Note that we show two complete seasons for clarity.

The three NOAA-SSU channels all show marked cooling in the tropical stratosphere that is juxtaposed against warming both in the NH and in the SH polar regions during December and during SH winter, respectively. Although the distinct meridional structure in the trends is consistent with a strengthening of the upper branch of the BDC in both hemispheres during the winter season in the last three decades, trends are not statistically significantly different from the global mean trend for most of the channels. Only some seasonal T* trends at the top of the stratosphere (CH3) are significant at 2σ level at high latitudes during summer seasons in both hemispheres and during equinox months in the SH (Fig. 3.7). The lack of significance is attributable to the large interannual variability of high latitude temperatures compared with the relatively weak magnitude of such trends. Zonally asymmetric patterns at high latitudes may dilute the zonal mean warming signals, contributing also to the lack of significance [Young et al. 2011 and references therein]. The only region marked by cooling in the polar-regions is over the far NH during January-February for NOAA-SSU CH3 and during February-March for CH2 and CH1. The cooling of the NH polar cap during midwinter can only be partially explained by radiative cooling from ozone loss because the Arctic ozone depletion is much smaller than that in the Antarctic [Randel and Wu 1999; Solomon 1999]. Moreover, the cooling of the NH polar cap during January-February is paired with weak warming over the subtropics that indicate a possible dynamical contribution to the observed cooling. Fu et al. [2010] noted that similar cooling found in MSU4 is consistent with a weakening of the BDC in the NH spring. Nevertheless, neither the high latitude cooling nor the weak tropical warming is statistically significantly different from the zonal mean trends at any level.

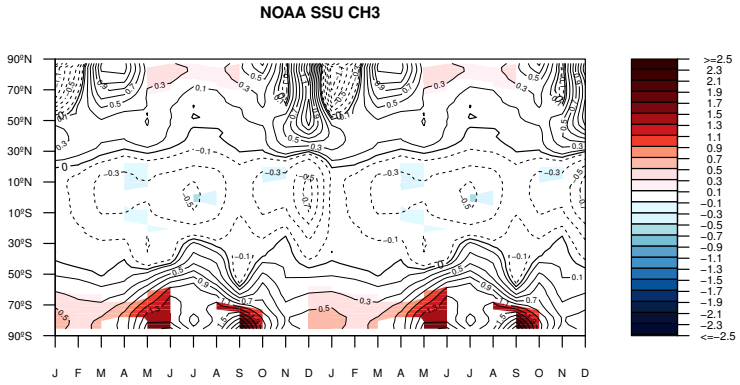

Figure 3.7: Zonal-mean T* trends as a function of month and latitude for the NOAA-SSU CH3 with shaded regions showing zonal temperature trends statistically significantly different from the global mean trend at 2σ level.

The MetOffice-SSU dataset yields a very different picture of recent stratospheric temperature trends than NOAA-SSU. The trend pattern of MetOffice-SSU3 is char-

acterized by a year-round warming trend centered at 40º S and 40º N that is most marked in winter months. These warming trends observed in the departure temperature field are in agreement with the minimum cooling in the MetOffice-SSU3 temperatures reported by Randel et al. [2009] and Young et al. [2012] but removing the effect of trends in the GHGs concentration. The out of phase pattern of the trends between tropical and polar latitudes observed in NOAA-SSU3 data is not apparent during any month. The Met Office SSU2 shows a very weak cooling in the tropics that is juxtaposed against a weak warming over SH during SH winter, and against a weak warming in the NH polar cap during December. The same warming pattern, although weaker, is derived from MetOffice-SSU1 at high latitudes in the winter hemisphere but no simultaneous tropical cooling is detected. Any zonal MetOffice-SSU trend is significantly different from the trend in the global-mean.

In the lower stratosphere, the MSU4 temperature trends show a high-latitude warming centered on December-January in the NH and a weak warming in the SH during August-September that are not linked with any tropical cooling. In the SH, temperature trends show a strong cooling of more than -1.4 K/decade centered on November-December that is attributable to the late spring radiative ozone cooling. Lin et al. [2009] pointed out that the near-zero trend in October is a consequence of zonal asymmetries in the SH high latitudes that almost cancel the zonal-mean trend meanwhile the radiative induced ozone cooling overwhelms the dynamical warming. In any case zonal mean trends in the lower stratosphere are not statistically significantly from the global-mean.

Figure 3.8 shows BDCI trends computed from December to April in the NH and from June to November in the SH. Statistically significant BDCI trends are represented with filled triangles and non-significant ones with open triangles. The shaded areas indicate the two-sigma error bars of the BDCI trends for each NOAA-SSU and MetOffice-SSU channels and for MSU4. The interannual variance in the BDCI time series is larger than the trends for almost every month in each channel and hence the trends in the BDCI are not significant. The only exceptions are for NOAA-SSU3 in the SH during October and November and in the NH during April where the variance is smaller. Despite that, it is worthy of note that for all of the NOAA-SSU channels as well as for the MSU4, trends in the BDCI are significant and positive during December assuming a 90% significant level instead of the 95% level considered in this analysis.

Our analysis leads different conclusions than Young et al. [2012] and Fu et al. [2010]. To construct the BDCI, Young et al. [2012] first calculated the tropical (20°S-20°N) and extratropical (>40° N for NH and >40°S for SH) mean temperature anomalies for each month and then the regression coefficients between the detrended tropical and extratropical time series. The significant anticorrelation between tropical and extratropical temperatures was used to “remove” the common BDC-like interannual variability.

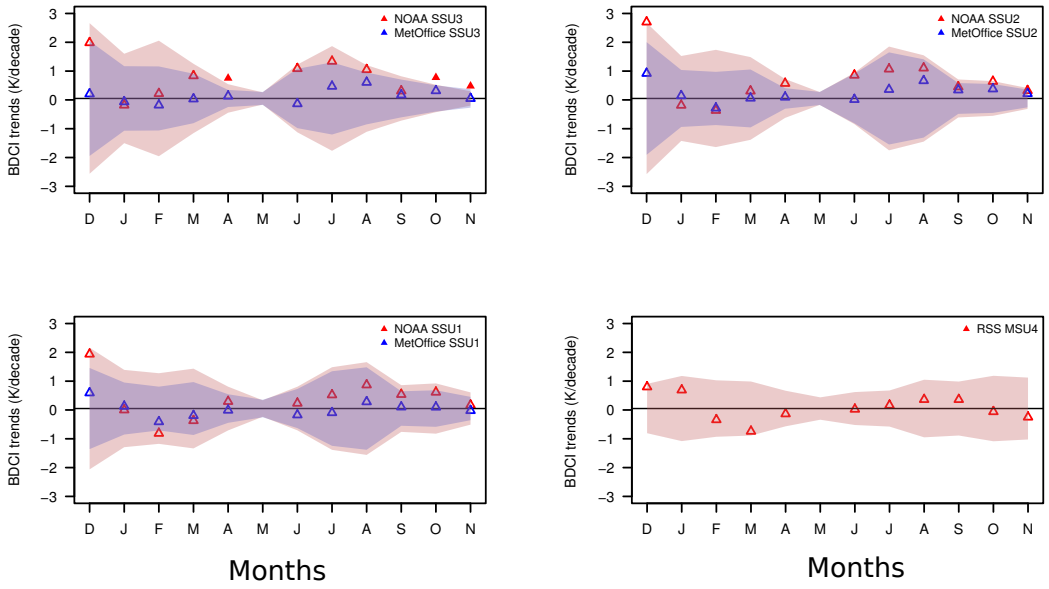

Figure 3.8: BDCI_T trends as a function of month for the four layers sampled by the MSU4 and the NOAA and MetOffice SSU products. Shaded areas represent the two sigma error bars of the BDCI_T trends for each level and data product. Note that from December to April the BDCI_T trends are computed for the NH and from June to November for the SH. May has been excluded to the analysis because the extratropical temperatures are well correlated with the tropical ones neither in the NH nor in the SH. Filled (open) triangles indicate statistically (non-statistically) significantly different from the global mean trends.

Finally, the original time series were adjusted and the BDCI computed (Eqs. 3.5 to 3.7).

$$T^*_{trop} = T_{trop} - r_1 T'_{extr} \tag{3.5}$$

$$T^*_{extr} = T_{extr} - r_2 T'_{trop} \tag{3.6}$$

$$BDCI^* = T^*_{extr} - T^*_{trop} \tag{3.7}$$

Where "trop" and "extr" subscripts refer to tropical and extratropical; T*, T' and T correspond to adjusted, detrended and original temperature time series and r1 and r2 are the regression coefficients for the tropics against extratropics and extratropics against tropics, respectively. BDCI* stands for adjusted BDC Index. Using temperature anomalies from the MetOffice-SSU, the MSU4 and the Iterative Universal Kriging (IUK) radiosonde dataset [Sherwood et al. 2008], Young et al. [2012] show that the trends in the BDCI* are consistent with an acceleration of the NH branch of the BDC during December throughout the depth of the stratosphere. They found statistically significant positive trends in the BDCI* for January and February and a significant negative trend during March both in the MSU4 and the IUK datasets. In the SH they show significant positive trends during August from the MSU4 level to the SSU-CH2 level that may indicate an acceleration of the SH branch of the BDC. Nevertheless, they stated that the trends in the non-adjusted BDCI are not statistically significant. Here we argue that removing the "BDC-like" variability lead to unrealistically significant trends and hence trends in the BDC should be viewed in the non-adjusted BDCI instead of in the adjusted BDCI. Therefore the actual satellite based temperature time series are not consistent with an acceleration of the BDC in the last three decades. If a real trend actually exists, it is still not possible to distinguish from the large variability in the time series.

Fu et al. [2010] argue that MSU4 temperature trends for the period 1980-2008 are consistent with a significant acceleration of the BDC from June to November in the SH and from December to February in the NH. They also show that the trends are consistent with a weakening of the BDC during March. Our analysis of the MSU4 temperatures reproduces the main features found by Fu et al. [2010]: strong warming over NH pole cap during December-January followed by a strong cooling juxtaposed against subtropical warming during March. Nevertheless, here we argue that trends in the BDC should be better represented by trends from T* instead of by trends from Tzonal (Eq. 3.2). Our zonal T* trends are not statistically significantly different from the global mean and moreover the high latitude warming both in the NH and in the SH are not linked with any tropical cooling. Presumably, direct radiative forcing has only induced stratospheric cooling over the last three decades [Shine et al. 2003; Ramaswamy et al. 2006]. Hence, if there were a positive trend in tropical upwelling, we would also expect to find cooling in the tropics when removing the temperature global mean anomalies from our zonal time series. Therefore, unlike Fu et al. [2010], our MSU4 trends are not consistent with an acceleration of the BDC over the last three decades in the lower stratosphere. Even so, an acceleration of the NH lower branch of the BDC cannot be completely discarded because the MSU4 weighting function contains part of the upper troposphere that has warmed up during the last decades, possibly masking the lower-stratosphere tropical cooling.

3.4.4.2 Temperature trends in Radiosonde datasets

Radiosondes are an invaluable source of temperature data. In order to assess

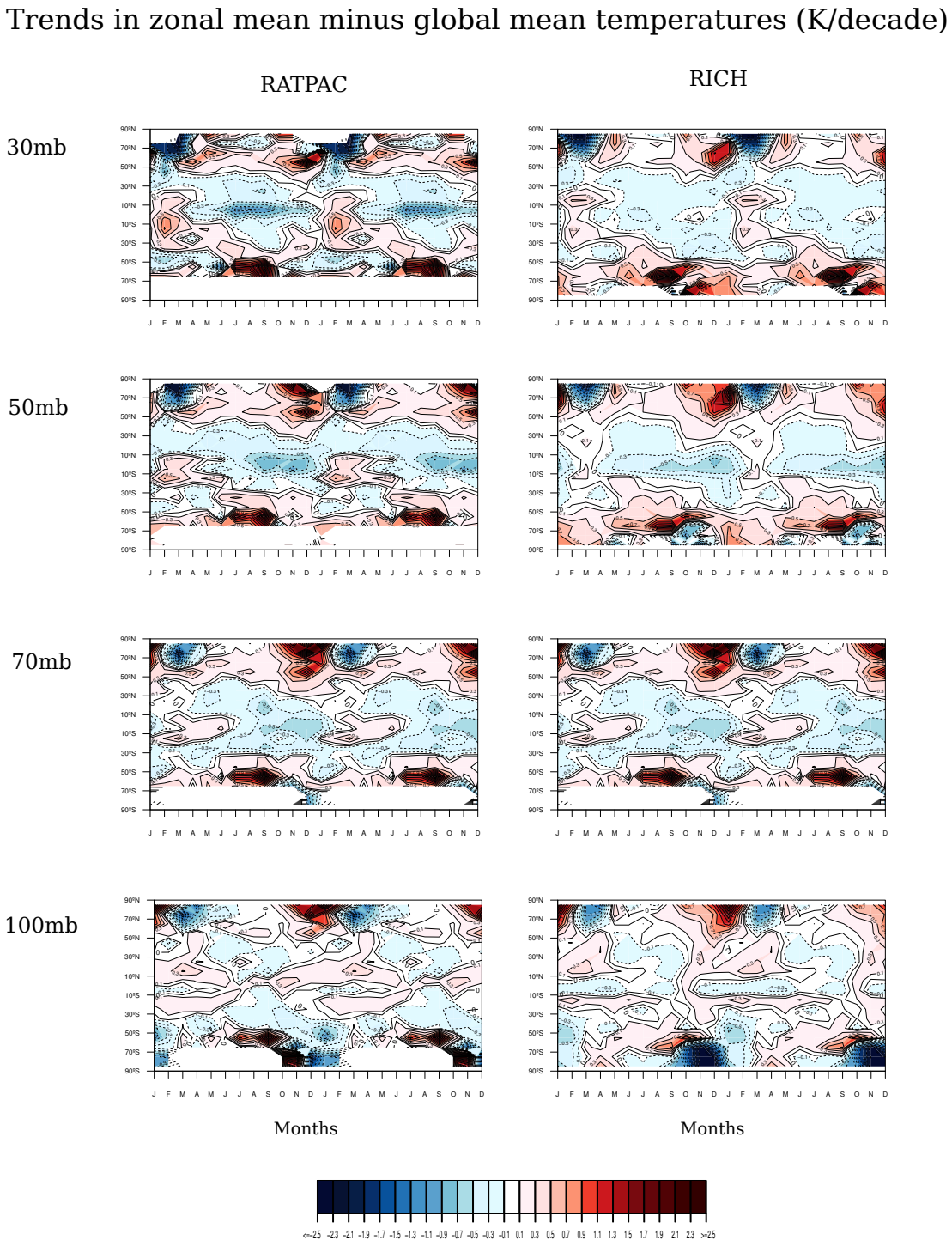

Figure 3.9: Figure 3.9 Zonal-mean T* trends as a function of month and latitude at four pressure levels sampled by RATPAC and RICH radiosonde products. No filled areas indicate that no data is available over this latitude for the month considered. Note that we show two complete seasons for clarity.

the robustness of the observed trend structure, we computed trends for the RICH andRATPAC radiosonde datasets that by construction are almost completely independent of satellite radiances.

Figure 3.9 shows the trends in T* as a function of month and latitude at four individual pressure levels from 100 mb to 30 mb, so mainly covering the lower and mid-stratosphere. Radiosonde data have a limited and irregular spatial coverage, especially over oceans and high latitudes, and the sparse longitudinal distribution can bias some latitudinal bands to certain longitudes. Despite that, both RATPAC and RICH datasets reasonably reproduce the pattern and magnitude of temperature trends for the MSU4 and NOAA SSU1, although the structures are noisier, especially for RATPAC data due to the irregular spatial distribution. At 50 mb and 70 mb both RATPAC and RICH show extended cooling in the tropics juxtaposed against warming in the NH polar cap and against warming in the SH high latitudes during late spring although none of this trends are statistically significantly different from the global mean. The cooling observed in March is also well reproduced at 50 mb and 70 mb for both datasets. Similar results were found by Young et al. [2011] using IUK radiosonde data at 30 mb. In the SH, the ozone-induced cooling in late spring is well reproduced for RICH data which has better coverage than RATPAC in the SH high-latitudes. The largest discrepancies between radiosonde datasets are detected in SH high latitudes during spring when a strong warming at 100 mb is observed in RATPAC but not in RICH radiosondes. The sampling longitude bias in the binned means, as well as the individual adjustment procedures might be responsible for these differences.

Figure 3.10 displays the BDCI trends and the 2σ error bars (shaded region) for the RATPAC and RICH datasets. RATPAC shows positive and statistically significant trends of the order of 3 K/decade during December and January at 50 mb and 30 mb and from December to February at 70 mb; this indicates a possible acceleration of the lower branch of the BDC in the NH in winter months. RICH also exhibits a positive and significant BDCI trend in December at 50 mb and 70 mb although the magnitude is weaker compared with RATPAC. All three RATPAC levels show positive and significant BDCI trends in April of the order of 2K/decade that are not reproduced by RICH. In the SH, RATPAC is characterized by a very large variance due to the sparse radiosonde coverage. The process of homogenization in RICH largely reduces the variance in the SH, but as is the case for RATPAC, the BDCI does not show any significant trend for any month.

3.4.4.3 Temperature trends in Reanalysis

Figure 3.11 shows the trends in T* for MERRA and ERA-Interim reanalysis as a function of month and latitude. Temperature anomalies are weighted by the MSU4 and the three SSU channel weighting functions to obtain data layers comparable to the NOAA, MetOffice and MSU4 datasets. Trends are computed depending on the

level top of the dataset, so no reanalysis has high enough model top to accurately represent the top stratosphere, and ERA-Interim is only representative

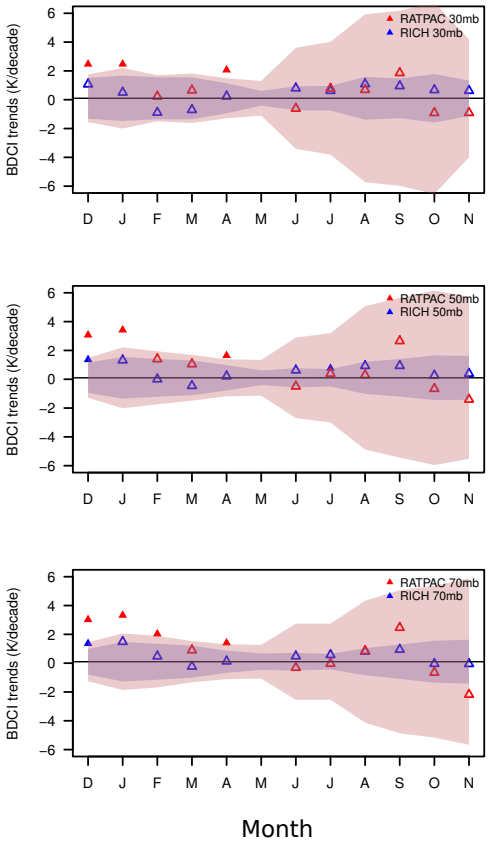

Figure 3.10: BDCI_T trends as a function of month for three layers sampled by RATPAC and RICH radiosonde products. Shaded areas represent the two sigma error bars of the BDCI_T trends for each level and data product. Note that from December to April the BDCI_T trends are computed for the NH and from June to November for the SH. May has been excluded to the analysis because the extra-tropical temperatures are no well correlated with the tropical ones neither in the NH nor in the SH. Filled (open) triangles indicate statistically (non-statistically) significantly different from the global mean trends.

for the low and mid-stratosphere. The three MERRA levels plotted in Fig. 3.11 show weak warming in the tropics throughout the year except during December for MERRA-CH1 and during January for MERRA-MSU4. The December-January tropical cooling is juxtaposed with a strong warming over the NH pole cap that is followed by a strong cooling during March coinciding with warming in the tropics. In the SH high latitudes, the MERRA-CH2 and MERRA-CH1 show a warming trend during September-October whereas MERRA-MSU4 displays a strong cooling

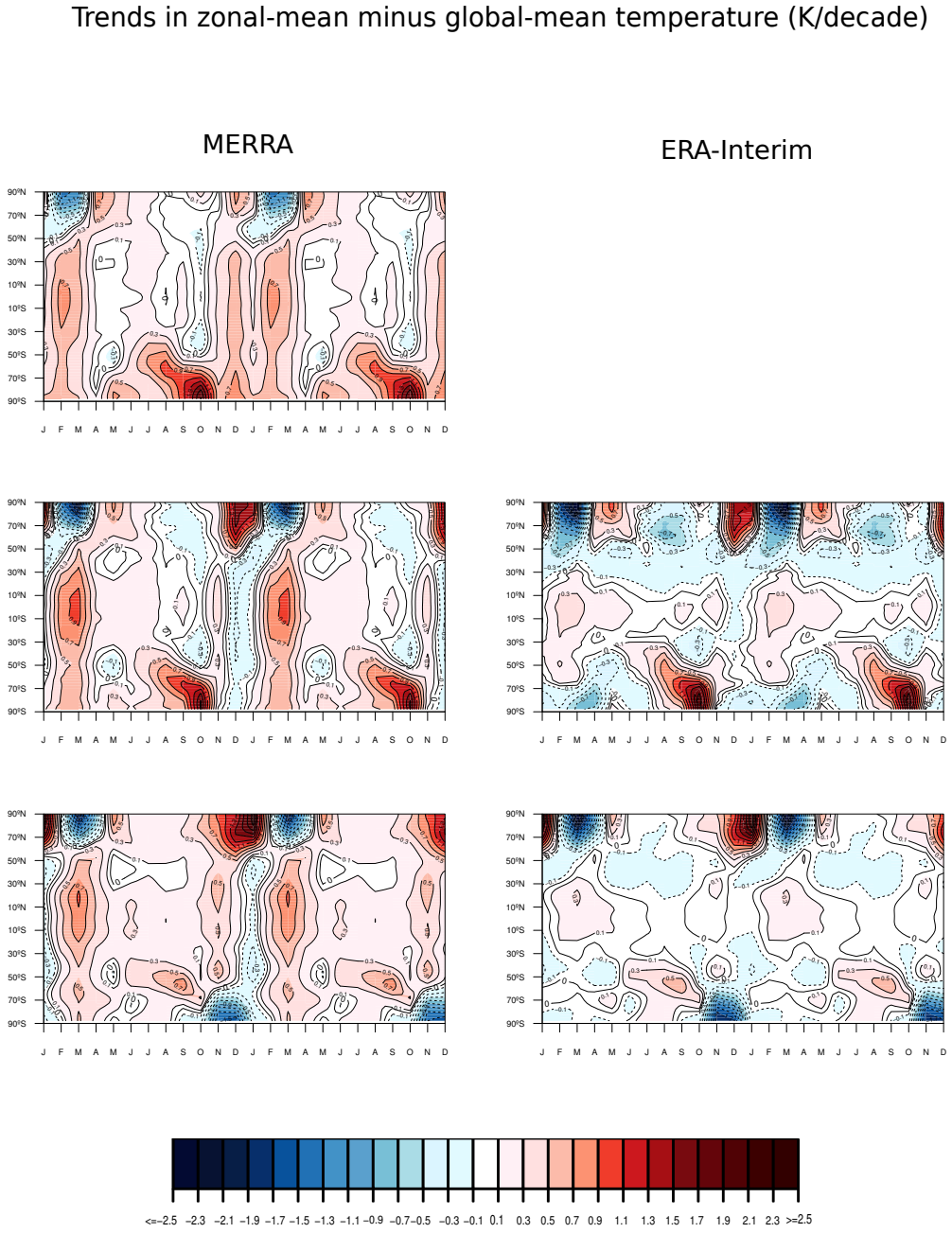

Figure 3.11: Zonal-mean T* trends for the MERRA and ERA-Interim as a function of month and latitude. Temperature anomalies are weighted by the MSU4 and the three SSU channel weighting functions to obtain data layers comparable to the NOAA, MetOffice and MSU4 datasets. Trends are computed depending on the level top of the dataset. Note that we show two complete seasons for clarity.

during late spring that could be attributable to radiative ozone cooling. The main features of MERRA reanalysis are displayed by ERA-Interim but the tropical warming trends as well as the tropical cooling found in December-January are weaker. Both reanalysis are in better agreement with MSU4 and MetOffice-SSU than with NOAA-SSU trends, although temperature trends at high latitudes, as well as in the tropics, are stronger. However, trends in the zonal temperature from MERRA and ERA-Interim reanalysis are not statistically significantly different from their global means assuming a 95% confidence level.

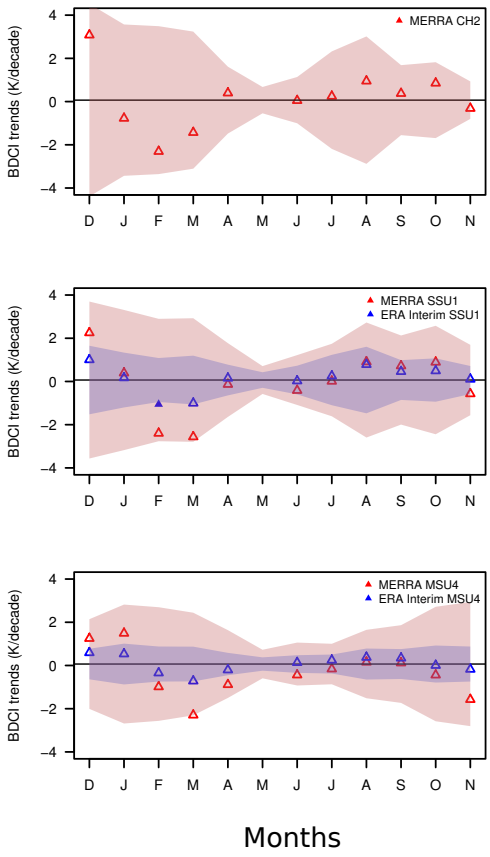

Figure 3.12: BDCI_T trends for MERRA and ERA-Interim as a function of month for the MSU4 and SSU CH1 and SSU CH2 equivalent layers. Trends are computed depending on the level top of the dataset. Shaded areas represent the two sigma error bars of the BDCI_T trends for each level and data product. Note that from December to April the BDCI_T trends are computed for the NH and from June to November for the SH. May has been excluded to the analysis because the extratropical temperatures are no well correlated with the tropical ones neither in the NH nor in the SH. Filled (open) triangles indicate statistically (non-statistically) significantly different from the global mean trends.

Seviour et al. [2012] found statistically significant negative trends in the tropical upwelling at 70 mb using ERA-Interim reanalysis. Nevertheless, this result was inconsistent with the statistically significant warming at 70 mb that they attributed in part to the effect of ozone trends not included in ERA-Interim. With a different approach, Iwasaki et al. [2009] also concluded that the BDC trends using output from reanalyses were unreliable.

The BDCI_T trends from MERRA show larger seasonal variability than ERA-Interim, especially in the NH with values of about 2 K/decade during December and -3 K/decade during March (Fig. 3.12). The BDCI determined from ERA-Interim is close to that from MSU4 and MetOffice SSU1. Tropical warming coinciding with SH high latitude cooling in the lower stratosphere result in large negative trend in the BDCI_T from MERRA reanalysis during November. Nevertheless trends are not larger than the interannual variance and hence they are not statistically significant.

3.5 Summary

In this chapter, we presented an updated and extended analysis of trends in stratospheric temperatures from multiple satellite retrievals, radiosondes and reanalysis to determine if they are consistent with a strengthening of the BDC during the past three decades. The estimated trends in the BDC are weak in all datasets and not exceed the 95% threshold. Moreover there are large discrepancies between different observational products as well as between observations and reanalysis.

Large discrepancies are found between the NOAA and MetOffice SSU products. While the three NOAA-SSU channels all show extended tropical cooling juxtaposed against warming both in the NH and in the SH polar regions during December and during SH winter, respectively, the MetOffice-SSU channels only show a weak cooling for CH2 during December juxtaposed with weaker high latitude warming. Both MetOffice and NOAA are working on a new version of the SSU dataset that should address these large discrepancies.

Our results differ from previous studies that found MetOffice, MSU4 and radiosonde temperature anomalies to be consistent with an acceleration of the BDC during the boreal winter. While all of these studies infer trends in the BDC from zonal mean temperature anomalies, we examine all temperature trends as “departures” from the global-mean (Eq. 3.2). Presumably, trends in the departure temperature field (T*) are not strongly affected by trends due to well-mixed greenhouse gases and hence they mainly respond to changes in dynamics (BDC). Therefore, any trend in the BDC should be projected into the T* field.

Finally, we also analyzed trends for the ERA-Interim and MERRA reanalysis. The spatial temporal structure of trends for both reanalysis is similar to MetOffice-SSU and MSU4. Nevertheless, temperature trends at high latitudes, as well as in the tropics, are stronger but still not statistically significant.

In the light of the discrepancies between observations of stratospheric temperatures, we conclude that it is essential a better constrain in the accuracy of these observational datasets if we want to monitor the strengthening of the BDC predicted by most of the models for the 21st century in response to GHG induced climate change.

4 Are the models correctly reproducing the observed stratospheric temperature trends?

4.1 Overview

This chapter presents a brief comparison between simulated and observed stratospheric temperatures over the last three decades. Simulated time series analyzed are from the current generation of AOGCMs and CCMs and the observed data, from the MSU4 and the two SSU satellite products available. Firstly, temperature anomalies from the AOGCMs runs available from the Coupled Model Intercomparison Project Phase 5 (CMIP5) are examined in section 4.3. Finally, section 4.4 examines results from the CCMs available from the CCM validation project phase two (CCMVal2). This chapter is partially based on Thompson et al. [2012].

4.2 Introduction

AOGCMs as well as CCMs are our best tools to simulate the state of the atmosphere and anticipate its response to both natural and anthropogenic forcings. These models are built on the bases of our current theoretical understanding of the physical processes governing the atmosphere. On the other hand, these numerical simulations test the reliability of the theory when their predictions are compared against observations. This is the process by which means our knowledge of the atmosphere advances (Figure 4.1).

This chapter just pretends to show that there are still important discrepancies between the observed and simulated stratospheric temperature trends, as well as large differences among models. Attribution of these discrepancies falls outside the scope of this thesis. We just point out some current problems:

1. Most of the current AOGCMs have poor vertical resolution at high altitudes. Therefore they do not adequately resolve the stratosphere.
2. Similarity between CCMs simulations might be due in part to the similarity of the orographic gravity wave parametrization [WMO 2011].

3. There is a lack of long term diagnostic data for model intercomparison studies. For example stratospheric temperature observations rely only on a few bunches of data sources that do not expand longer than three decades. In addition there are significant discrepancies between observational data sets.

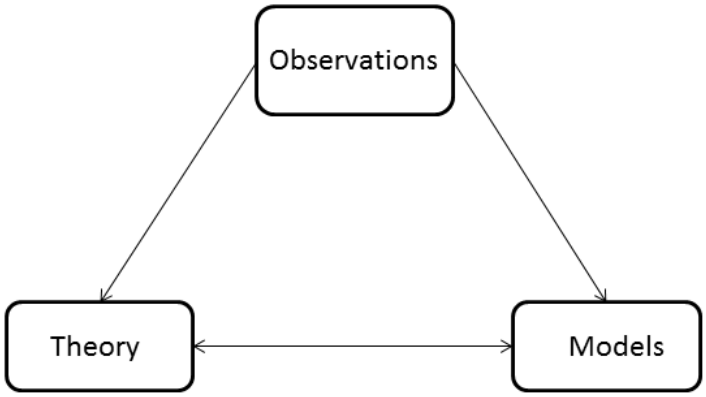

Figure 4.1: "The virtuous cycle of knowledge".

4.3 AOGCMs from the CMIP5 archive

Figure 4.2 shows that globally the CMIP5 models indicate less cooling in the upper stratosphere (40-50 km) than both SSU products, lie between them at 35-45 km and reasonably match the MetOffice-SSU product at 25-35 km. Where do these discrepancies come from?

Changes in stratospheric circulation should be reflected in the latitudinal structure of temperature trends. Figure 4.3 shows the standard deviation of trends in the stratospheric temperature anomalies from the CMIP5 runs as a function of latitude and month. This figure indicates that there is large disparity among different CMIP5 models, especially at high latitudes during winter months. This picture calls into question the ability of these models to simulate changes in the stratospheric circulation.

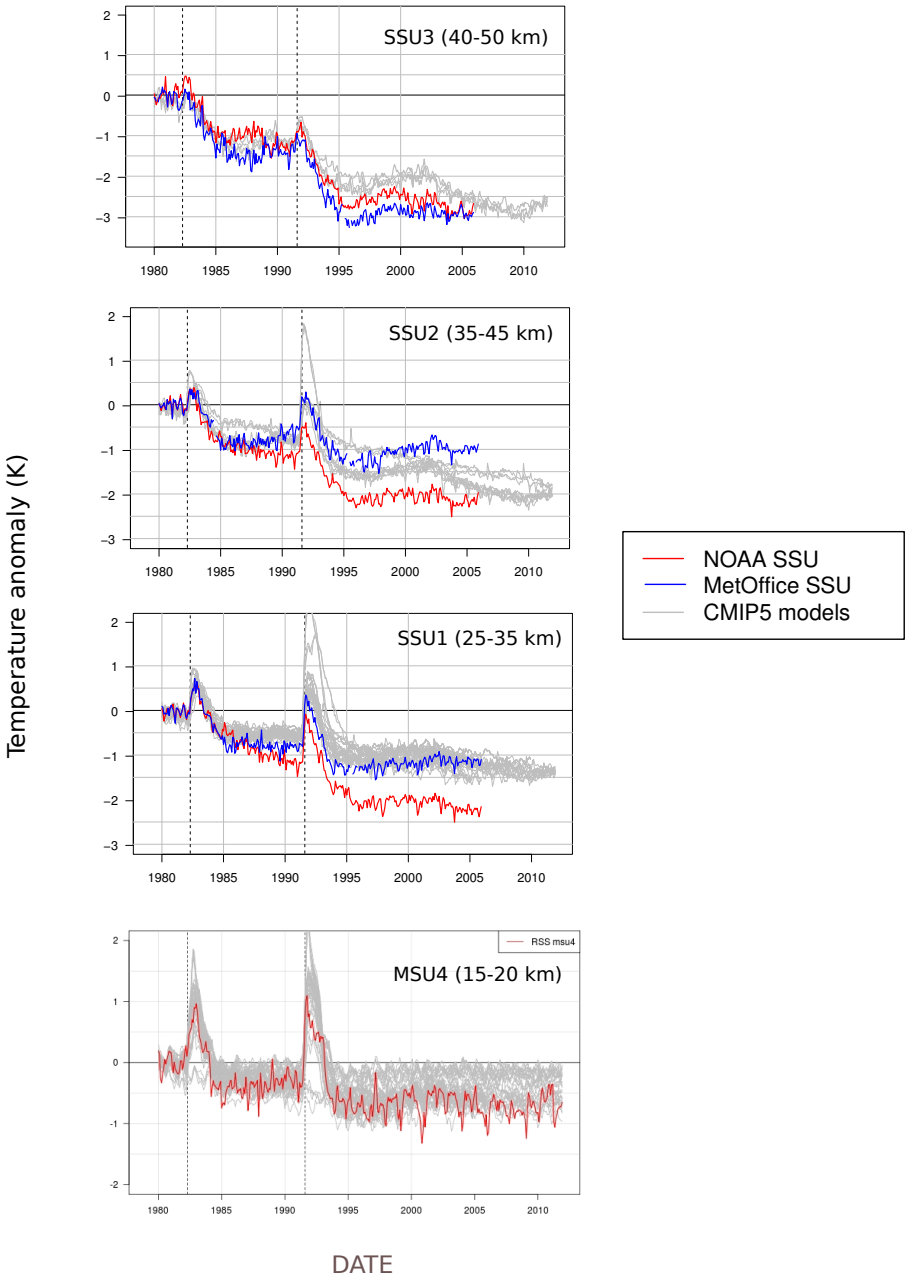

Figure 4.2: Monthly mean global-mean stratospheric temperatures anomalies for the altitude ranges and data sets indicated. AOGCM runs are from the CMIP5 archive. CMIP5 runs were converted to SSU and MSU time series using the appropriated weighting functions. Several CMIP5 runs have poor vertical resolution in the middle and upper stratosphere, therefore less models are used at higher altitudes (see table 4.1).

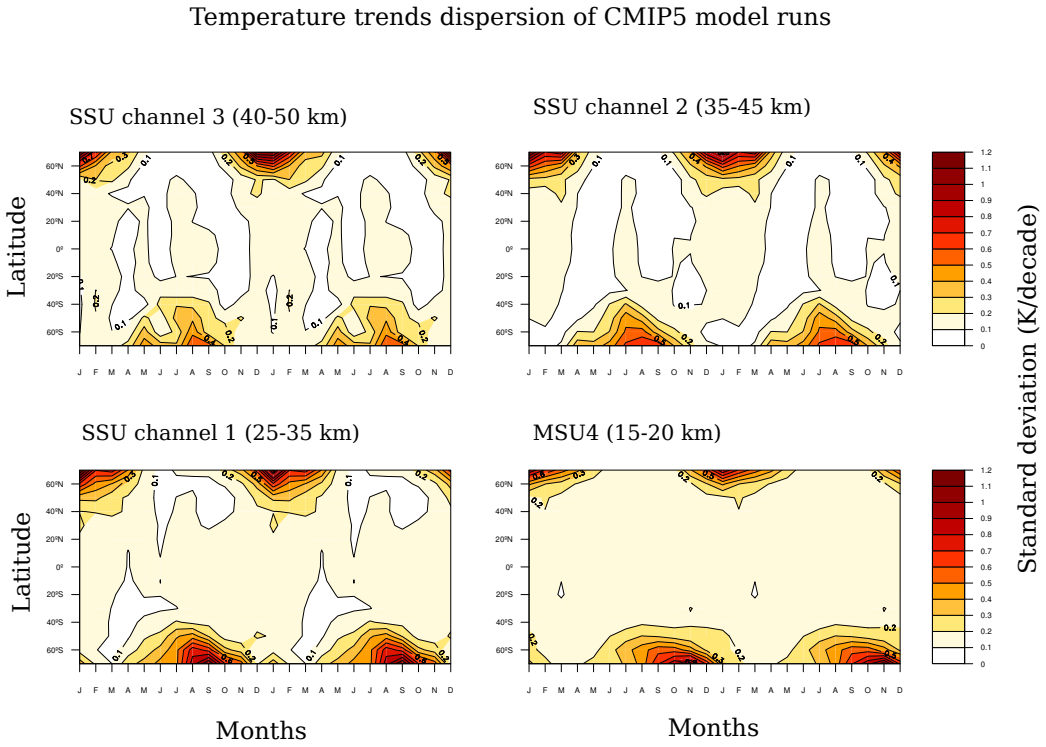

Figure 4.3: Standard deviation (K/decade) of the stratospheric temperature trends from the CMIP5 model runs. Trends were calculated for the period 1979-2005. CMIP5 time series were converted to MSU4 and SSU time series using the appropriate weighting functions. Models were used depending on the vertical resolution and the model top.

4.4 CCMs from the CCMVal2 archive

AOGCMs are primarily built to simulate tropospheric processes. On the contrary, CCMs specifically treat the stratospheric chemistry and are primarily focused on studying the processes of the stratosphere. Surprisingly stratospheric temperature anomalies derived from the models of the CCMVal2 archive are very similar to the ones derived from the CMIP5 archive. Figure 4.4 shows that the global-mean temperature anomalies derived from CCMVal2 runs are very similar to the ones derived from CMIP5 runs. Thus CCMs also show less cooling in the upper stratosphere (40-50 km) than both SSU products, lie between them at 35-45 km and reasonably match the MetOffice-SSU product at 25-35 km.

Finally, figure 4.5 shows a boxplot for the trends of the stratospheric temperatures derived from the CCMVal2 model runs. Trends are shown by three key latitude 70ºN, 70ºS and 0ºN.

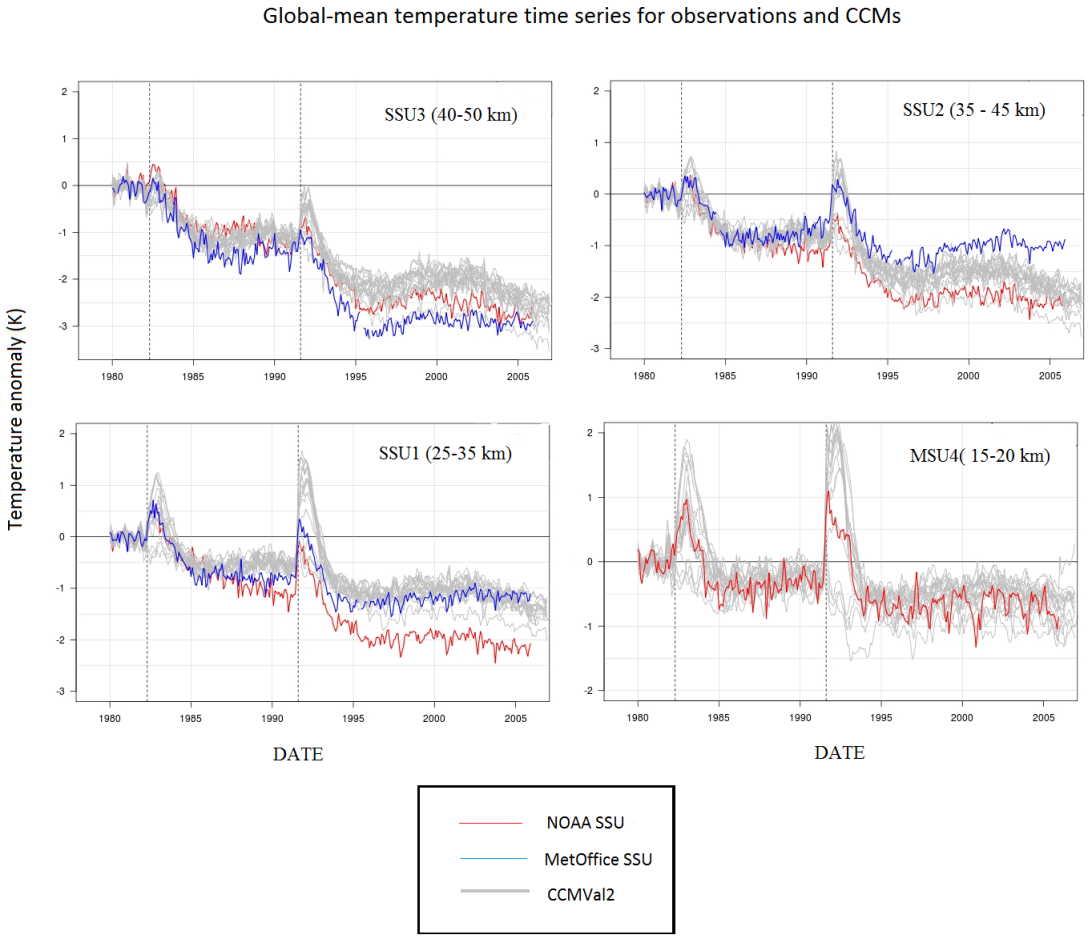

Figure 4.4: Time series of monthly mean global-mean stratospheric temperature anomalies. Anomalies are shown for the altitude ranges and data sets indicated. CCMVal2 model runs were converted to MSU and SSU time series using the appropriated weighting functions. See table 4.1 for a list of the models used.

In the upper stratosphere (40-50 km), trends from the CCMVal2 model runs show large dispersion during winter months, both at 70º N and 70º S. Such dispersion might indicate different representations of the BDC and ozone depletion. Moreover the magnitude of the trends throughout the year lies between the two SSU products. In the middle stratosphere (25-35 km) the picture is similar although the models seem to better agree with SSU products. In the upper stratosphere tropical regions, the models show less dispersion but they seem to underestimate the cooling measured by the SSU products. In the other hand in the middle stratosphere the models reasonably match with MetOffice-SSU whereas NOAA-SSU shows globally more cooling.

CMIP5 model runs	CCMVal2 model runs
CanESM2* (5)	AMTRAC3
CCSM4 (6)	CCSRNIES
CSIRO-Mk3.6.0 (10)	CMAM (3)
FGOALS-s2 (3)	EMAC
GFDL-CM3* (5)	LMDZrepro (3)
GFDL-ESM2G (1)	MRI (4)
GFDL-ESM2M (1)	NIWA SOCOL
GISS-E2-H (15)	SOCOL (3)
GISS-E2-R (16)	ULAQ
HadCM3 (10)	UMSLIMCAT
HadGEM2-CC** (3)	WACCM (4)
HadGEM2-ES (4)	
MIROC4h* (3)	
MIROC5 (4)	
MIROC-ESM*** (3)	
MIROC-ESM-CHEM*** (1)	
MRI-CGCM3** (5)	
NorESM1-M (3)	
NorESM1-ME (1)	

Table 4.1: Model runs used in this study. Numbers in parentheses indicate the number of ensemble members. Three asterisks (***) indicate that the model was used in all levels considered. ** used in MSU4, SSU channel 1 and SSU channel 2. * used in SSU channel. No asterisks used only in MSU4. All model runs were converted to MSU4 and SSU time series using the appropriated weighting functions.

4.5 Where do these discrepancies come from?

There is currently no definitive answer for this problem. Thompson et al. [2012] suggested some possible causes:

- One or both of the SSU products are in error.
- Trends in the global-mean temperature anomalies are driven by radiative pro-

cesses associated with changes in stratospheric composition and are at first order independent of changes in stratospheric circulation. Therefore it is possible that the models miss some key aspects associated with radiative processes. A misrepresentation of ozone trends is suggested.

- Changes in the BDC are not completely understood. Different representations of the BDC between models together with different representations of the ozone trends might explain the differences they exhibit in the latitudinal structure of the trends.

5 Discussion and Outlook

5.1 Overview

In this concluding chapter the main results of the thesis are summarized. In addition an outlook with suggestions for future research is given.

5.2 Discussion

In this thesis, the following questions have been addressed:

- To what extent are the long-term trends of total ozone affected by the North Atlantic Oscillation during winter and summer seasons?

This question has been addressed in Chapter 2 by examining the correlation between the NAO and TOC in the Northern Hemisphere during the period 1980-2009 for the high summer and winter seasons. TOC anomalies were based on TOMS and OMI satellite retrievals, while the NAO time series used were the principal component time series of the leading EOF of the gridded Atlantic sea level pressure anomalies from the NCEP/NCAR data set. Moreover correlation between the NAO and thermal tropopause pressure and geopotential heights at 200 hPa and 500 hPa were also calculated. This study has shown that during winter, the TOC variability associated with the NAO is particularly important over Northern Europe, the US East Coast and Canada explaining up to 30% of the TOC variance for these regions. Further the explained variance reaches up to 60% over North Eastern Asia. One central finding of this work is the inverse relation found over Southern Europe between the winter NAO and SNAO on TOC values. It is shown that a positive SNAO produces a retrograde circulation over the Eastern Mediterranean favoring the generation of two relatively small low pressure systems at 200 hPa over the central Mediterranean and west of Iberian Peninsula positively correlated with TOC values.

- How robust are the observed trends in the Brewer-Dobson Circulation?

This question has been addressed in Chapter 3 by examining the out of phase stratospheric temperature trends between the tropics and the extratropics. Trends were examined as departures from the global-mean for a range of observational data (NOAA-SSU, MetOffice-SSU, MSU TLS, RATPAC and RICH radiosondes) and two primary reanalysis products (ERA-Interim and MERRA). To gain further insight, trends of a Brewer-Dobson Circulation index (BDCI) based on temperatures were also calculated. The ability of this BDCI to capture the evolution of the BDC was tested using the TEM diagnosis of residual vertical velocities from the WACCM model. This study showed that the estimated trends in the BDC are weak in all data sets and not exceed the 95% significance threshold. Moreover it has been shown that there are large discrepancies between different observational products as well as between observations and reanalysis.

- Is the current generation of coupled atmosphere-ocean global circulation models (AOGCMs) and coupled climate-chemistry models (CCMs) correctly reproducing the observed stratospheric temperature trends over the last three decades?

This question has been addressed in Chapter 4 by examining stratospheric temperature trends from the MSU4 and SSU products and from the CCMVal2 and CMIP5 model runs. This study showed that there are large discrepancies betweem models and observations and also among models. These divergences are apparent in the global-mean trends and more strikingly in the latitudinal structure of trends. The cause of such divergences is not completely clear, although errors in the SSU products and a misrepresentation of ozone trends in the models are more likely involve.

5.3 Outlook

Several questions have arisen on the present study that require further research:

As we stated in chapter 3, most of CCM runs robustly predict a strengthening of the BDC over the next decades as a response to GHGs concentration increase. “Climate change” would change the propagation properties of the atmosphere resulting in more waves breaking into the stratosphere. Nevertheless, there are still important uncertainties on which type of waves are responsible for the predicted BDC strengthening. Moreover as we discussed before these predictions must be contrasted against observations to test its reliability. We showed that stratospheric temperatures can be a good observational proxy to infer trends in the BDC. Nevertheless some problems should be taken into consideration:

- It is absolutely crucial to better constraint the stratospheric temperatures. We hope that the forthcoming release of newly repossessed SSU radiances will help to shed light to the current discrepancies between data sets.
- Trends in the difference between the zonal-mean and the global-mean stratospheric temperature anomalies primarily reflect changes in the BDC but also at second order to any forcing that includes a latitudinal gradient (e.g., the ozone hole or the meridional gradient of the GHG heating rates). Future research could be directed towards building a temperature based BDC-Index that discount the effects of ozone depletion. This could be done by subtracting the temperature anomalies linearly congruent with ozone from the original time series:

$$T^{dyn}(\theta,t) = T(\theta,t) - T^{O_3}(\theta,t) - \left[T^{CO_2}\right] \tag{5.1}$$

where $T^{O_3}(\theta,t)$ is the zonal component of $T(\theta,t)$ that are linearly congruent with variations of $O_3(\theta,t)$ and $\left[T^{CO_2}\right]$ is the global-mean temperature no linearly congruent with global mean ozone variations. The last term should remove the effects of the well-mix GHGs.

We know that changes in wave penetration into the stratosphere determine the BDC variability. Nevertheless, some questions have still to be investigated. Here we just propose some possible lines of research that the author finds very interesting:

- To what extend do tropical waves such as generated by strong convection contribute to stratospheric wave penetration and thus to BDC?

- Is the variability of the NAO/NAM influencing the stratospheric wave penetrations and thus the BDC? If so, to what extend?

Bibliography

[1] Ambaum, M.P.H., and B.J. Hoskins, 2002: The NAO troposphere-stratosphere connection. J. Climate, 15, 1969-1978.

[2] Andrews, D.G., J.R. Holton, and C.B. Leovy, 1987: Middle Atmosphere Dynamics, Academic Press, 487 pp.

[3] Andrews, D. G., and M. E. McIntyre 1976: Planetary waves in horizontal and Vertical shear: The generalized Eliassen-Palm relation and the mean zonal acceleration, J. Atmos. Sci., 33, 2031-2048.

[4] Appenzeller, C., A.K. Weiss, and J. Staehelin 2000: North Atlantic Oscillation modulates total ozone winter trends, Geophys. Res. Lett., 27, 1131-1134.

[5] Austin, J., and F. Li, 2006: On the relationship between the strength of the Brewer-Dobson circulation and the age of stratospheric air, Geophys. Res. Lett. 33, L17807.

[6] Austin, J., J. Wilson, F. Li, and H. Voemel, 2007: Evolution of water vapor and age of air in coupled chemistry climate model simulations of the stratosphere. J. Atmos. Sci.64, 905-921.

[7] Baldwin MP, Dunkerton TJ, 1999: Propagation of the Arctic Oscillation from the stratosphere to the troposphere, J. Geophys. Res. 104, 30937-46.

[8] Baldwin MP, Dunkerton TJ, 2001: Stratospheric harbingers of anomalous weather regimes. Science 294: 581-84.

[9] Bhartia, P.K. 2002 : Algorithm theoretical basis documentation, NASA Goddard Space Flight Center, Greenbelt, Maryland, USA.

[10] Birner, T., and H. Bönisch, 2011: Residual circulation trajectories and transit times into the extratropical lowermost stratosphere, Atm. Chem. Phys., 11, 817-827.

[11] Bladé, I., Fortuny, D., van Oldenborgh, G. J. and Liebmann, B., 2012: The summer North Atlantic Oscillation in CMIP3 models and related uncertainties in projected summer drying in Europe, J. Geophys. Res., 117, D16104.

[12] Bladé, I., Liebmann, B., Fortuny, D., and Oldenborgh, G. J., 2011: Observed and simulated impacts of the summer NAO in Europe: implications for projected drying in the Mediterranean region. ClimateDyn., 39, 3-4.

[13] Bojkov, R., L. Bishop, and V. Fioletov, 1995: Total ozone trends from quality-controlled ground-based data (1964-1994), J. Geophys. Res., 100, D12.

[14] Bönisch, H., A. Engel, T. Birner, P. Hoor, D.W. Tarasick, and E.A. Ray, 2011: On the structural changes in the Brewer-Dobson circulation after 2000. Atmos. Chem. Phys., 11, 3937-3948.

[15] Braesicke, P., A. Jrrar, P. Hadjinicolaou, and J. Pyle, 2003: Variability of total ozone due to the NAO as represented in two different model systems, Meteorol. Z., 12(4), 203-208. Brewer, A.W., 1949: Evidence for a world circulation provided by the measurements of helium and water vapour distribution in the stratosphere. Q. J. Roy. Meteor. Soc., 75, 351-363.

[16] Butchart, N., and A.A. Scaife, 2001: Removal of chlorofluorocarbons by increased mass exchange between the stratosphere and troposphere in a changing climate. Nature, 410, 799-802.

[17] Butchart, N., A.A. Scaife, M. Bourqui, J. de Grandpré, S.H.E. Hare, J.Kettleborough, U. Langematz, E. Manzini, F. Sassi, K. Shibata, D. Shindell, and M. Sigmond, 2006: Simulations of anthropogenic change in the strength of the Brewer-Dobson circulation, ClimateDyn., 27, 727-741.

[18] Butchart, N., I. Cionni, V. Eyring, T.G. Shepherd, D.W. Waugh, H. Akiyoshi, J. Austin, C. Brühl, M.P. Chipperfield, E. Cordero, M. Dameris, R. Deckert, S. Dhomese, S.M. Frith, R.R.. Garcia, A.Gettelman, M.A. Giorgetta, D.E. Kinnison, F. Li, E. Mancini, C.McLandress, S. Pawson, G. Pitari, D.A. Plummer, E. Rozanov, F.Sassi, J.F. Scinocca, K. Shibata, B. Steil, and W. Tian, 2010: Chemistry-climate model simulations of twenty-first century stratospheric climate and circulation changes. J. Climate, 23, 5349-5374.

[19] Butchard, 2014: The Brewer Dobson Circulation. Accepted in press. doi: 10.1002/2013RG000448.

[20] Calvo, N., and R.R. Garcia, 2009: Wave forcing of the tropical upwelling in the lower stratosphere under increasing concentrations of greenhouse gases. J. Atmos. Sci., 66, 3184-3196.

[21] Chapman, S., 1930: A theory of upper atmospheric ozone. Mem. Roy. Meteorol. Soc., 3, 103.

[22] Charney, J. G., and P. G. Drazin, 1961: Propagation of planetary-scale disturbances from the lower into the upper atmosphere, J. Geophys. Res., 66, 83-109.

[23] Cook, P. A., and H. K. Roscoe, 2009: Variability and trends in stratospheric NO2 in Antarctic summer, and implications for stratospheric NOy, Atmos. Chem. Phys., 9, 3601–3612.

[24] Corral A., A. Ossó, and J.E. Llebot, 2010: Scaling of tropical-cyclone dissipation, Nature Phys., 6, 693-696.

[25] Dall'amico, M., L.J. Gray, K.H. Rosenlof, A.A. Scaife, K.P. Shine, and P.A. Stott, 2010: Stratospheric temperature trends: impact of ozone variability and the QBO, Climate Dyn., 34, vol. 2-3, 381-398.

[26] Daniel, J. S., S. Solomon, and D.L. Albritton, 1995: On the evaluation of halocarbon radiative forcing and global warming potentials, J. Geophys. Res., 100 (D1), 1271–1285.

[27] Dee, D.P., with 35 co-authors, 2011: The ERA-Interim reanalysis: configuration and performance of the data assimilation system, Q. J. R. Meteor. Soc., 137, 553-597.

[28] Derber, J.C., R.J. Purser, W.-S. Wu, R. Treadon, M. Pondeca, D. Parrish, and D. Kleist, 2003: Flow-dependent Jb in a global grid-point 3D-Var.Proc. ECMWF annual seminar on recent developments in data assimilation for atmosphere and ocean, Reading, UK.

[29] Deser C., 2000: On the teleconnectivity of the "Arctic Oscillation", Geophys. Res. Let., 779-782.

[30] Dickinson, R. E., 1968: On the excitation and propagation of zonal winds in an atmosphere with Newtonian cooling, J. Atmos.Sci., 25, 269-279.

[31] Dobson, G.M.B., 1956: Origin and distribution of the polyatomic molecules in the atmosphere, Proc. Roy. Soc. Ldn., Series a-Mathematical and Physical Sciences, 236, 187-193.

[32] Dragani, R., 2010: On the quality of the ERA-Interim ozone reanalysis. Part I: Comparisons with in situ measurements, ECMWF Technical Report, ERA Report Series (2).

[33] Durre, I., S.V. Russell, and D.B. Wuertz, 2006: Overview of the Integrated Global Radiosonde Archive, J. Climate, 19(1), 53-68.

[34] Echer, E., V.W.J.H. Kirchhoff, Y. Sahai, and N. PaesLeme 2001: A study of the solar cycle signal on total ozone over low-latitude Brazilian observation stations, Adv. Space Res., 27(12), 1983-1986.

[35] Echer, E., F.L. Guarnieri, N.R. Rigozo, L.E.A. Vieira 2004: A study of latitudinal dependence of the quasibiennial oscillation in total ozone mapping spectrometer total ozone, Tellus, 56A, 527-535.

[36] Eliassen, A., 1951: Slow thermally or frictionally controlled meridional circulation in a circular vortex, Astrophys.Norv., 5(2), 19-60.

[37] Emanuel, K., 2007: Environmental factors affecting tropical cyclone power dissipation, J. Climate 20, 5497-5509.

[38] Emanuel, K., 2010: Stratospheric cooling and Tropical Cyclones, paper presented at 29th Conference on Hurricanes and Tropical Meteorology, Am. Meterol. Soc., Tucson, Arizona.

[39] Engel, A., T. Möbius, H. Bönisch, U. Schmidt, R. Heinz, I. Levin, E. Atlas, S. Aoki, T. Nakazawa, S. Sugawara, F. Moore, D. Hurst, J. Elkins, S. Schauffler, A. Andrews, and K. Boering, 2009: Age of stratospheric air unchanged within uncertainties over the past 30 years, Nature Geosci., 2, 28-31.

[40] Farman, J. C., R. J. Murgatroyd, A. M. Silnickas, and B. A. Thrush, 1985. Ozone photochemistry in the Antarctic stratosphere in summer. *Q. J. R. Meteorol. Soc.*, *111*, 1013–1028.

[41] Folland, C.K., J. Kinght, H.W. Linderholm, D. Fereday, S. Ineson, and J.W. Hurrell, 2009: The summer North Atlantic Oscillation: Past, Present, and Future, J. Climate, 22, 1082-1103. Forster, P.M., and D.W.J. Thompson (Coordinating Lead Authors), 2011: Stratospheric changes and climate. Scientific Assessment of Ozone Depletion: 2010, Global Ozone Research and Monitoring Project Report no. 52, World Meteorological Organization, 4.1-4.60.

[42] Free, M., D.J. Seidel, J.K. Angell, J. Lanzante, I.Durre, and T.C. Peterson, 2005: Radiosonde Atmospheric Temperature Products for Assessing Climate (RATPAC): A new data set of large-area anomaly time series, J. Geophys. Res., 110, D22101.

[43] Fu, Q., S. Solomon, and P. Lin, 2010: On the seasonal dependence of tropical lower-stratospheric temperature trends. Atmos. Chem. Phys., 10, 2643-2653.

[44] Garcia, R.R., D.R. Marsh, D.E. Kinnison, B.A. Boville, and F. Sassi, 2007: Simulation of secular trends in the middle atmosphere, 1950-2003, J. Geophys. Res., 112, D09301.

[45] Fusco, A. C. and Salby, M. L., 1999: Interannual variations of total ozone and their relationship to variations of planetary wave activity, J. Clim., 12, 6, 1619-1629, Corrigendum 12, 10, 3165.

[46] Garcia, R.R. and W.J. Randel, 2008: Acceleration of the Brewer-Dobson circulation due to increases in greenhouse gases.J. Atmos. Sci., 65, 2731–2739.

[47] Garny, H., M. Dameris, W. Randel, G.E. Bodeker, and R. Deckert, 2011: Dynamically forced increase of tropical upwelling in the lower stratosphere, J. Atmos. Sci., 68, 1214-1233.

[48] Gillett, Nathan P., Hans F. Graf, and Tim J. Osborn, 2003: Climate change and the North Atlantic oscillation, Geophysical Monograph Series, 134, 193-209.

[49] Hadjinicolaou, P., A. Jrrar, J.A. Pyle, and L. Bishop, 2002: The dynamically driven long-term trend in stratospheric ozone over northern middle latitudes, Q.J.R. Meteorol. Soc., 128, 1393-1412.

[50] Haimberger, L., C. Tavolato, and S. Sperka, 2012: Homogenization of the Global Radiosonde Temperature Dataset through combined comparison with reanalysis background series and neighboring stations, J. Climate, 25, 8108-8131.

[51] Hall, T.M., and R.A. Plumb, 1994: Age as a diagnostic of stratospheric transport, J. Geophys. Res., 99 (D1), 1059-1070.

[52] Harris, N.R.P., E. Kyrö, J. Staehelin, D. Brunner, S-B. Andersen, S. Godin-Beekmann, S. Dhomse, P. Hadjinicolaou, G. Hansen, I. Isaksen, A. Jrrar, A.

Karpetchko, R. Kivi, B. Knudsen, P. Krizan, J. Lastovicka, J. Maeder, Y. Orsolini, J.A. Pyle, M. Rex, K. Vanicek, M. Weber, I. Wohltmann, P. Zanis, and C. Zerefos 2008: Ozone trends at northern mid- and high latitudes- A European perspective, Ann. Geophys., 26(5), 1207-1220.

[53] Hartmann, D. L., J. M. Wallace, V. Limpasuvan, D. W. J. Thompson and J. R. Holton, 2000: Can Ozone Depletion and Global Warming Interact to Produce Rapid Climate Change? Proc. Nat. Acad. Sci., 97, 1412-1417.

[54] Haynes, P. H., C. J. Marks, M. E. McIntyre, T. G. Shepherd, and K. P. Shine, 1991: On the"downward control"of extratropical diabatic circulations by eddy-induced mean zonal forces, J. Atmos. Sci., 48, 651–678.

[55] Haynes, Peter, 2005: Stratospheric dynamics, Annu. Rev. Fluid Mech., 37, 263-293.

[56] Hegglin, M. I., and T. G. Shepherd, 2009: Large climate-induced changes in ultraviolet index and stratosphere-to-troposphere flux. Nat. Geosci., 2, 687–691.

[57] Hood, L.,1997: The solar cycle variation of total ozone: Dynamical forcing in the lower stratosphere, J. Geophys. Res., 102, D1, 1355-1370.

[58] Hood, L., S. Rossi, and M. Beulen, 1999: Trends in lower stratospheric zonal winds, Rossby wave breaking behavior, and column ozone at northern midlatitudes, J. Geophys. Res., 104, D20, 24321-24339.

[59] Hood, L.L, and B.E. Soukharev 2005: Interannual variations of total ozone at northern midlatitudes correlated with stratospheric EP flux and potential vorticity, J. Atmos. Sci., 62, 3724-3740.

[60] Holton, J.R., P.H. Haynes, M.E. McIntyre, A.R. Douglass, R.B. Rood, and L. Pfister, 1995: Stratosphere-troposphere exchange, Rev. Geophys., 33, 403-439.

[61] Holton and Hakim, 2013. An Introduction to Dynamic Meteorology. Academic Press.

[62] Hoskins, Brian J., M. E. McIntyre, and Andrew W. Robertson, 1985: On the use and significance of isentropic potential vorticity maps, Quarterly Journal of the Royal Meteorological Society 111.470, 877-946.

[63] Hurrell, J.W., 1995: Decadal trends in the North Atlantic Oscillation: regional temperatures and precipitation, Science, 269, 676-679.

[64] Hurrell, J.W., and H. van Loon, 1997: Decadal variations in climate associated with the North Atlantic Oscillation, Climate Change, 36, 301-326.

[65] Hurrell, J.W., and C. Deser, 2009: North Atlantic climate variability: The role of the North Atlantic Oscillation, J. Mar. Syst., 78(1), 28-41.

[66] Hurrell, J.W., Y. Kushnir, M. Visbeck, and G. Ottersen 2003: An Overview of the North Atlantic Oscillation, in The North Atlantic Oscillation: Climate Significance and Environmental Impact, Geophys. Monogr. Ser., vol. 134, edited

by J.W. Hurrell, Y. Kushnir, G. Ottersen, and M. Visbeck, pp. 1-35. AGU, Washington, DC.

[67] IPCC/TEAP (2005), IPCC/TEAP Special report on safeguarding the ozone layer and the global climate system: Issues related to hydrofluorocarbons and perfluorocarbons, Cambridge University Press, Cambridge, UK and New York.

[68] Iwasaki, T., H. Hamada, and K. Miyazaki, 2009: Comparisons of Brewer-Dobson circulations diagnosed from reanalysis, J. Meteor. Soc. Jpn, 87, 997-1006.

[69] Kalnay, E., Kanamitsu, M., Kistler, R., Collins, W., Deaven, D., Gandin, L., and Joseph, D.,1996: The NCEP/NCAR 40-year reanalysis project, Bulletin of the American meteorological Society, 77(3), 437-471.

[70] Kanamitsu, M., W. Ebisuzaki, J. Woollen, S-K. Yang, J.J. Hnilo, M. Fiorino, and G.L. Potter, 2002: NCEP-DOE AMIP II Reanalysis (R-2), Bull. Amer. Meteorol. Soc., 1631-1643.

[71] Kang S.M., L.M. Polvani, J.C. Fyfe, and M. Sigmond 2011: Impact of Polar Ozone Depletion on Subtropical Precipitation, Science, 332, no. 6032, 951-954.

[72] Kawatani, Y., K. Hamilton, and S. Watanabe 2011: The Quasi-Biennial Oscillation in a Double CO2 Climate, J. Atmos. Sci., 68(2).

[73] Kerr, J.B., and C.T. McElroy, 1995: Evidence for large upward trends of ultraviolet-B radiation linked to ozone depletion, Science, 262, nº 5183, 1032-1034.

[74] Knudsen, B.M., and S.B. Andersen 2001: Longitudinal variation in springtime ozone trends, Nature, 413, 699-700.

[75] Lander, M.A., 1994: An exploratory analysis of the relationship between tropical storm formation in the Western North Pacific and ENSO, Month. Weather Rev. 122, 636-651.

[76] Latif, M., 2001: Tropical Pacific/Atlantic Ocean Interactions at Multi-Decadal Time Scales, Geophys. Res. Lett., 28, 539-542.

[77] Li, F., J. Austin, and J. Wilson, 2008: The strength of the Brewer-Dobson Circulation in a changing climate: couple chemistry-climate model simulations, J. Climate, 21, 40-57. Lin, P. and Q. Fu, 2013: Changes in various branches of the Brewer-Dobson circulation from an ensemble of chemistry climate models, J. Geophys. Res., 118, 73-84.

[78] Lin, P., Q. Fu, S. Solomon, and J.M. Wallace, 2009: Temperature trend patterns in Southern Hemisphere high latitudes: Novel indicators of stratospheric change, J. Climate, 22, 6325-6341.

[79] Mäder, J.A, J. Staehelin, T. Peter, D. Brunner, H.E. Rieder, and W.A. Stahel 2010: Evidence for the effectiveness of the Montreal Protocol to protect the ozone layer, Atmos. Chem. Phys., 10, 12161-12171.

[80] McLandress, C., and T.G. Shepherd, 2009: Simulated anthropogenic changes in the Brewer-Dobson circulation, including its extension to high latitudes, J. Climate, 22, 1516-1540.

[81] McPeters, R., 1996: Total Ozone Mapping Spectrometer (TOMS) & Ozone Monitoring Instrument (OMI), NCAS British Atmospheric Data Centre, 1996, NASA. Available from: http://badc.nerc.ac.uk/view/badc.nerc.ac.uk___ATOM___dataent_TOMS

[82] McPeters, R.D., A.J. Krueger, P.K. Bhartia, and J.R. Herman 1998: Earth Probe Total Ozone Mapping Spectrometer (TOMS) Data Products User's Guide, NASA/TP-1998-206895, NASA, Washington, D.C.

[83] McPeters, R., M. Kroon, G. Labow, E. Brinska, D. Balis, I. Petropavlovskikh, J.P. Veefkind, P.K. Bhartia, and P.F. Levelt, 2008: Validation of Aura Ozone Monitoring Instrument total column ozone product, J. Geophys. Res., 113, D15S14.

[84] Mears, C.A., and F.J. Wentz, 2009: Construction of the Remote Sensing Systems V3.2 atmospheric temperature records from the MSU and AMSU microwave sounders, J. Atmos. Oceanic Tech., 26, 1493-1509.

[85] Meehl, G.A., C. Covey, B. McAveney, M. Latif, and R.J. Stouffer, 2005: Overview of the coupled model intercomparison project. Bull. Amer. Meteor. Soc., 86, 89-93.

[86] Nash, J., and G.F. Forrester, 1986: Long-term monitoring of stratospheric temperature trends using radiance measurements obtained by the TIROS-N series of NOAA spacecraft, Adv. Space Res., 6, 37-44.

[87] Nash, J., 1988: Extension of explicit radiance observations by the Stratospheric Sounding Unit into the lower stratosphere and lower mesosphere. Q. J. R. Meteor. Soc., 114, 1153-1171.

[88] Newman, P.A., and E.R. Nash, 2005: The unusual Southern Hemisphere stratospheric winter of 2002. J. Atmos. Sci., 62, 614-628.. Plumb, R.A., 2002: Stratospheric transport. J. Meteor. Soc. Jpn, 80, 793-809.

[89] Orsolini, Y.J., and F.J. Doblas-Reyes, 2003: Ozone signatures of climate patterns over the Euro-Atlantic sector in the spring, Q.J.R. Meteorol. Soc., 129, 3251-3263.

[90] Ossó, A., Y. Sola, J. Bech, and J. Lorente, 2011: Evidence for the influence of the NAO on total ozone column at northern low- and mid-latitudes during winter and summer season. J. Geophys. Res., 116, D24.

[91] Peters, D.H.W., A. Gabriel, and G. Entzian, 2008: Longitude-dependent decadal ozone changes and ozone trends in boreal winter months during 1960-2000. Ann. Geophys., 26, 1275-1286.

[92] Purser, R.J., W.-S. Wu, D.F. Parrish, and N.M. Robers, 2003a: Numerical aspects of the application of recursive filters to variational statistical analysis.

Part I: Spatially homogeneous and isotropic Gaussian covariances. Mon. Wea. Rev., 131, 1524-1535.

[93] Purser, R.J., W.-S. Wu, D.F. Parrish, and N.M. Robers, 2003b: Numerical aspects of the application of recursive filters to variational statistical analysis. Part II: Spatially inhomogeneous and anisotropic general covariances. Mon. Wea. Rev., 131, 1536-1548.

[94] Pyle, J., T. Shepherd, et al. 2005: Ozone and Climate: A Review of Interconnections, in IPCC/TEAP Special Report: Safeguarding the Ozone Layer and the Global Climate System, edited by B. Metz, L. Kuijpers, S. Solomon, S.O. Andersen, O. Davidson, J. Pons, D. de Jager, T. Kestin, M. Manning, and L.A. Meyer, pp. 83-132, Cambridge University Press, Cambrige, UK, and New York, USA.

[95] Ramaswamy, V., M.-L.Chanin, J. Angell, J. Barnett, D. Gaffen, M. Gelman, P. Keckhut, Y. Koshelkov, K. Labitzke, J.-J.R. Lin, A. O'Neill, J. Nash, W.J. Randel, R. Rood, K. Shine, M. Shiotani, and R. Swinbank, 2001: Stratospheric temperature trends: observations and model simulations.Rev. Geophys., 39, 71-122.

[96] Randel, W.J., and F. Wu, 1999: A stratospheric ozone trends data set for global modeling studies.Geophys. Res. Lett., 26, 3089-3092.

[97] Randel, W.J., F. Wu, A. Gettelman, J.M. Russell III, J.M. Zawodny, and S.J. Oltmans, 2001: The seasonal variation of water vapor in the lower stratosphere observed in HALOE data. J. Geophys. Res., 106, 14313-14325.

[98] Randel, W. J., Wu, F. and Stolarski, R., 2002: Changes in column ozone correlated with the stratospheric EP flux, J. Meteor. Soc. Jap., 80, 4b, 849-862.

[99] Randel, W.J., K.P. Shine, J. Austin, J. Barnett, C. Claud, N.P. Gillett, P. Keckhut, U. Langematz, R. Lin, C. Long, C. Mears, A. Miller, J. Nash, D.J. Seidel, D.W.J. Thompson, F. Wu, and S. Yoden, 2009: An update of observed stratospheric temperature trends. J. Geophys. Res., 114, D02107.

[100] Rieder, H.E., J. Staehelin, J.A. Maeder, T. Peter, M. Ribatet, A.C. Davison, R. Stübi, P. Weihs, and F. Holawe 2010a: Extreme events in total ozone over Arosa –Part 1: Application of extreme value theory, Atmos. Chem. Phys., 10, 10021-10031.

[101] Rieder, H.E., J. Staehelin, J.A. Maeder, T. Peter, M. Ribatet, A.C. Davison, R. Stübi, P. Weihs, and F. Holawe 2010b: Extreme events in total ozone over Arosa –Part 2: Fingerprints of atmospheric dynamics and chemistry and effects on mean values and long-term changes, Atmos. Chem. Phys., 10, 10033-10045. Rieder, H. E., Jancso, L. M., Rocco, S. D., Staehelin, J., Maeder, J. A., Peter, T., and Vaníček, K., 2011: Extreme events in total ozone over the Northern mid-latitudes: an analysis based on long-term data sets from five European ground-based stations. Tellus B, 63(5), 860-874.

[102] Rienecker, M.M., and Coauthors, 2008: The GEOS-5 Data Assimilation System—Documentation of versions 5.0.1 and 5.1.0, and 5.2.0. NASA Tech. Rep. Series on Global Modeling and Data Assimilation, NASA/TM-2008-104606, Vol. 27, 92 pp.

[103] Rienecker, M.M., and Coauthors, 2011: MERRA: NASA's Modern-Era Retrospective Analysis for Research and Applications. J. Climate, 24, 3624-3648.

[104] Rind, D., D. Shindell,P. Lonergan, and N.K. Balachandran, 1998: Climate change and the middle atmosphere. Part III: The double CO2 climate revisited. J. Climate, 11, 876-894.

[105] Rind, D., J. Perlwitz, and P. Lonergan 2005: AO/NAO response to climate change: 1. Respective influences of stratospheric and tropospheric climate changes, J. Geophys. Res., 110, D12107.

[106] Rosenlof, H.K., 1995: Seasonal cycle of the residual mean meridional circulation in the stratosphere. J. Geophys. Res., 100, 5173-5191.

[107] Rosenlof, K.H., and J.R. Holton, 1993: Estimates of the stratospheric residual circulation using the downward control principle. J. Geophys. Res., 98, 10, 465-10,479.

[108] Salby, M.L., and P.F. Callaghan 2005: Interaction between the Brewer–Dobson Circulation and the Hadley Circulation, J. Climate, 18, 4303-4316.

[109] Schoeberl, M.R., P. K. Bhartia, E. Hilsenrath, and O. Torres 1993: Tropical ozone loss following the eruption of Mt. Pinatubo. Geophys. Res. Lett., 20(1), 29-32

[110] Seviour, W.J.M., N. Butchard, and S.C. Hardiman, 2012: The Brewer-Dobson circulation inferred from ERA-Interim.Q. J. R. Meteor. Soc., 138, 878-888.

[111] Shepherd, T.G., 2008: Dynamics, stratospheric ozone, and climate change, Atmos.-Ocean, 46, 371-392. Shindell, Drew T., et al. "Simulation of recent northern winter climate trends by greenhouse-gas forcing." Nature 399.6735 (1999): 452-455.

[112] Shine, K.P., M.S. Bourqui, P.M.F. Forster, S.H.E. Hare, U. Langematz, P. Braesicke, V. Grewe, M. Ponater, C. Schnadt,C.A. Smith, J.D. Haigh, J. Austin, N. Butchart, D.T. Shindell, W.J. Randel, T. Nagashima, R.W. Portmann, S. Solomon, D.J. Seidel, J. Lanzante, S. Klein, V. Ramaswamy, and M.D. Schwarzkopf, 2003: A comparison of model-simulated trends in stratospheric temperatures. Q. J. R. Meteor. Soc., 129, 1565-1588.

[113] Shine, K.P., J.J. Barnett, and W.J. Randel, 2008: Temperature trends derived from stratospheric sounding unit radiances: The effect of increasing CO2 on the weighting function. Geophys. Res. Lett., 35, L02710.

[114] Sigmond, M., P.C. Siegmund, E. Manzini, and H. Kelder, 2004: A simulation of the separate climate effects of middle-atmospheric and tropospheric CO2 doubling. J. Climate, 17, 2352-2367.

[115] Simmons, A., C. Uppala, D. Dee, and S. Kobayashi, 2007: ERA-Interim: New ECMWF reanalysis products from 1989 onwards. ECMWF Newsletter, 110, 25-35.

[116] Sitnov, S.A., 2004: QBO effects manifesting in ozone, temperature and wind profiles, Ann. Geophys., 22, 1495-1512.

[117] Solomon, S., 1999: Stratospheric ozone depletion: a review of concepts and history. Rev. Geophys., 37, 275-316.

[118] SPARC CCMVal, 2010: SPARC Report on the Evaluation of Chemistry-Climate Models, V. Eyring, T. G. Shepherd, D. W. Waugh (Eds.), SPARC Report No. 5, WCRP-132, WMO/TD-No. 1526, http://www.atmosp.physics.utoronto.ca/SPARC.

[119] Staehelin, J., J. Mäder, A.K. Weiss, and C. Appenzeller, 2002: Long-term ozone trends in Northern mid-latitudes with special emphasis on the contribution of changes in dynamics. Phys. Chem. Earth, Parts A/B/C, 27(6-8), 461-469.

[120] Steinbrecht W., H. Claude, U. Köhler, and K.P. Hoinka, 1998: Correlations between tropopause height and total ozone: implications for long-term changes, J. Geophys. Res., 103(D15), 19183-19192. Steinbrecht, W., H. Claude, U. Köhler, and P. Winkler (2001), Interannual changes of total ozone and northern hemisphere circulation patterns, Geophys. Res. Lett., 28(7), 1191-1194.

[121] Stolarski, R.S., P. Bloomfield, R.D. McPeters, and J.R. Herman 1991: Total ozone trends deduced from Nimbus-7 TOMS data, Geophys. Res. Lett., 18, 1015-1018.

[122] Stephenson, D. B.,H. Wanner, S.Brönnimann, and J. Luterbacher, 2003: The history of scientific research on the North Atlantic Oscillation. Geophysical Monograph 134.

[123] Sung, M.-K., G.-H. Lim, J.-S.Kug, and S.-I.An 2011: A linkage between the North Atlantic Oscillation and its downstream development due to the existence of a blocking ridge, J. Geophys. Res., 116, D11107. Thompson, D.W.J., and J.M. Wallace, 1998: The Arctic Oscillation signature in the wintertime geopotential height and temperature fields. Geophys. Res. Lett., 25, 1297-1300.

[124] Thompson, D.W.J., and J.M. Wallace, 2000: Annular modes in the extratropical circulation. Part I: Month-to-month variability. J. Climate, 13, 1000-1016.

[125] Thompson, D.W.J., S. Lee, and M.P. Baldwin, 2003: Atmospheric Processes Governing the Northern Hemisphere Annular Mode/North Atlantic Oscillation. AGU Monograph: North Atlantic Oscillation: Climatic Significance and Environmental Impact, 134, 81-112.

[126] Thompson, D.W.J., and S. Solomon, 2009: Understanding Recent Stratospheric Climate Change. J. Climate, 22, 1934–1943.

[127] Thompson, D.W.J., D.J. Seidel, W.J. Randel, C.-Z.Zou, A.H. Butler, C. Mears, A. Ossó, C. Long, and R. Lin, 2012: The mystery of recent stratospheric temperature trends. Nature, 491, 692-697.

[128] Timmermann, A., J.M. Oberhuber, A. Bacher, M. Esch, M. Latif., and E. Roeckner, 1999: Increased El Niño frequency in a climate model forced by future greenhouse warming. Nature, 398, 694-696.

[129] Tung, K. and H. Yang, 1994: Global QBO in circulation and ozone, part I, Reexamination of observational evidence, J. Atmos. Sci., 51, 2699-2707.

[130] Ueyama, R., and J.M. Wallace, 2010: To what extent does high latitude wave forcing drive tropical upwelling and the Brewer-Dobson circulation? J. Atmos. Sci., 67, 1232-1246.

[131] Varotsos, C., 2004: The extraordinary events of the major, sudden stratospheric warming, the diminutive Antarctic ozone hole, and its split in 2002. Environ. Sci. Pollut. Res., 11(6), 405-411.

[132] Wang, L., and D.W. Waugh, 2012: Chemistry-climate model simulations of recent trends in lower stratospheric temperature and stratospheric residual circulation. J. Geophys. Res., 117, D09109.

[133] Wang, L., C.-Z.Zou, and H. Qian, 2012: Construction of Stratospheric Temperature Data Records from Stratospheric Sounding Units. J. Climate, 25, 2931-2946.

[134] Wanner H., S. Brönnimann, C. Casty, D. Gyalistras, J. Luterbacher, C. Schmutz, D. Stephenson, and E. Xoplaki, 2001: North Atlantic Oscillation Concepts and Studies. Surveys Geophys., 22, 321-382.

[135] Watanabe M., 2004: Asian jet waveguide and a downstream extension of the North Atlantic Oscillation. J Clim 17: 4674–4691.

[136] Waugh, D., and T. Hall, 2002: Age of stratospheric air: Theory, observations, and models. Rev. Geophys., 40, 1010.

[137] Weatherhead, E.C., and S.B. Andersen, 2006: The search for signs of recovery of the ozone layer, Nature, 441, 39-45.

[138] Wilks, D.S., 2006: Statistical methods in atmospheric sciences, Int. Geophys. Ser., vol. 91, edited by R. Dmowska, D. Hartmann, and H.T. Rossby, Academic Press, Wiley, New York.

[139] WMO, 2007: Scientific Assessment of Ozone Depletion 2006, Global ozone research and monitoring project report 50, Geneva, Switzerland.

[140] WMO, 2011: Scientific Assessment of Ozone Depletion 2010, Global ozone research and monitoring project report 52, Geneva, Switzerland.

[141] Wohltmann, I., R. Lehmann, M. Rex, D. Brunner, and J.A. Mäder, 2007: A process-oriented regression model for column ozone, J. Geophys. Res., 112, D12304.

[142] World Meteorological Organization, 2011: Scientific Assessment of Ozone Depletion: 2010, Global Ozone Research and Monitoring Project Report 52, Geneva, Switzerland.

[143] World Meteorological Organization, 2012: Antarctic Ozone Bulletin, http://www.wmo.int/pages/prog/arep/WMOAntarcticOzoneBulletins2012.html.

[144] Wu, W.-S., R.J. Purser, and D.F. Parrish, 2002: Three-dimensional variational analysis with spatially inhomogeneous covariances. Mon. Wea. Rev., 130, 2905-2916.

[145] Young, P.J., D.W.J. Thompson, K.H. Rosenlof, S. Solomon, and J.-F.Lamarque, 2011: The seasonal cycle and interannual variability in stratospheric temperatures and links to the Brewer-Dobson circulation: An analysis of MSU and SSU data. J. Climate, 24, 6243-6258.

[146] Young, P.J., K.H. Rosenlof, S. Solomon, S.C. Sherwood, Q. Fu, and J.-F.Lamarque, 2012: Changes in stratospheric temperatures and their implications for changes in the Brewer-Dobson circulation, 1979-2005. J. Climate, 25, 1759-1772. Yulaeva, E., J. Holton, and J.M. Wallace, 1994: On the cause of the annual cycle in tropical lower-stratospheric temperatures. J. Atmos. Sci., 51, 169-174.

[147] Zerefos, C.S., K. Tourpali, I.S.A. Isaksen, and C.J.E. Schuurmans, 2001: Long term solar induced variations in total ozone stratospheric temperatures and the troposphere, Adv. Space Res., 27(12), 1943-1948.